

MODELLING THE INFLUENCE OF TRANSITIONS IN DIKES ON GRASS COVER EROSION BY WAVE OVERTOPPING

MSc-thesis in Civil Engineering and Management



M. Frankena
July 2019

**UNIVERSITY
OF TWENTE.**

Cover picture:

Grass cover erosion at the lower part of the slope and at the geometrical transition at the landward toe after wave overtopping tests at test section Boonweg 3 (Van der Meer, 2014).

MODELLING THE INFLUENCE OF TRANSITIONS IN DIKES ON GRASS COVER EROSION BY WAVE OVERTOPPING

*Master thesis Civil Engineering and Management
University of Twente
Faculty of Engineering Technology
Department of Water Engineering and Management*

July 2019
Enschede

Author: Marc Frankena

<i>Graduation committee:</i>	Prof. dr. S.J.M.H. Hulscher	University of Twente
	Dr. J.J. Warmink	University of Twente
	V.M. van Bergeijk MSc	University of Twente
	P. van Steeg MSc	Deltares

Preface

This report presents the thesis that forms the conclusion of my Master in Civil Engineering and Management. This graduation research was carried out at the Department of Water Engineering and Management at the University of Twente in collaboration with Deltares. Hopefully, the findings of this thesis provide a valuable contribution to the research regarding modelling grass cover erosion by wave overtopping.

I would like to thank the members of my graduation committee for their supervision and support throughout this research. First of all, I want to express my gratitude to Vera van Bergeijk for her creative suggestions and critical reflections for improving both modelling aspects and academic writing. Secondly, I would like to thank Paul van Steeg for suggesting interesting points of improvement and specifically for emphasizing aspects that cause discrepancies between grass cover erosion in models and in practice. Furthermore, I want to thank Jord Warmink and Suzanne Hulscher for their critical views to increase the academic level and the scientific value of the research. I also want to thank André van Hoven, Roy Mom and Jaap Bronsveld for providing their expert opinions during the interviews.

Finally, I want to thank my family, friends and fellow students who supported me during my life as a student and especially during this research.

Marc Frankena

Enschede, July 2019

Abstract

Transitions in dikes appear to be weak spots for grass cover erosion by wave overtopping. Erosion models are available to predict and evaluate grass cover erosion on dikes. However, it is currently not known how the influence of transitions on grass cover erosion must be included in these computational models. The objective of this thesis is therefore to set up a model approach to analyse the effects of transitions on grass cover erosion and to derive representative influence factors for one transition type.

Suitable transition types for the model analysis are selected based on expert opinions and the availability of data from wave overtopping tests. A general approach is introduced for analysing the influence of transitions on grass cover erosion by wave overtopping. The approach describes how the grass cover strength is determined considering the damage along the slope and, next, how representative influence factors for the transitions are calibrated based on the damage at the transition. The approach is specified for two erosion models: the hydrodynamic-erosion model and the cumulative overload method. Also, three methods for flow acceleration along the landward slope are considered for the cumulative overload method. Next, the model analysis is applied to seven test sections with a geometrical transition at the landward toe.

The influence of the geometrical transition is calibrated in terms of the turbulence intensity parameter r_0 and the load factor α_M for the hydrodynamic-erosion model and the cumulative overload method, respectively. The calibration of turbulence intensity parameter r_0 for the load increase at geometrical transitions results in $r_0 = 0.25$ for mild slopes and $r_0 = 0.45$ for relatively steep slopes. The calibrated load factors for the three flow acceleration methods vary between $\alpha_M = 1.4$ and $\alpha_M = 1.6$ for mild slopes and range from $\alpha_M = 1.4$ to $\alpha_M = 1.8$ for relatively steep slopes. Generally, the calibrated load factor α_M exceeds the theoretical value for the load increase at geometrical transitions as function of the slope steepness by Hoffmans et al. (2018). It is concluded that the hydrodynamic-erosion model is better applicable for determining representative influence factors for transitions on grass cover erosion than the cumulative overload method.

The modelled erosion depth is linearly related to the inverse strength parameter C_E in the hydrodynamic-erosion model. Model results showed that the erosion rate of the grass sod is relatively high compared to the erosion rate of the clay layer. It is therefore recommended to distinguish between erosion of the grass sod and erosion of the clay layer to improve the hydrodynamic-erosion model. Finally, it is recommended to apply the calibration approach to other transition types to determine representative influence factors for each transition type using the hydrodynamic-erosion model.

Table of content

Preface.....	i
Abstract	ii
1. Introduction	1
1.1. Background	1
1.2. Problem definition and research objective	2
1.3. Method	4
1.4. Report outline.....	4
2. Influence of transitions on grass cover erosion	5
2.1. Problematic transition types	6
2.1.1. Expert judgment.....	6
2.1.2. Wave overtopping tests and transitions	9
2.1.3. Synthesis.....	16
2.2. Model cases	16
3. Model analysis	20
3.1. Model description.....	20
3.1.1. Boundary conditions	20
3.1.2. Model 1: Hydrodynamic-erosion model	22
3.1.3. Model 2: Cumulative overload method	24
3.2. Modelling the effects of transitions	27
3.2.1. Model 1: Hydrodynamic-erosion model	27
3.2.2. Model 2: Cumulative overload method	28
3.3. Application to transition landward toe	29
3.3.1. Model 1: Hydrodynamic-erosion model	30
3.3.2. Model 2: Cumulative overload method	32
4. Results.....	34
4.1. Model 1: Hydrodynamic-erosion model.....	34
4.2. Model 2: Cumulative overload method	35
4.3. Comparison of the model results	36
4.3.1. Grass cover strength parameter	36
4.3.2. Influence factor geometrical transition	38

5. Discussion.....	41
5.1. Sensitivity analysis	41
5.1.1. Grass cover strength parameter	41
5.1.2. Erosion rate parameter	43
5.1.3. Flow acceleration method.....	45
5.1.4. Influence factors.....	47
5.2. Model approach	48
5.2.1. Modelling the influence of transitions on grass cover erosion.....	49
5.2.2. Model applicability.....	49
6. Conclusions and recommendations.....	51
6.1. Conclusions.....	51
6.2. Recommendations.....	53
7. References	55
Appendix 1 Wave overtopping tests in Vietnam and the USA	58
Appendix 2 Damage numbers per flow acceleration method	61
Appendix 3 Results hydrodynamic-erosion model	64
Appendix 4 Results cumulative overload method	66

1. Introduction

About 60% of the surface area of the Netherlands is vulnerable for flooding and the vulnerability of the Dutch delta will increase even further due to prospected sea level rise combined with ongoing land subsidence (Ministerie van Infrastructuur en Milieu & Ministerie van Economische Zaken, 2017). Therefore, the challenge remains to protect the inhabitants of the Netherlands and the economic value in the country against flooding.

Regional water authorities are responsible for maintenance of the dikes in their management area. These authorities are also obliged by law to assess the safety of the dikes once per twelve years to determine if a dike section is safe for all failure mechanisms. The introduction of multifunctional flood defences implies the increasing presence of many different types of transitions in dike covers. Despite the presence of all kinds of transitions on Dutch dikes, it is not prescribed by law how the regional water authorities must deal with the transitions. The regional water authorities do not know how the effect of transitions must be considered in the design and safety assessment of dikes.

1.1. Background

One major failure mechanism of dikes is grass cover erosion by wave overtopping. During storms, large waves run-up the waterside slope and, if the wave run-up height exceeds the crest freeboard, the wave overtops on the dike crest and eventually runs-down the landward slope (Schüttrumpf, 2001). The flow accelerates along the landward slope, until it reaches an equilibrium velocity (Van Bergeijk et al., 2019). The hydraulic loads that are exerted on the grass cover on dike crests and landward slopes are mainly determined by velocities and layer thicknesses of overtopping waves. The grass cover can withstand large deformations without shearing of the grass revetment due to the elastic character of grass. However, the repetition of the hydraulic loads by wave overtopping can eventually lead to rupture of the grass revetment ('t Hart et al., 2016).

Tests with wave overtopping simulators have shown that grass-covered dikes are not able to withstand high flow velocities of overtopping waves (Van der Meer et al., 2010). From the tests is also concluded that grass cover erosion typically starts at weak spots, for example at damaged parts of the grass cover or at transitions and obstacles. The experiments have shown that erosion at transitions and obstacles differs with respect to erosion at horizontal parts and slopes, which is related to both load increases and grass strength decreases (Hoffmans et al., 2018). In case of a revetment transition, from a smooth to a rough surface, turbulence increases near the transition. Similarly, objects that interrupt the flow cause a redistribution of forces, resulting in turbulence around the objects. Geometrical changes, for example from a slope to a berm, cause a flow jet and result in increasing hydraulic loads. Furthermore, transitions frequently have got an indirect influence on the grass cover strength due to damage and a decreased grass quality near the transition (Van Steeg, 2015).

Calle and Van der Meer (2012) made a first attempt for identifying the most problematic transitions in flood defences. An expert meeting resulted in ten transitions that were identified as most problematic. The high number of transition types that were considered by Calle and Van der Meer (2012) were rearranged to limit the number of transitions in dikes in general (Van Steeg and Van Hoven, 2013a) and specifically for transitions in grass revetments (Van Steeg and Van Hoven 2013b). The latter categorization was elaborated and distinguishes transitions on four levels: (1) loads, (2) orientation, (3) slope discontinuity and (4) height- and

roughness difference (Van Steeg, 2014). This resulted in a categorization including sixteen transition types.

Computational models were developed to improve understanding of grass cover erosion by wave overtopping. Examples are the cumulative overload method and the hydrodynamic-erosion model.

The cumulative overload method (Hoffmans et al., 2018) compares the overtopping flow velocities to the critical flow velocity of the grass cover. The cumulative overload method results in a damage number (D) for the simulated overtopping waves. Comparison of the calculated damage numbers with the damage categorization results in a safety assessment of the stability of the grass cover for wave overtopping. The categories for damage numbers are empirically derived from the Dutch wave overtopping tests at the Vechtdijk: no damage, first damage, various damages and failure (Van der Meer et al., 2015). However, it is disputable if the derived damage categories are representative for all type of dike characteristics.

The cumulative overload method requires an acceleration factor (α_a) for the initial overtopping flow velocity to calculate the damage number at a specific distance along the dike profile. The common method is to determine the acceleration factor from a graph based on the slope angle and the distance along the landward slope (Van der Meer et al., 2015). This means that a constant acceleration factor is applied to all wave volumes. This approach is a simplification of the iterative method for flow acceleration by Schüttrumpf and Oumeraci (2005) in which the flow acceleration is determined as function of the initial velocity and layer thickness of overtopping waves.

The hydrodynamic-erosion model combines a model for overtopping flow velocities with an erosion model. The analytical model by Van Bergeijk et al. (2019) results in maximum overtopping flow velocities along dike crests and landward slopes per simulated wave volume. Subsequently, the flow velocities along the dike profile are used as input for the erosion model by Hoffmans (2012) to calculate the cumulative erosion depths (d) along the dike profile for all simulated wave volumes.

1.2. Problem definition and research objective

The required height of a dike crest is determined as the sum of the design water level and the required free crest height. The required free crest height depends on the maximum mean overtopping discharge that is allowed during normative storm events. To save the costs of dike reinforcement projects, the required free crest height should be limited. Therefore, from an economic perspective, a high maximum allowed overtopping discharge is desired. The computational erosion models can be used to calculate the maximum allowed overtopping discharge for which the dike is safe for grass cover erosion by wave overtopping. Despite transitions are identified as weak spots for this failure mechanism, a general approach to include the effects of transitions on grass cover erosion in the computational models is not yet provided.

The cumulative overload method includes a load factor (α_M) and a strength factor (α_S) to account for increases of the hydraulic load and decreases of the grass cover strength, respectively. Theoretical formulas are provided to determine load factors for transitions to account for roughness differences, slope angle changes and concentrated flows along objects (Hoffmans et al., 2018). The cumulative overload method is applied to derive representative load factors for revetment transitions, geometrical transitions and objects for the wave

overtopping tests at Nijmegen and Millingen (Van Hoven et al., 2013). The derived load factors are compared, which shows that the derived load factors are variable between the test sections. An additional analysis shows that the derived load factors for geometrical transitions do not agree with the theoretical values (Hoffmans, 2015). So, the existing studies show that the application of the cumulative overload method for a limited number of wave overtopping tests did not result in generalizable load factors for a specific transition type.

The hydrodynamic-erosion model does not yet consider load and strength factors to include the effects of transitions on grass cover erosion. However, this model can be further adapted to account for load increases and strength transitions near transitions. Van Bergeijk et al. (2019a) describes three formulations for the turbulence intensity parameter r_0 to account for the hydraulic load changes near transitions. The formulations were applied to the Afsluitdijk. From the model analysis is concluded that the modelled erosion depths are sensitive to erosion parameters like r_0 and therefore it is recommended to improve the formulations for those parameters to make the model generally applicable.

Bomers et al. (2018) applied a CFD-simulation to the hydrodynamic-erosion model to study the influence of a road on top of a dike on grass cover erosion. Furthermore, Aguilar-López et al. (2018) used CFD-simulations for a probabilistic assessment method to determine the influence of an asphalt road on top of a dike to the probability of failure locally and for an entire dike profile. The computation time of a CFD-simulation of a single wave is relatively large. Therefore, it is not practical to use such CFD-simulations to reanalyse the erosion process at transitions during wave overtopping tests. To calibrate influence factors for transitions in grass covers using the results of wave overtopping tests, it is therefore more appropriate to use erosion models with a relatively short computational time.

Different models are available for analysing grass cover erosion by wave overtopping. Those models include parameters that can be adapted to account for the influences of transitions on grass cover erosion. However, representative values that are generally applicable for all transition types are not available yet. Besides, no general approach is available to account for the influence of transitions on grass cover erosion.

This leads to the main objective of this research, which is stated as follows:

To set up a general approach for the model analysis of the effects of transitions on grass cover erosion and to derive representative influence factors for a transition type.

To meet this research objective, the following research questions will be addressed:

- 1. Which transition types are most relevant for calibration of load and/or strength parameters using the hydrodynamic-erosion model and the cumulative overload method?*
- 2. What are calibrated values of the turbulence intensity parameter (r_0) to represent the load increase at the geometrical transition at the landward toe using the hydrodynamic-erosion model?*
- 3. What are calibrated values of the load factor (α_M) to represent the load increase at the geometrical transition at the landward toe using the cumulative overload method?*

1.3. Method

Four problematic transition types for grass cover erosion by wave overtopping are selected based on the findings from wave overtopping tests and the opinions of four experts. A two-step approach is developed to derive factors from wave overtopping tests that represent the influence of the transition on erosion of the grass cover. First, the minimum strength of the grass cover is determined based on no damage at the slope and next the influence of the transition is calibrated considering the damage at the transition.

The model approach is applied to one problematic transition type: the geometrical transition at the landward toe. Two erosion models are considered: the hydrodynamic-erosion model and the cumulative overload method. Both erosion models are applied to seven test sections where grass cover erosion was observed at the geometrical transition.

Representative values for the threshold flow velocity U_t and the critical flow velocity U_c are derived based on no damage at the landward slope using the hydrodynamic-erosion model and the cumulative overload method, respectively. Subsequently, the turbulence intensity parameter r_0 is calibrated using the observed erosion depth at the transition. Similarly, the grass cover strength is expressed in terms of the critical flow velocity U_c based on the comparison of the modelled damage numbers for different critical flow velocities to the observed damage number. The effect of the transition is determined by calibration of the load factor α_M with respect to the observed damage number at the transition. Three approaches are used in the cumulative overload method to account for the acceleration of overtopping waves along the landward slope. Finally, the model analysis results in values for r_0 and α_M that are representative for the load increase at the geometrical transition for each test section.

1.4. Report outline

- Chapter 2** This chapter contains an analysis of problematic transition types for grass cover erosion according to expert judgement and the outcomes of wave overtopping tests. This chapter results in the selection of one problematic transition type and seven test sections that are included in the model analysis. The characteristics and test results are described in detail per test section.
- Chapter 3** This chapter describes the model approach. It is described how the hydraulic boundary conditions for overtopping wave volumes are derived. Both erosion models, the hydrodynamic-erosion model and the cumulative overload method, are introduced. Besides, it is described how the representative grass cover strength is determined and how the influence factors for the transitions are calibrated.
- Chapter 4** The results of the analysis of the influence of transitions on grass cover erosion using the hydrodynamic-erosion model and the cumulative overload method are provided in this chapter.
- Chapter 5** This chapter contains the discussion of the research method and the results.
- Chapter 6** The conclusions and recommendations from this research are presented here.

2. Influence of transitions on grass cover erosion

From wave overtopping tests was concluded that erosion at transitions shows a different behaviour compared to erosion along dike crests, slopes and berms (Hoffmans et al., 2018). In case of a revetment transition, from a smooth to a rough surface, turbulence increases near the transition. Similarly, objects that interrupt the flow cause a redistribution of forces, resulting in turbulence around the objects. Geometrical changes, for example from a slope to a berm, cause a flow jet and result in increasing hydraulic loads. Next to the increasing hydraulic loads, the strength of the grass is often reduced near transitions.

A categorization of transition types in grass revetments is provided by Van Steeg (2014). Transitions are categorized based on four characteristics: (1) the hydraulic load zone, (2) orientation, (3) inclination change and (4) height and roughness differences (Figure 2.1). Because this research focuses on wave overtopping, the part of the categorization that regards to transitions in the wave impact zone is not further included. The grey categories (T4, T10, T11 and T12) indicate transition types that are not frequently found in practice.

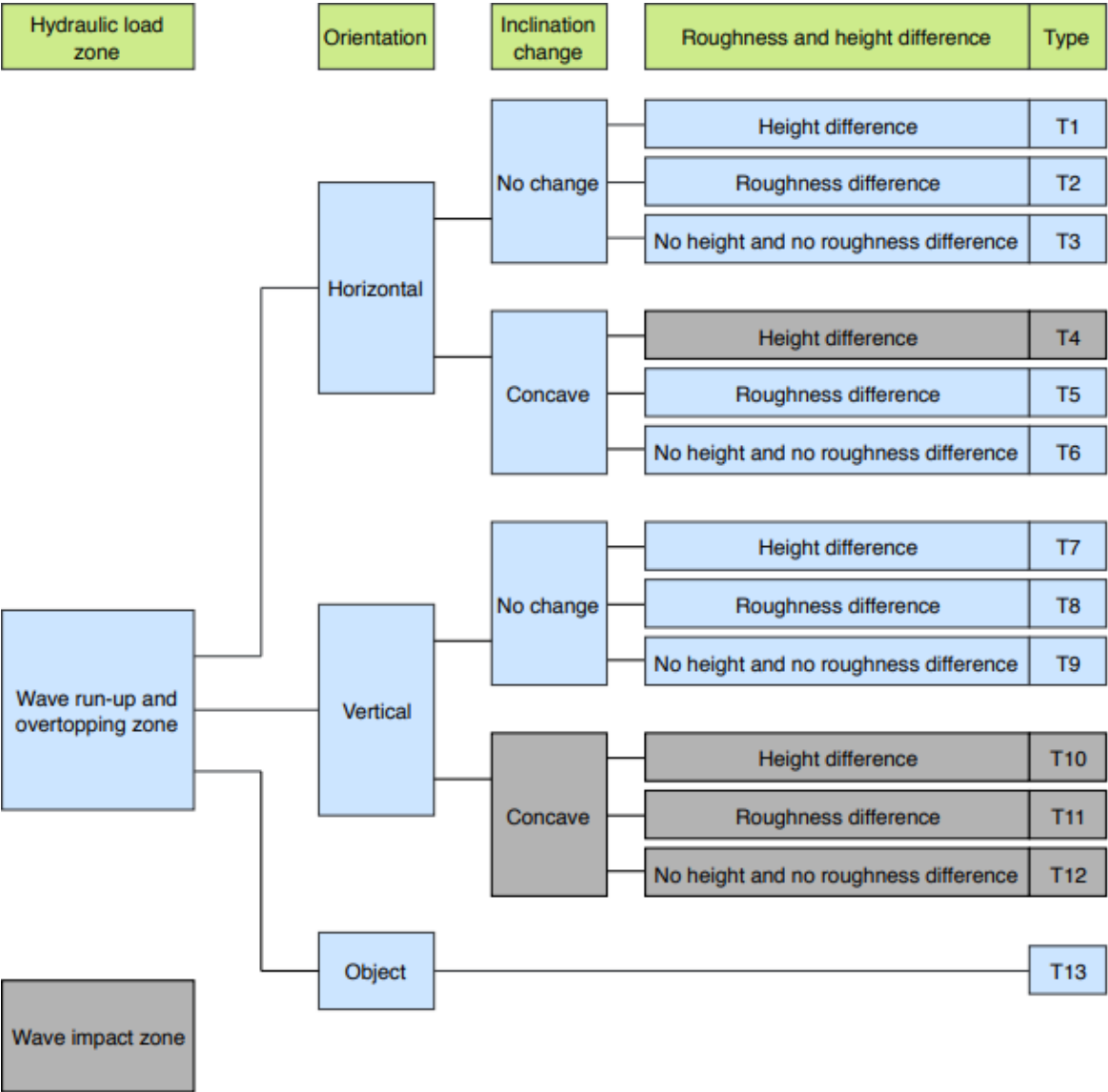


Figure 2.1 Categorization of transition types. Overview adapted from Van Steeg (2014).

This chapter provides an analysis of the influence of different transition types on grass cover erosion by wave overtopping. Section 2.1. includes an analysis of expert judgment and wave overtopping tests to determine problematic transition types for grass cover erosion. One of the problematic transition types is selected for the model analysis using both the hydrodynamic-erosion model and the cumulative overload method. Subsequently, the model cases are introduced and described in Section 2.2.

2.1. Problematic transition types

Problematic transition types for grass cover erosion by wave overtopping are determined based on expert judgment (Subsection 2.1.1.) and based on overtopping tests with transitions (Subsection 2.1.2.). The outcomes of both parts are aggregated and result in a selection of transition types that could further be analysed using erosion models (Section 2.1.3.).

2.1.1. Expert judgment

Four experts were asked to participate in an individual interview to discuss which transition types are problematic regarding its influence on the erosion resistance of the grass revetment. The experts were selected based on their background in the field of wave overtopping, grass revetments and transitions in dikes. The number of experts was supposed to be limited, due to time constraints. Four experts, covering perspectives from research, test operation and flood defence management, were selected. Those experts are introduced below.

1. *André van Hoven – Deltares:*

André van Hoven is an advisor in geo-engineering at the Dutch research institute Deltares. Since 2008, he was involved in research programmes SBW (Strength and Loads on Water Defences) and WTI 2017 (Research and Development of Flood Defence Assessment Tools) as project leader. Van Hoven is therefore familiar with wave overtopping tests and the problematic role of transitions regarding the erosional resistance of grass revetments.

2. *Paul van Steeg – Deltares:*

Paul van Steeg is an expert in coastal structures at Deltares. From a research perspective, Van Steeg is involved in a project regarding the vulnerability of transitions in grass slopes from 2013 to present. Results of this research project are a categorization of transition types (Van Steeg, 2014) and an analysis of transition types that are most important for further research, according to representatives from regional water authorities (Van Steeg, 2015). This shows the expertise of Van Steeg with respect to the problematic influence of different transition types on grass cover erosion.

3. *Roy Mom – Infram-Hydren:*

Roy Mom works as an advisor at Infram-Hydren, which is a Dutch company involved in innovation and research in hydraulic engineering. Since 2007, he was involved during the wave overtopping tests and has been co-author of the factual reports. Later on, Mom has served as project leader of the tests. Therefore, Mom has got expertise regarding transition types that appeared to be most vulnerable for grass cover erosion during the wave overtopping tests.

4. *Jaap Bronsveld – Waterschap Rivierenland & STOWA:*

Jaap Bronsveld works as an expert in flood defences at the regional water authority Waterschap Rivierenland. Besides, he is “*grasregisseur*” (lit. grass director) at STOWA, which

is the central organization for sharing knowledge between the regional water authorities. Due to his role at both organizations, Bronsveld frequently has to deal with the complications of transitions during the safety assessment and reinforcement projects of flood defences.

In the interviews, a distinction is made between primary and secondary effects that take place at transitions following Van Steeg (2015). Primary effects relate to the direct influence of a transition on the hydraulic load or revetment strength. These primary effects are (i) increase of the load at roughness differences due to turbulence, (ii) increase of the load at geometrical transitions and (iii) increase of the load due to flow disturbance by objects. Secondary effects relate to management issues like inadequate maintenance and damaged grass revetments, for example due to tire tracks near a road.

Multiple questions were asked to discuss with the experts which transition types are problematic regarding grass cover erosion. The core questions of the interviews are listed below:

1. *Which transition types have got the largest primary effects?*
2. *Which transition types have got the largest secondary effects?*
3. *Which issues regarding maintenance of transitions occur in practice?*
4. *Which transition types are most problematic regarding to grass cover erosion?*

The experts often expressed problematic transition in terms of objects, for example a transition with an asphalt road or a transition with stairs. Therefore, the outcomes of the interviews were arranged according to the categorization in Van Steeg (2014). The similarities and differences between the expert interviews were compared to conclude which transition types are most problematic for grass cover erosion according to expert knowledge. The main findings are discussed below.

Considering transition types with the largest primary effects, two transition types were mentioned most frequently by the experts. Those are transitions from a smooth to a rough surface (type T2) and geometrical transitions (type T6). Transition type T5 considers a roughness difference and also a geometrical transition and is therefore a combination of both types T2 and T6. Van Hoven explained that, according to theory, the primary effect is largest at a transition from a smooth to rough surface, for example at the transition from an asphalt road to a grass revetment. The roughness difference between both surface types causes a sudden jump of the shear stress, resulting in an increased hydraulic load near the transition. Mom stated that interruption of the grass sod is a dominant factor regarding a decreased grass cover strength at T2- and T5-transitions. Mom and Van Steeg both explained that damage was often observed at the landward toe (type T6) during the wave overtopping tests. Both experts emphasized that the landward toe is a weak spot for erosion due to two processes. First, the flow accelerates along the slope and therefore the largest flow velocity is observed near the landward toe and, second, the geometrical transition results in a jet of the overtopping flow.

The experts provided several examples where secondary effects play a major role regarding grass cover erosion. Bronsveld explained that the secondary effects often take place at locations that are frequently used by humans. Grass covers near roads (types T2 and T5) and stairs (types T7 and T8) are often damaged. Van Steeg stated that tire tracks and sheep tracks probably have a significant influence on the erosion resistance of grass covers. Van Hoven explained that secondary effects of transitions can also be related to the construction of the transition. For example, stairs are often constructed directly on top of a sand layer. The

erosion resistance of sand is negligible compared to clay, resulting in vulnerable spots for grass cover erosion near stairs and also near roads. Besides, Mom explained that the grass cover is often not well-connected to the stairs, resulting in bare spots with a low resistance to erosion.

Secondary effects are often related to issues regarding maintenance at transitions. Bronsveld mentioned three secondary effects due to the same cause. He explained that soil subsidence does frequently occur near founded objects, like pumping stations and sheet piles. The height difference caused by soil subsidence around objects impede mowing of the grass revetment and results in a lower grass quality and a lower erosion resistance. Furthermore, a height difference causes shadow effects which also affect the quality of the grass sod. This means that irregular constructions (types T1 and T7) at dikes result in challenges for the dike manager. Bronsveld further emphasized that, from a maintenance perspective, it is of interest to know how to strengthen a certain transition to guarantee the stability of the grass revetment near the transition during normative storm conditions. This means that dike managers are mainly interested in constructive solutions and less in model results.

All experts provided their opinion regarding most problematic transition types regarding grass cover erosion and they used various arguments to substantiate their opinions. Van Hoven considered the costs of solving the issues with certain transition types to formulate two problematic transition types. Van Hoven explained that the transition from asphalt roads to grass revetments (types T2 and T5) and transitions at buildings (types T1 and T7) are probably most problematic. For both transition types yields that conflicting interests play a major role. Asphalt roads on top of dikes should be wide enough to prevent tire tracks near the road, but the width of the road should also be limited to limit the dike reconstruction costs. Similarly, buildings in dike should be removed to limit the number of transitions and thus to limit the number of weak spots. However, it is not feasible to buy off the house owners to remove their buildings.

Van Steeg explained that he analysed the opinions of Dutch dike managers regarding problematic transition types in one of his researches. The report *Monitoring en fysieke modelproeven overgangen met grasbekledingen 2016-2020* (Van Steeg, 2015) therefore describes the expert opinion of Van Steeg regarding problematic transition types regarding grass cover erosion. In the analysis is concluded that it is prioritized to test horizontal (T2) and vertical (T8) transitions at the seaward slope by wave run-up simulations and to study the geometrical transition at the landward toe (T6) by wave overtopping tests. Van Steeg further expects that the findings of those wave run-up tests are also representative for the influence of the transition type on erosion by wave overtopping.

Bronsveld stated that first damage is expected near transitions at which human activity often takes place (T2, T5, T7 and T8), because of the decreased erosion resistance of the grass cover due to secondary effects. Besides, Bronsveld explained that transitions with height differences (T1 and T7) are generally problematic, because hindrance during maintenance and shadow effects result in a decreased grass cover strength. Mom pointed out that the geometrical transitions (T5 and T6) and flows along stairs (T7 and T8) are normative for the erosion resistance of the grass revetment. Besides, Mom argued that transitions types where primary as well as secondary effects take place, for example at stairs, are most problematic for grass cover erosion. Finally, all experts agree that the secondary effects are often dominant for erosion compared to primary effects. The outcomes of the expert interviews are summarized in Table 2.1. Six transition types are identified as problematic: types T1, T2, T5, T6, T7 and T8.

Table 2.1 Overview of problematic transition types according to four experts. For each transition type is determined if large primary and secondary effects are expected and if maintenance issues occur in practice.

Type	Primary effects	Secondary effects	Maintenance issues	Problematic transition types
T1			X	X
T2	X	X		X
T3				
T5	X	X		X
T6	X			X
T7		X	X	X
T8		X		X
T9				
T13				

2.1.2. Wave overtopping tests and transitions

Since 2007, multiple tests with wave overtopping simulators have been performed in the Netherlands, Belgium, Vietnam and the United States. The wave overtopping simulator was developed in the Netherlands for simulating overtopping waves on in-situ test sections to develop understanding of the behaviour of the grass revetment during wave overtopping (Van der Meer et al., 2006). The wave overtopping simulator is used to release a number of wave volumes that are representative for normative storm events. The Dutch wave overtopping simulator (Figure 2.2a) was used during wave overtopping tests at nine locations in the Netherlands and two locations in Belgium from 2007 to 2015. A second wave overtopping simulator was developed in Vietnam (Figure 2.2b) and was used to test representative, Vietnamese grass types from 2009 to 2012. A wave overtopping facility was constructed at Colorado State University in the United States. This fixed-in-place overtopping simulator (Figure 2.2c) was used to test prepared grass mats at the facility (Thornton et al., 2010).

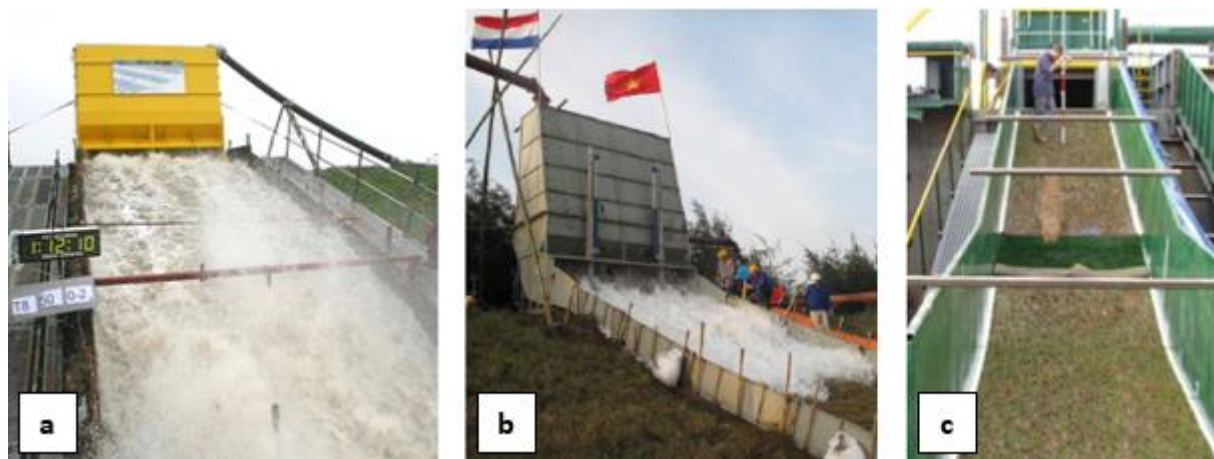


Figure 2.2 Wave overtopping simulators in a. the Netherlands, b. Vietnam and c. the United States. Figures retrieved from a. ComCoast (2007), b. Le et al. (2012) and c. Hughes et al. (2013).

Various test conditions and transition types have been considered during the wave overtopping tests. Reports generally provide specific information per test location regarding test conditions, site characteristics and observed erosion. However, a summary of the wave overtopping tests that are performed worldwide is not available. Therefore, this subsection provides an overview of the wave overtopping tests to investigate which range of test conditions and which site characteristics were considered. Also, an inventory of the data that

is available per test section was made. The overview in this subsection is limited to tests in the Netherlands and Belgium. Appendix 1 provides a similar overview of the wave overtopping tests in Vietnam and the United States.

The Dutch wave overtopping simulator was used at seven locations in the Netherlands as part of the research programme SBW (*Strength and Loads on Water Defences*) from 2007 to 2012. Additionally, wave overtopping tests at two locations were performed in 2013 as part of the WBI 2017 framework. This framework is the current legal safety assessment of primary flood defences in the Netherlands. The Dutch wave overtopping simulator was also used during tests in Belgium in 2010 and 2015.

The wave overtopping simulator is placed on top of the dike crest and each test section is 4 m wide. During the tests, the simulator releases a number of wave volumes, causing an overtopping flow along the dike crest, the landward slope and the berm. The simulated wave volumes are determined using a probability exceedance function and depend on the significant wave height and wave period for each mean overtopping discharge. The simulated mean overtopping discharges vary from 0.1 to 75 l/s/m and each simulation lasts 6 hours. Intervals of 2 hours of testing are used to describe the erosional damage along the test section and to capture erosion using photos. If the stop criterium, an erosion depth of 30 cm, is reached, the wave overtopping test is terminated.

Van der Meer (2014) provides a comprehensive overview of the wave overtopping tests in the Netherlands and Belgium. This overview summarizes the characteristics of each test, for example in terms of simulated mean overtopping discharges, while also pictures of erosion are provided for each test section. More detailed information regarding tests with the Dutch wave overtopping simulator are provided in a factual report for each test location. Those factual reports include a more detailed description of the development of erosion during the tests, while also measurements and photos are provided.

For each test, the hydraulic test conditions are specified in terms of the significant wave height (H_S) and the wave period (T_P), while the characteristics of the test sections are expressed in terms of the steepness of the landward slope ($\cot(\alpha)$) and the revetment type (Table 2.2).

The wave regimes are defined in terms of wave height (H_S) and wave period (T_P). Three regimes were applied during the tests: a river regime ($H_S = 1.0$ m; $T_P = 4.0$ s), a sea regime ($H_S = 2.0$ m; $T_P = 5.7$ s) and a severe sea regime ($H_S = 3.0$ m; $T_P = 6.9$ s). These are assumed to be representative regimes that cover the range of hydraulic loads during normative conditions for Dutch dikes. The sea regime was applied most frequently in the Netherlands, at 21 sections, while the river regime (four sections) and the severe sea regime (one section) were considered a few times. The wave regimes that were used during wave overtopping tests in Belgium are comparable to Dutch river regimes. A regime with large waves ($H_S = 3.0$ m and $T_P = 6.2$ s) was applied to one test section in Belgium.

Another condition for the wave overtopping tests is the steepness of the landward slope. The flow will accelerate more on a steep slope compared to a mild slope. So, the critical flow velocity, which represents the strength of the grass revetment, is more likely to be exceeded in case of a steep slope compared to a mild slope. The steepness of the landward slope is therefore a parameter with a significant influence regarding erosion of the grass revetment.

Table 2.2 Overview test conditions of wave overtopping tests in the Netherlands and Belgium including the wave height H_s , the wave period T_p and the steepness of the landward slope $\cot(\alpha)$. The revetment type is classified according to VTV 2006 (Ministerie van Verkeer en Waterstaat, 2007).

Location – year (reference)	Section	H_s [m]	T_p [s]	$\cot(\alpha)$ [-]	Revetment type
<i>The Netherlands</i>					
Delfzijl – 2007 (Akkerman et al., 2007)	1	2.0	5.7	3.0	Grass (type w1)
	2	2.0	5.7	3.0	Grass (reinforced)
	3	2.0	5.7	3.0	Bare clay
Boonweg – 2008 (Bakker et al., 2008a)	1	2.0	5.7	2.9	Grass (type w2)
	2	2.0	5.7	2.9	Grass (type w2)
	3	2.0	5.7	2.9	Grass (type h3)
	4	2.0	5.7	2.9	Grass (type w2)
St. Philipsland – 2008 (Bakker et al., 2008b)	1	2.0	5.7	2.4	Grass (type h3)
Kattendijke – 2008 (Bakker et al., 2008b)	1	2.0	5.7	3.0	Grass (type h3)
	2	2.0	5.7	3.0	Grass (type h3)
	3	2.0	5.7	3.0	Elastocoast
	4	2.0	5.7	3.0	Open rock asphalt
Afsluitdijk – 2009 (Bakker et al., 2009)	1	2.0	5.7	2.6	Grass (type w2)
	2	2.0	5.7	2.6	Grass (type w2)
	3	2.0	5.7	2.6	Grass (type w2)
Vechtdijk – 2010 (Bakker et al., 2010)	1	2.0	5.7	2.8/7.5/3.8	Grass (type w2)
	2	2.0	5.7	4.8	Grass (type w2)
	3	1.0	4.0	4.8	Grass (type w2)
	4	3.0	6.9	4.8	Grass (type w2)
Tholen – 2011 (Bakker et al., 2011)	1	2.0	5.7	3.0	Grass (type h1)
	2	2.0	5.7	2.4	Grass (type r/h1)
	3	2.0	5.7	2.4	Grass (type w2/w3)
	4	2.0	5.7	2.4	Grass (type w2/w3)
Nijmegen – 2013 (Bakker et al., 2013)	1	1.0	4.0	5.5/1.9	Grass (type h2)
	2	1.0	4.0	2.7	Grass (type h1/h2)
Millingen – 2013 (Bakker et al., 2013)	1	1.0	4.0	3.5	Grass (type h2)
<i>Belgium</i>					
Tielrode – 2010 (Peeters et al., 2012)	1	0.75 & 1.0	3.1 & 3.6	2.5	Grass (type h2/h3)
	2	0.75 & 1.0	3.1 & 3.6	2.5	Grass (type r/h2)
	3	0.75 & 1.0	3.1 & 3.6	3.5	Grass (type h2)
	4	3.0	6.2	2.5	Grass (type h2/h3)
Wijmeers – 2015 (Pleijter et al., 2018)	1	0.4 & 1.3	2.5 & 4.6	1.9	Grass (type h2)
	2	1.2	4.4	1.9	Grass (type r)

The steepness of the landward slope is expressed in terms of $\cot(\alpha)$, which is the cotangent of the landward slope angle α . Table 2.2 shows that $\cot(\alpha)$ ranges from 1.9 (steep slope) to 4.8 (mild slope), while $\cot(\alpha) = 3.0$ was applied most frequently. At the Vechtdijk (section 1), the landward slope consisted of three parts with different slope angles due to the presence of a maintenance road halfway the slope. The landward slope at Nijmegen (section 1) consisted of a mild upper slope and a steep lower slope.

The governing factor for the erosion resistance of a grass revetment is the root density (Young, 2005). The critical flow velocity of a grass revetment is therefore high in case of a dense root structure. The root density of grass depends on the grass type, which means that the grass type is a major determinant for the critical flow velocity. The grass type is therefore a test condition with a major influence on the erosion process.

Table 2.2 shows the revetment type per test section. The grass type is classified according to VTV 2006 (Ministerie van Verkeer en Waterstaat, 2007). VTV 2006 provides a categorization of grass types based on the vegetation type and the root density. Vegetation types are identified by capitals P (pioneer vegetation), W (meadow grass), R (rough hay grass) and H (hay grass). The root density is identified by numbers 1 (poor density), 2 (moderate density) and 3 (good density).

Figure 2.3 provides an overview of the number of wave overtopping tests per grass category. Pioneer vegetation (≤ 4 years) is not tested with the wave overtopping simulator. Meadow type W2 (moderate sod quality) is tested frequently, while tests with a good or a poor sod quality are scarce. Each hay type (or combination of two hay types) was tested at one to four test sections.

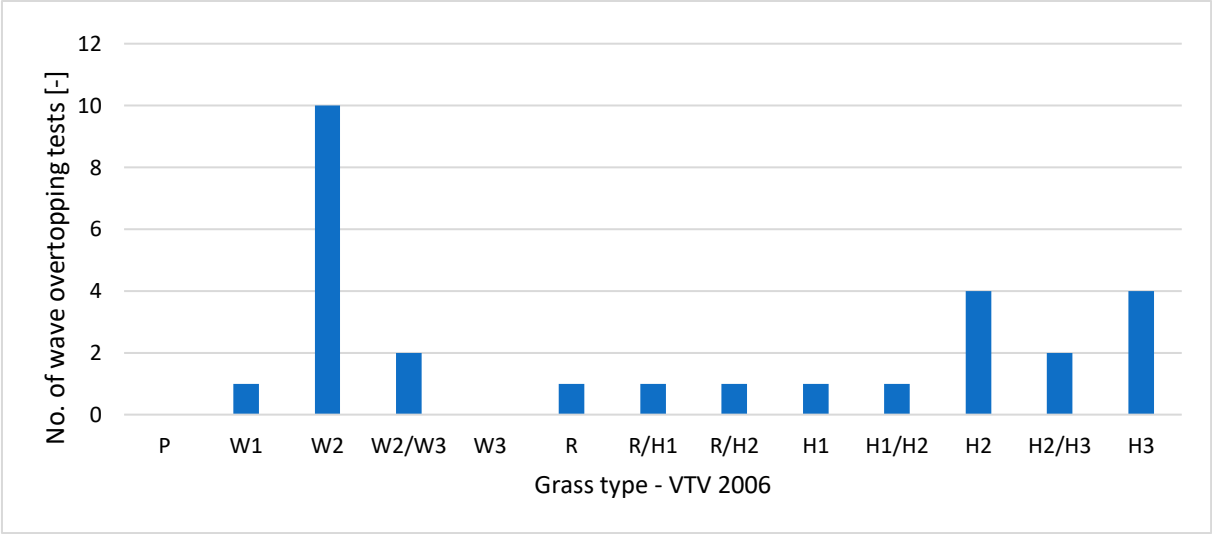


Figure 2.3 Number of wave overtopping tests per VTV 2006 grass type.

Despite the wave overtopping simulator was designed for testing the erosional resistance of grass revetments, the simulator is also used to test other types of dike revetments. During the first tests at Delfzijl in 2007, a test section with a grass reinforcement system and a test section with bare clay were considered. Besides, two hard revetments, Elastocoast and open rock asphalt, were tested at Kattendijke in 2008.

Table 2.3 provides an overview of the data that were obtained during the wave overtopping tests in the Netherlands. Data regarding the erosion depth along the test sections were visualized using different techniques. The factual report of a wave overtopping experiment generally includes a description of observed damage in terms of erosion surfaces and depths, resulting from manual measurements. For each test, these damage descriptions are supported by images from digital camera recordings and photographs. For test at Delfzijl (2007) and Nijmegen & Millingen (2013), 3D erosion profiles were composed by using laser scanners.

Table 2.3 Overview erosion data and flow data of wave overtopping tests in the Netherlands.

	Delfzijl (2007)	Boonweg St. Philipsland Kattendijke (2008)	Afsluitdijk (2009)	Vechtdijk (2010)	Tholen (2011)	Nijmegen Millingen (2013)
<i>Erosion data</i>						
Digital camera recordings	X	X	X	X		X
Photographs	X	X	X	X	X	X
Manual measurements	X	X	X	X	X	X
3D patterns	X					X
<i>Flow data</i>						
Flow velocity			X	X	X	X
Front velocity	X	X	X	X		X
Layer thickness	X	X	X	X	X	X
Overtopping duration		X				
Turbulence				X		
Void fraction			X	X		
Water pressure						X

The results further show that data regarding different flow characteristics are available. The layer thickness was measured during each wave overtopping test, while also measurements of the flow velocity and/or front velocity of overtopping waves were obtained. Also, overtopping durations, turbulence, void fractions and water pressures were measured at some locations.

Erosion data was obtained during the tests at Tielrode (2010) and Wijmeers (2015) in Belgium. Photographs and manual measurements of erosion are available in the factual reports for both tests. During the tests at Wijmeers, also flow data were captured. The data consist of measurements of layer thicknesses, flow velocities and water pressures.

The factual reports of the wave overtopping tests in the Netherlands and Belgium were also studied to make an overview of the transitions that were tested. The transition types were arranged according to the categorization of transition types by Van Steeg (2014). For each transition type and test section was determined if the tested transition could possibly be included in the model analysis with the cumulative overload method and the hydrodynamic-erosion model. Different considerations were made to determine if a certain tested transition is suitable to include in the analysis with the erosion models. Two major requirements for inclusion of a test in the analysis were (1) that erosion was observed at the transition and (2) that the first damage took place at the transition. Furthermore, the grass cover at a certain test section should not be damaged before the wave overtopping test started and sufficient data regarding the operation and results of the wave overtopping test should be available.

Table 2.4 provides an overview of the transition types that were subjected to wave overtopping tests in the Netherlands and Belgium. A description of the transition type is given and remarks regarding the suitability for including the transition test as case study for model analysis are provided.

Table 2.4 Overview of tested transition types in the Netherlands and Belgium.

Type	Location	Description	Remarks	Case
T1	Nijmegen 1	Concrete beam (culvert)	No erosion resistance of revetment	No
T1	Nijmegen 2	Concrete block (culvert)	No erosion at transition	No
T2	St. Philipsland 1	Road (asphalt)	-	Yes
T2	Afsluitdijk 2	Road (bricks) at berm	-	Yes
T2	Tholen 1	Road (asphalt) at berm	Initial damage before test	No
T2	Millingen 1	Road (asphalt) at crest	-	Yes
T2	Tielrode 3	Road (asphalt) at crest	-	Yes
T3	Vechtdijk 1	Road (grass blocks) at crest	-	Yes
T3	Vechtdijk 1	Road (grass blocks) at slope	-	Yes
T3	Vechtdijk 2	Road (grass blocks) at crest	No erosion at transition	No
T3	Vechtdijk 3	Road (grass blocks) at crest	No erosion at transition	No
T3	Vechtdijk 4	Road (grass blocks) at crest	No erosion at transition	No
T5	Tielrode 1	Road (asphalt) at landward toe	No erosion at transition	Yes
T5	Tielrode 2	Road (asphalt) at landward toe	No erosion at transition	Yes
T5	Tielrode 4	Road (asphalt) at landward toe	Initial damage before test	Yes
T6	Boonweg 1	Landward toe	Bricks underneath grass revetment	Yes
T6	Boonweg 2	Landward toe	Bricks underneath grass revetment	Yes
T6	Boonweg 3	Landward toe	Erosion starts at slope	No
T6	Boonweg 4	Landward toe	Erosion starts at slope	No
T6	St. Philipsland 1	Landward toe	Erosion related to transition type T2	No
T6	Kattendijke 1	Landward toe	-	Yes
T6	Kattendijke 2	Landward toe	-	Yes
T6	Afsluitdijk 1	Landward toe	-	Yes
T6	Afsluitdijk 2	Landward toe	-	Yes
T6	Afsluitdijk 3	Landward toe	Erosion related to transition type T8	No
T6	Vechtdijk 1	Landward toe	No erosion at transition	No
T6	Vechtdijk 2	Landward toe	No erosion at transition	No
T6	Vechtdijk 4	Landward toe	Erosion starts at slope	No
T6	Tholen 1	Berm	Initial damage before test	No
T6	Tholen 3	Landward toe	Erosion starts at slope	No
T6	Tholen 4	Landward toe	-	Yes
T6	Nijmegen 1	Landward toe	No erosion resistance of revetment	No
T6	Nijmegen 2	Landward toe	Insufficient data wave conditions	No
T6	Millingen 1	Landward toe	No erosion at transition	No
T6	Tielrode 3	Landward toe	No erosion at transition	No
T7	Tholen 3	Fencing	-	Yes
T7	Nijmegen 1	Concrete beam	No erosion at transition	No
T8	Afsluitdijk 3	Stairs	Initial damage before test	No
T8	Tholen 2	Stairs	Initial damage before test	No
T13	Vechtdijk 2	Tree (Ø 0.80 m)	-	Yes
T13	Tholen 3	Pole (0.20 m x 0.20 m)	No erosion resistance of revetment	No
T13	Tielrode 3	Tree (Ø 0.40 m)	No erosion at transition	No

Transition types T1, T2 and T3 regard to horizontal transitions with a height difference, a roughness difference or no height and roughness difference, respectively. Transition type T1 has been tested at two sections in Nijmegen. At one section, the erosion resistance of the semi-hard revetment was negligible, because it existed of loose materials, while no erosion was observed at the second test section. Therefore, both T1-tests do not fit in the model studies. Five tests considered T2-transitions, existing of four asphalt roads and one brick road.

At Tholen, the grass cover was already damaged before the wave overtopping test started, so this test is not suitable to include in the model analysis. However, the four remaining tests with roads (type T2) could be considered in the model analysis. T3-transitions were also tested five times. Those transitions were found at the Vechtdijk at which grass block roads were present. Damage at the T3-transitions (grass-blocks) was only observed at the crest and the slope at the section Vechtdijk 1, so only the first T3-test should be considered in the model analysis.

Transition types T5 and T6 are defined as concave geometrical transitions with and without a roughness difference respectively. Three T5-transitions were tested at Tielrode: an asphalt road was present at the landward toe at three test sections. Erosion was only observed at the third section, which is related to initial damage at the transition at the test section. The three tests with T5-transitions could therefore be compared to compare the erosion resistance at a T5-transition in case of a damaged grass cover with a grass cover without initial damage. Transition type T6 was tested twenty times and is therefore most frequently included in the wave overtopping tests. The landward toe appeared to be a weak spot for grass cover erosion, because first damage did often take place at this transition. Fourteen T6-tests are not suitable to include in the model analysis, for various reasons, which means that only seven tests with T6-transitions are assumed to be representative to include in the model analysis (Table 2.4).

Transition types T7, T8 and T9 regard to vertical transitions with respectively a height difference, a roughness difference or no height and roughness difference. T7- and T8-transitions were both tested twice, while no T9-transitions have been tested (Table 2.4). Two stairs (T8) at the Afsluitdijk and Tholen, appeared to be vulnerable for grass cover erosion, but this was likely related to the initially damaged grass cover along the stairs. Severe erosion was also observed around a fence (T7) at Tholen. No erosion was observed near a raised edge (T7) at Nijmegen.

Transition type T13 refers to objects that are located in the dike profile. The results show that two trees and one pole have been tested. While severe erosion took place around the tree at the Vechtdijk, no grass cover erosion was observed at the three at Tielrode. Severe erosion took place around the pole at Tholen, however, this test is not representative to include in the model analysis, because the erosion resistance of the semi-hard revetment (loose material) was negligible.

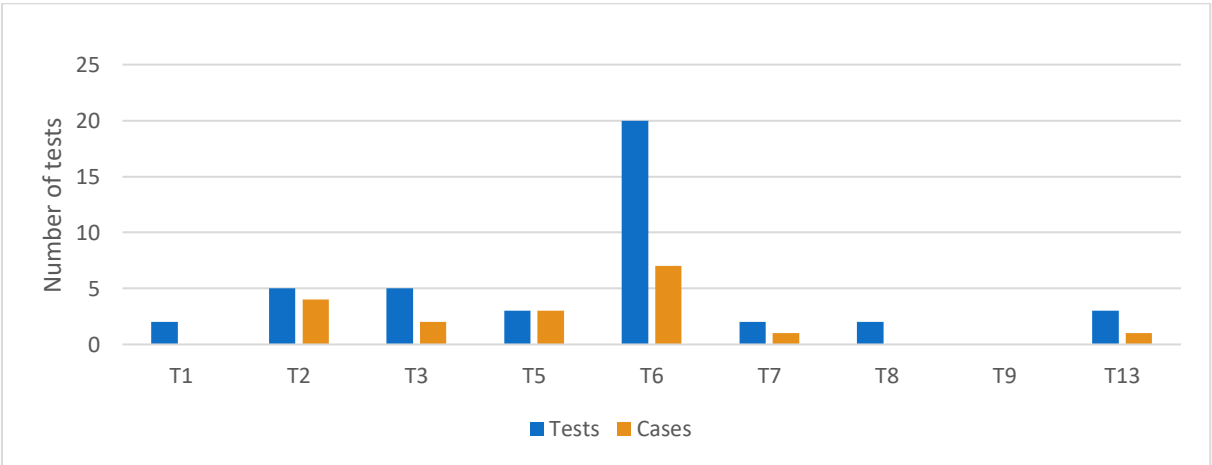


Figure 2.4 Number of tests and appropriate model cases per transition type

An overview of the number of tests per transition type and the number of cases that could be studied in the model analysis is provided (Figure 2.4). It appears that most cases (eights tests) are appropriate to consider for T6-transitions, while one to four tests cases could be used for modelling transition types T2, T3, T5, T7 and T13. No suitable cases regarding types T1, T8 and T9 are available from the wave overtopping tests in the Netherlands, Belgium and Vietnam.

2.1.3. Synthesis

Section 2.1. has provided an analysis of the influence of transition types on erosion of the grass cover as well as an overview of the transition types that were considered during the wave overtopping tests. The transitions types that are problematic according to the experts and the tested transitions are compared in this subsection.

In Subsection 2.1.1., problematic transition types for grass cover erosion, according to four experts, were identified and were compared. The experts agree that both horizontal and vertical transitions can have a severe influence to grass cover erosion. Generally, the experts agreed that transitions with a roughness difference (types T2, T5 and T8) are vulnerable to grass cover erosion, due to interruption of the grass revetment, increasing shear stress and initial damage by human activity at the transition. Furthermore, the experts pointed out that geometrical transitions (types T5 and T6), for example the landward toe, are weak spots for grass cover erosion, due to acceleration of the flow velocity along the slope and also due to increased hydraulic loads. Also, transitions with height differences (types T1 and T7) are assessed as vulnerable for erosion, due to secondary aspects, for example by inadequate maintenance.

Subsection 2.1.2. has provided an overview of the transition types that were tested during wave overtopping simulations in the Netherlands and Belgium and has given a selection of wave overtopping tests that are suitable to include in the model analysis. From the results can be concluded that T1 and T7 are the only transition types for which no appropriate model case is available. One case could be considered to model transition types T13, however, this transition type is not identified as problematic by the experts. Most cases (seven) can be used to analyse T6-transitions, while one to four cases are suitable for modelling the remaining transition types T2, T3, T5 and T7.

Based on both the analysis of the expert opinions and the analysis of suitable cases for the model analysis, four transition types are selected: T2, T3, T5 and T6. Plane, horizontal transitions with and without a roughness difference, types T2 and T3 respectively, should be included in the model analysis. In this way, the influence of the interruption of the grass sod and also the effect of a roughness difference to grass cover erosion could be determined. Geometrical, horizontal transitions T5 and T6, respectively with and without a roughness difference, could also be analysed to determine the influence of an inclination change and also the effects of an interrupted sod and roughness differences.

2.2. Model cases

The model analysis in this thesis is limited to transition type T6: the geometrical transition at the landward toe. Based on the analysis of wave overtopping tests with transitions (Subsection 2.1.2), seven test sections are selected: Boonweg 1 and 2, Kattendijke 1 and 2, Afsluitdijk 1 and 2 and Tholen 4. This section provides a description of the characteristics of the test sections that are used as model cases for the analysis using the hydrodynamic-erosion model and the cumulative overload method.

For all test sections, the dike consisted of a sandy core covered with a clay layer. The erosion resistance of the clay layer at each test section is assessed as moderate (type C3) according to VTV 2006 (Van der Meer, 2014). Other aspects, like grass type characteristics, erosion development during the tests, failure mechanisms and secondary aspects are described per test section.

Boonweg 1 and Boonweg 2:

The grass type at test sections Boonweg 1 and Boonweg 2 is categorized as type w2: meadow grass with a moderate root density. The grass quality according to VTV 2006 is assessed as good (Van der Meer, 2014). Initial damage, consisting of multiple mouse holes and tire tracks, were found at the landward slope at Boonweg 2.

The mean wave overtopping discharges that were applied during the tests are $q_m = 0.1$ l/s/m, $q_m = 1$ l/s/m, $q_m = 10$ l/s/m, $q_m = 30$ l/s/m, $q_m = 50$ l/s/m and $q_m = 75$ l/s/m. No grass cover erosion was observed at the dike crests and landward slopes at both test sections. During the test, it was observed that bricks were located underneath the grass cover after the transition at the landward toe.

At Boonweg 1, the grass cover at the transition started to erode during the simulation with $q_m = 50$ l/s/m. Due to the bricks, the root depth was limited and the roll-up mechanism was observed. This resulted in three gullies with a mean depth of 0.10 m directly after the landward toe. The gullies continued to erode and a number of bricks were washed away during the simulation with $q_m = 75$ l/s/m. The final damage can be described as a large hole with a depth of approximately 0.30 m (Figure 2.5a).

During the tests at Boonweg 2, only slight erosion was observed at the transition during the simulation with $q_m = 50$ l/s/m. The grass cover started to erode at the transition during the simulation with $q_m = 75$ l/s/m. Similarly, to the erosion development at Boonweg 1, the roll-up mechanism was observed and a gully was formed. Next, the gully continued to erode and some bricks were washed away. The depth of the eroded hole is around 0.30 m (Figure 2.5b).



Figure 2.5 Grass cover erosion at the landward toe at test sections (a) Boonweg 1 and (b) Boonweg 2 after wave overtopping tests with a maximum mean overtopping discharge $q_m = 75$ l/s/m. Figures obtained from Van der Meer (2014).

Kattendijke 1 and Kattendijke 2:

The grass type is categorized as hay grass with a good density (h3) and the grass quality is assessed as good for test sections Kattendijke 1 and 2 (Van der Meer, 2014). At section 1,

several mole holes were present at the landwards slope, while tire tracks were present at the landward toe. Initial damage (5 cm deep carves) caused by a manure injector were present on top of the dike crest and at the end of the landward slope at section 2. The mean wave overtopping discharges that were applied during the tests are $q_m = 0.1$ l/s/m, $q_m = 1$ l/s/m, $q_m = 10$ l/s/m, $q_m = 30$ l/s/m, $q_m = 50$ l/s/m and $q_m = 75$ l/s/m.

During the wave overtopping tests at Kattendijke 1, the loose material was washed away, but no severe erosion was observed at the landward slope. However, holes started to erode (roll-up mechanism) at the geometrical transition during the simulation with $q_m = 30$ l/s/m. Erosion of the holes continued and the failure criterium (erosion depth = 0.30 m) was met after the simulation with $q_m = 50$ l/s/m. The test was continued with the simulation with $q_m = 75$ l/s/m and this resulted in severe head-cut erosion. This failure pattern was related to the damage at the maintenance road after the geometrical transition. For the analysis of this transition, it is therefore most appropriate to consider the simulations with $q_m = 30$ l/s/m and $q_m = 50$ l/s/m and to exclude the simulation with $q_m = 75$ l/s/m.

At Kattendijke 2, erosion was observed at the end of the landward slope directly above the geometrical transition. Grass cover erosion started during the simulation with $q_m = 30$ l/s/m at the spot that was damaged by the manure injector. The spot continued to erode during the test with $q_m = 50$ l/s/m and resulted in a final erosion depth of 0.20 m. It is likely that the grass cover strength was locally reduced by the initial damage from the manure injector. It is therefore recommended to exclude the lower part of the slope for deriving the representative strength parameters for the grass cover for Kattendijke 2.

During the tests with $q_m = 30$ l/s/m, the loose material was removed from the berm and grass particles started to wash away. Subsequently, the damage started to develop at the transition to a depth of 0.20 m during the simulation with $q_m = 50$ l/s/m. The damage at the transition at Kattendijke 2 is comparable to the damage at Kattendijke 1. It is difficult to assess to which extent the damage at the transition at Kattendijke 2 is related to the initial damage by the manure injector.

Afsluitdijk 1 and Afsluitdijk 2:

The grass type at Afsluitdijk 1 and 2 is categorized as meadow grass with a moderate root density (w2). The grass quality is assessed as moderate and good for section 1 and section 2, respectively.

The applied mean wave overtopping discharges at Afsluitdijk 1 are $q_m = 1$ l/s/m, $q_m = 10$ l/s/m, $q_m = 30$ l/s/m, $q_m = 50$ l/s/m and $q_m = 75$ l/s/m. First damage was observed at the transition after the simulation with $q_m = 10$ l/s/m. During the test with $q_m = 30$ l/s/m, the damaged spot continued to erode by the roll-up mechanism and resulted in an eroded surface with a length of 2.4 m, a width of 4.0 m and a maximum depth of 0.20 m at the transition. Subsequently, the erosion depth at the transition was 0.35 m after the final simulation with $q_m = 75$ l/s/m. Grass cover erosion at the end of the landward slope started to develop during the simulation with $q_m = 50$ l/s/m. After the final simulation, a gully with a length of 7.8 m over the full slope and with a maximum depth of 0.15 m was observed (Figure 2.6a).

The simulations at Afsluitdijk 2 were limited to $q_m = 1$ l/s/m and $q_m = 10$ l/s/m. Initial damage with a depth of 0.13 m was observed halfway the landward slope. A paved parking spot was present at the berm, 3.0 m after the geometrical transition.



Figure 2.6 Grass cover erosion at the slope and the landward toe at test sections (a) Afsluitdijk 1 and (b) Afsluitdijk 2 after wave overtopping tests with maximum mean overtopping discharges $q_m = 75$ l/s/m and $q_m = 10$ l/s/m. Figures obtained from Van der Meer (2014).

During the simulation with $q_m = 1$ l/s/m, the damaged hole halfway the started to erode. Next, this damaged spot continued to erode in the downward direction during the simulation with $q_m = 10$ l/s/m. This resulted in an erosion depth of 0.13 m at the lower part of landward slope. Besides, erosion at the geometrical transition started to develop during the simulation with $q_m = 10$ l/s/m. The final erosion depth at the transition was around 0.20 m (Figure 2.6b).

Tholen 4:

A meadow grass type with a moderate to good root density was present at section Tholen 4. The quality of the grass cover was assessed as poor (Van der Meer, 2014). Simulated mean overtopping discharges are $q_m = 1$ l/s/m, $q_m = 5$ l/s/m, $q_m = 10$ l/s/m and $q_m = 30$ l/s/m.

Loose materials were washed away during the simulations with $q_m = 1$ l/s/m, $q_m = 5$ l/s/m and $q_m = 10$ l/s/m. However, no severe erosion was observed at the landward slope. During the test with $q_m = 30$ l/s/m, a concentrated seepage flow was developed. This resulted in soil subsidence over a large surface halfway the landward slope.

Grass cover erosion at the landward toe started during the simulation with $q_m = 5$ l/s/m. A number of holes with a depth varying from 0.10 m to 0.20 m were observed at the transition. During the simulation with $q_m = 10$ l/s/m, severe erosion was observed and resulted in failure of the grass cover landward toe. The maximum erosion depth was 0.40 m. The landward toe was protected using geotextiles during the simulation with $q_m = 30$ l/s/m.

3. Model analysis

This chapter provides an overview of the methodology that was set up to model the effects of transitions on grass cover erosion by wave overtopping. The model description (Section 3.1.) shows how the boundary conditions were derived and introduces both erosion models: the hydrodynamic-erosion model and the cumulative overload method. Next, the approach for modelling the effect of transitions on grass cover erosion is explained (Section 3.2.). The application of both erosional models to the geometrical transition at the toe (type T6) is described in Section 3.3. The model analysis shows how the existing erosion models were adjusted to account for increased loads and decreased cover strength at transitions. The velocity threshold (grass cover strength) must first be determined and, subsequently, influence factors can be applied to model load increases or strength decreases at transitions.

3.1. Model description

The model description consists of three parts. It is first described how the distributions of wave overtopping volumes were determined and how the hydraulic boundary conditions were determined for each wave overtopping volume (Subsection 3.1.1.). Next, both models for grass cover erosion are introduced: the hydrodynamic-erosion model (Subsection 3.1.2.) and the cumulative overload method (Subsection 3.1.3.).

3.1.1. Boundary conditions

The wave volumes that were simulated during the wave overtopping tests in the Netherlands and Belgium were determined according to a probability exceedance distribution. Multiple mean overtopping discharges (q_m) were simulated, varying from $q_m = 0.1$ l/s/m to $q_m = 75$ l/s/m. The hydraulic boundary conditions are input for both erosion models and are defined in terms of the flow velocity at the start of the crest ($u_{o,i}$), the layer thickness at the start of the crest ($h_{o,i}$), the overtopping discharge (q_i) and the wave overtopping period ($T_{o,i}$) per individual wave (i).

Wave volumes are randomly generated according to an exceedance function (Equation 1). The scale parameter (a) is calculated using Equation 2. The definitions of the parameters are given in Table 3.1.

$$P_{Vi} = P(V_i \leq V) = 1 - \exp \left[- \left(\frac{V}{a} \right)^{0.75} \right] \quad \text{Equation 1}$$

$$a = 0.84 \cdot q_m \cdot t_{storm} / N_{ow} \quad \text{Equation 2}$$

Table 3.1 Definitions parameters exceedance distribution.

Parameter	Definition	Unit
P_{Vi}	Probability of exceedance volume V by V_i	-
V_i	Wave overtopping volume for wave i	m ³ /m
V	Wave overtopping volume	m ³ /m
a	Scale parameter	-
q_m	Mean overtopping discharge	m ³ /s/m
t_{storm}	Duration of the storm	s
N_{ow}	Number of overtopping waves	-

To generate random wave volumes, it is required to determine the probability that a certain wave volume V_i is selected. This probability of occurrence is determined by using incremental steps for the wave volumes with $\Delta V = 0.001 \text{ m}^3/\text{s}$. Equation 3 shows that the probability of occurrence $P(V_i = V)$ is determined by the difference between the exceedance probabilities of two consecutive wave volumes, $P(V_{i-1} > V)$ and $P(V_i > V)$.

$$P(V_i = V) = P(V_{i-1} > V) - P(V_i > V) \quad \text{Equation 3}$$

Wave volumes are generated using MATLAB-function *randsample*. This function uses an array with wave volumes and an array with corresponding probabilities of occurrence to sample a predefined number of wave volumes according to the exceedance probability function.

Representative storm conditions that were considered during the tests are the significant wave height ($H_s = 2.0 \text{ m}$), the peak period ($T_p = 5.7 \text{ s}$), the total number of waves ($N_w = 4596$), the 2%-wave run-up level ($R_{u,2\%} = 3.98 \text{ m}$), the steepness of the seaward slope ($\cot(\alpha) = 4.0$) and the storm duration ($t_{storm} = 6.0 \text{ h}$). The parameters per mean wave overtopping discharge (q_m) are defined in terms of the free crest height (R_c), the percentage of overtopping waves (P_{ow}), the number of overtopping waves (N_{ow}) and the maximum wave overtopping volume (V_{max}) (Table 3.2).

Table 3.2 Overview conditions per mean overtopping discharge q_m , including the free crest height R_c , the percentage of overtopping waves P_{ow} , the number of overtopping waves N_{ow} and the maximum overtopping volume V_{max} .

	Mean overtopping discharge q_m [l/s/m]						
	0.1	1	5	10	30	50	75
R_c [m]	5.06	3.84	2.98	2.61	2.03	1.76	1.54
P_{ow} [%]	0.2	2.7	11.4	18.9	36.6	47	56
N_{ow} [-]	9	126	525	867	1683	2160	2574
V_{max} [l/m]	769	1222	2018	2697	4707	6387	8278

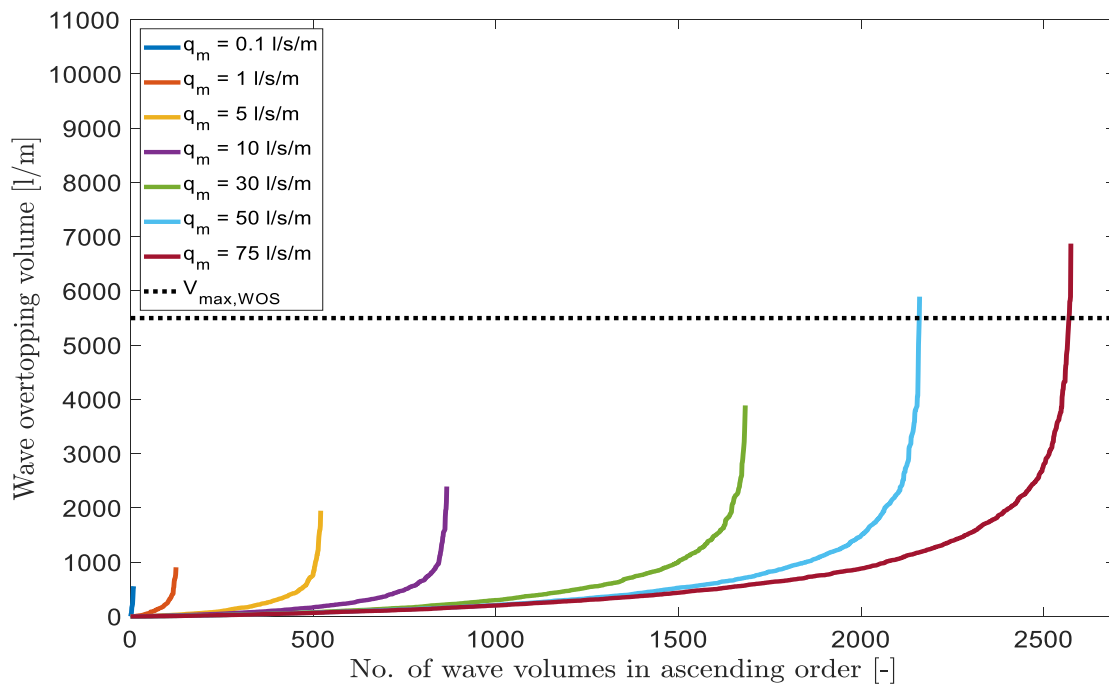


Figure 3.1 Distribution of wave volumes for various mean overtopping discharges q_m together with the maximum wave volume that can be simulated $V_{max,WOS}$.

Figure 3.1 shows the distribution of the simulated wave volumes per mean overtopping discharge q_m . The dotted line shows the maximum wave volume that can be simulated with the Dutch wave overtopping simulator $V_{max,WOS}$.

The hydraulic boundary conditions per simulated wave i are defined in terms of four parameters. The overtopping flow velocity at the start of the crest ($U_{0,i}$) is determined using Equation 4 (Van der Meer et al., 2015). The layer thickness at the start of the crest ($h_{0,i}$) and the overtopping discharge (q_i) per wave are determined using Equation 5 and Equation 6, respectively (Van der Meer et al., 2010). The overtopping period per wave is calculated using Equation 7 (Hughes et al., 2012). Definitions of the parameters are given in Table 3.3.

$$U_{0,i} = 4.5 \cdot V_i^{0.3} \quad \text{Equation 4}$$

$$h_{0,i} = 0.133 \cdot V_i^{0.5} \quad \text{Equation 5}$$

$$q_i = u_{0,i} \cdot h_{0,i} \quad \text{Equation 6}$$

$$T_{o,i} = 3.9 \cdot V_i^{0.46} \quad \text{Equation 7}$$

Table 3.3 Definitions of parameters hydraulic boundary conditions.

Parameter	Definition	Unit
V_i	Overtopping volume for wave i	m ³ /m
$U_{0,i}$	Flow velocity at start of the crest for wave i	m/s
$h_{0,i}$	Layer thickness at start of the crest for wave i	m
q_i	Overtopping discharge for wave i	m ³ /s/m
$T_{o,i}$	Wave overtopping period for wave i	s

3.1.2. Model 1: Hydrodynamic-erosion model

The hydrodynamic-erosion model is a combination of an analytical model for wave overtopping flow velocities along dike crests and landward slopes (Van Bergeijk et al., 2019b) and an erosion model (Hoffmans, 2012). This means that the combined model can be used to model the erosion depth along the dike profile for a number of overtopping wave volumes.

The analytical model of Van Bergeijk et al. (2019b) provides two formulas for the maximum overtopping flow velocity for an overtopping wave along horizontal parts, e.g. dike crests and berms, and along slopes (Equation 8 and Equation 9, respectively). The parameters μ , α and β are given in Equation 10 to Equation 12, respectively. Definitions are given in Table 3.4.

$$U_i(x) = \frac{1}{\frac{f \cdot x}{2 \cdot q_i} + \frac{1}{U_i(x=0)}} \quad \text{Equation 8}$$

$$U_i(s) = \frac{\alpha}{\beta} + \mu \cdot \exp(-3 \cdot \alpha \cdot \beta^2 \cdot s) \quad \text{Equation 9}$$

$$\mu = U_i(s=0) - \frac{\alpha}{\beta} \quad \text{Equation 10}$$

$$\alpha = \sqrt[3]{g \cdot \sin(\varphi)} \quad \text{Equation 11}$$

$$\beta = \sqrt[3]{f/(2 \cdot q_i)} \quad \text{Equation 12}$$

Table 3.4 Definitions of parameters analytical model for maximum overtopping flow velocities along dike crests and landward slopes (Van Bergeijk et al., 2019b).

Parameter	Definition	Unit
x	Horizontal dike crest coordinate	m
$U_i(x)$	Maximum flow velocity of wave i at horizontal coordinate x	m/s
s	Horizontal along-slope coordinate ($s = x/\cos(\varphi)$)	m
$U_i(s)$	Maximum flow velocity of wave i at slope coordinate s	m/s
α	Parameter	-
β	Parameter	-
μ	Parameter	-
φ	Angle landward slope	-
f	Bottom friction coefficient	-
q_i	Overtopping discharge of wave i	m ³ /s/m
g	Gravitational acceleration	m/s ²

The model for overtopping flow velocities is used to calculate the maximum flow velocity along the dike crest and the landward slope for each simulated wave volume. The flow velocities along the dike profile are input for the erosion model by Hoffmans (2012) to calculate the erosion depth d along the dike profile per overtopping wave. The erosion model by Hoffmans (2012) has been adapted to account for variations in the hydraulic load (r_0 & ω) and the grass cover strength (U_t) along the dike profile (Equation 13). The turbulence parameter ω depends on the depth-averaged turbulence intensity r_0 , see (Equation 14). The definitions of parameters are given in Table 3.5.

$$d(x) = \sum_{i=1}^N \left((\omega(x)^2 \cdot U_i(x)^2 - U_t(x)^2) \cdot T_o \cdot C_E \right) \quad \text{for} \quad \omega(x) \cdot U_i(x) \geq U_t(x) \quad \text{Equation 13}$$

$$\omega(x) = 1.5 + 5 \cdot r_0(x) \quad \text{Equation 14}$$

Table 3.5 Definitions of parameters adapted model for erosion depths along dike profiles (Hoffmans, 2012).

Parameter	Definition	Unit
x	Cross-dike coordinate	m
$d(x)$	Cumulative erosion depth at coordinate x	m
N	Number of waves	-
$\omega(x)$	Turbulence parameter at coordinate x	-
$U_i(x)$	Maximum flow velocity for wave i at coordinate x	m/s
$U_t(x)$	Threshold flow velocity at coordinate x	m/s
$T_{o,i}$	Overtopping period for wave i	s
C_E	Inverse strength parameter	s/m
$r_0(x)$	Depth-averaged turbulence intensity at coordinate x	-

The hydrodynamic-erosion model simplifies the process of grass cover erosion by wave overtopping using several assumptions. The overtopping flow accelerates along the dike profile, until an equilibrium between the gravitational forces and the bottom friction is reached. The major model assumption is that each wave for which the hydraulic load exceeds the grass cover strength contributes to the erosion depth along the dike profile. The hydraulic load is defined as the product of the turbulence parameter ω and the maximum overtopping flow velocity U_j . The grass cover strength is expressed in terms of the threshold flow velocity U_t . The model further assumes that the largest waves (largest hydraulic loads) have got a relatively large contribution to the modelled erosion depth compared to smaller wave volumes. The rate for grass cover erosion is expressed in terms of the inverse strength parameter C_E and the modelled erosion depth is linearly depending on this parameter.

3.1.3. Model 2: Cumulative overload method

The cumulative overload is introduced by Van der Meer et al. (2010) as an erosional index. An important model assumption is that each overtopping flow velocity that exceeds the critical flow velocity contributes to grass cover erosion (Equation 15). The amount of erosion is expressed in terms of the cumulative damage number D . Equation 16 shows the adapted cumulative overload method including three factors to account for the flow acceleration (α_a), the increase in load (α_M) and the decrease in cover strength (α_s) at transitions and obstacles (Hoffmans et al., 2018). The definitions of the parameters in the cumulative overload method are given in Table 3.6.

$$D = \sum_{i=1}^N (U_{0,i}^2 - U_c^2) \quad \text{for} \quad U_{0,i} > U_c \quad \text{Equation 15}$$

$$D = \sum_{i=1}^N (\alpha_M (\alpha_a \cdot U_{0,i})^2 - \alpha_s \cdot U_c^2) \quad \text{for} \quad \alpha_M (\alpha_a \cdot U_{0,i})^2 > \alpha_s \cdot U_c^2 \quad \text{Equation 16}$$

Table 3.6 Definitions of parameters cumulative overload method.

Parameter	Definition	Unit
D	Cumulative damage number	m^2/s^2
N	Number of waves	-
$U_{0,i}$	Overtopping flow velocity at the start of the crest for wave i	m/s
U_c	Critical flow velocity	m/s
α_a	Acceleration factor	-
α_M	Load factor	-
α_s	Strength factor	-

To account for acceleration of overtopping waves along the dike profile, the cumulative overload method includes the product of an acceleration factor α_a and the overtopping flow velocity at the start of the crest $U_{0,i}$. Generally, the acceleration factor is determined from a graph, based on the slope steepness $\cot(\alpha)$ and the distance between the end of the dike crest and the location on the landward slope (Van der Meer et al., 2015). The acceleration of overtopping waves depends on three parameters: the initial overtopping flow velocity, the steepness of the landward slope and the length of the slope. This means that the acceleration

of the overtopping waves differs for each wave volume, while the method by Van der Meer et al. (2015) considers a constant acceleration factor for each wave volume based on the characteristics of the dike profile.

The flow acceleration method by Van der Meer et al. (2015) is a simplification of the iterative model for overtopping flow velocities along the dike profile by Schüttrumpf and Oumeraci (2005). Recently, Van Bergeijk et al. (2019b) derived an analytical model to calculate overtopping flow velocities along dike crests and landward slopes (Section 3.1.2.). Both models consider the volume-dependency of the along-slope flow acceleration by using the initial flow velocity per overtopping wave $U_{0,i}$ as model input. Comparison of modelled overtopping flow velocities with measured flow velocities has shown that the analytical model results in more accurate approximations of the flow acceleration compared to the iterative model of Schüttrumpf and Oumeraci (Van Bergeijk et al., 2019b). For the model analysis with the cumulative overload method, three methods are considered to account for acceleration of overtopping waves along the slope:

1. Constant flow acceleration factor – Van der Meer et al. (2015) – $\alpha_{a,vdM}$
2. Acceleration factor per wave volume – Schüttrumpf and Oumeraci (2005) – $\alpha_{a,SO}$
3. Acceleration factor per wave volume – Van Bergeijk et al. (2019b) – $\alpha_{a,vB}$

The acceleration factor of an overtopping wave along the landward slope for the iterative model by Schüttrumpf and Oumeraci (2005) and the analytical model by Van Bergeijk et al. (2019) are compared (Figure 3.2). Two initial flow velocities were considered: $u(0) = 3.0$ m/s for moderate wave overtopping volumes and $u(0) = 6.0$ m/s for large wave overtopping volumes. Three values for the landward slope angle were considered: $\cot(\alpha) = 2.3$, $\cot(\alpha) = 2.7$ and $\cot(\alpha) = 3.0$.

Moderate overtopping waves show a relatively quick increase of the acceleration factor along the landward slope compared to large overtopping waves. In case of $u(0) = 3.0$ m/s, the overtopping flow quickly accelerates on the first 5 to 10 m along the slope before it reaches a constant flow velocity using the analytical model (Figure 3.2). The iterative model shows that the overtopping flow gradually accelerates along the full landward slope. The acceleration factor steadily increases for both the analytical model and the iterative method for larger wave volumes with $u(0) = 6$ m/s.

Comparison of the acceleration factors along the slope shows that the analytical model by van Bergeijk et al. (2019b) results in higher flow velocities than the iterative model by Schüttrumpf and Oumeraci (2005). Besides, the acceleration factor is higher for moderate wave volumes compared to larger wave volumes. For an initial flow velocity of $u(0) = 3.0$ m/s, the acceleration factor at the end of the slope ranges from 1.54 to 1.68 for the iterative model and from 1.64 to 1.76 for the analytical model. Considering a large initial flow velocity, the acceleration factor is between 1.26 and 1.38 for the iterative model and between 1.46 and 1.56 for the analytical model. The acceleration factor by Van der Meer et al. (2015) along the slope ranges from 1.44 for $\cot(\alpha) = 3.0$ to 1.54 for $\cot(\alpha) = 2.3$.

In this research, the model outcomes for different flow acceleration methods are compared to determine its influence on the derived critical flow velocities and the calibrated load factors.

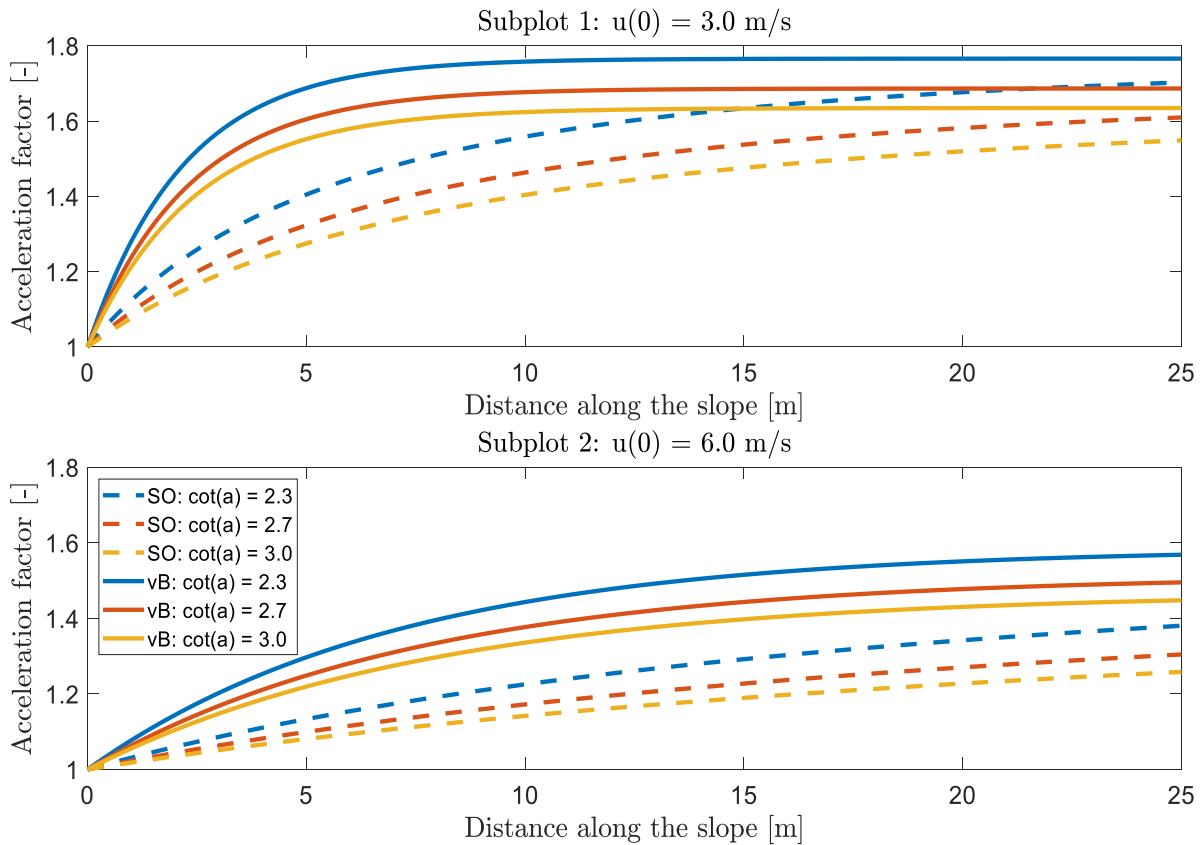


Figure 3.2 Comparison of the flow acceleration factor along the landward slope using the iterative model identified by SO (Schüttrumpf and Oumeraci, 2005) and the analytical model identified by vB (Van Bergeijk et al., 2019) for two initial flow velocities $u(0)$ and three landward slope angles $\cot(\alpha)$.

Four damage categories have been identified for the cumulative overload method: no damage, first damage, various damages and failure of the grass revetment. The model appeared to be most reliable for the prediction of failure and much less to predict ‘first damage’ and ‘various damages’ (Hoffmans et al., 2018).

The wave overtopping tests at the Vechtdijk in 2011 were considered to derive representative damage numbers for each damage category (Van der Meer et al., 2015). Constant flow acceleration factors ($\alpha_{\alpha, v d M}$) were assumed for this analysis. However, to apply the flow acceleration methods by Schüttrumpf and Oumeraci (2005) and Van Bergeijk et al. (2019b) to the cumulative overload method, the derived damage numbers should be recalculated. Therefore, the derivation of representative damage numbers by Van der Meer et al. (2015) is reproduced. Subsequently, the analysis is repeated to derive representative damage numbers per damage category for the volume-dependent flow acceleration methods by Schüttrumpf and Oumeraci (2005) and Van Bergeijk et al. (2019b).

Van der Meer et al. (2015) showed that the derived damage number per damage category for four test sections were most comparable for a critical flow velocity $U_c = 3.5$ m/s. Appendix 2 provides the model data and extensive model results for the re-analysis of damage numbers per damage category. Table 3.7 summarizes the results of the re-analysis of representative damage numbers.

Table 3.7 Representative damage numbers D per damage category for three flow acceleration methods.

Flow acceleration method	Damage number D per damage category [m^2/s^2]			
	No damage	First damage	Various damages	Failure
Van der Meer et al. (2015)	0 – 1000	1000	4000	7000
Schüttrumpf & Oumeraci (2005)	0 – 500	500	2000	3500
Van Bergeijk et al. (2019b)	0 – 2500	2500	9000	13000

3.2. Modelling the effects of transitions

This section provides a description of the methodology for analysing the influence of transitions on grass cover erosion. The general approach can be divided in two steps: (1) determining a representative parameter value for the strength of the grass cover and (2) calibrating a factor for the increase in load and/or the decrease in strength of the grass cover at the transition. The approach for modelling the effect of transitions is explained more specific for the hydrodynamic-erosion model (Subsection 3.2.1.) and the cumulative overload method (Subsection 3.2.2.).

3.2.1. Model 1: Hydrodynamic-erosion model

Two steps can be distinguished to analyse the influence of transitions on grass cover erosion using the cumulative overload method. First, a representative threshold flow velocity U_t needs to be determined and, next, the turbulence intensity parameter r_0 needs to be calibrated (Figure 3.3).

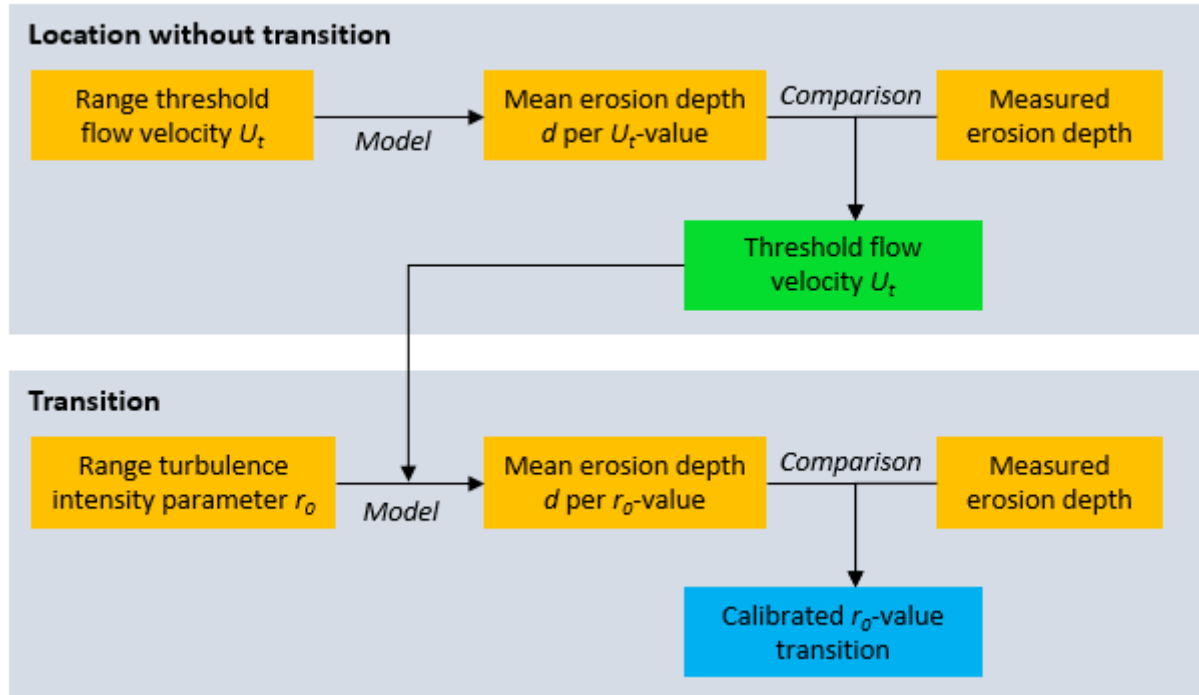


Figure 3.3 Overview of the approach for determining influence factors for a transition on grass cover erosion using the hydrodynamic-erosion model.

The strength of the grass cover is included in the hydrodynamic-erosion model in terms of the threshold flow velocity U_t . To analyse the influence of transitions on grass cover erosion, it is

first required to determine a representative value for U_t . From grass sod pulling tests is concluded that the grass cover strength generally varies along a dike profile (Bijlard, 2015). Therefore, it is difficult to determine parameters like the threshold flow velocity at a test section. In this research, it is assumed that a representative threshold flow velocity can be derived based on the measured erosion depth at a spot along the dike profile where no transition is present.

First, a range of threshold flow velocity values needs to be defined and, subsequently, the erosion depth at the spot along the dike profile is calculated for each threshold flow velocity value. The modelled erosion depths are compared to the measured erosion depth. The threshold flow velocity value for which the modelled erosion depth is closest to the measured erosion depth is selected as representative threshold flow velocity U_t . A minimum threshold flow velocity can be determined in case the grass cover did not erode during the wave overtopping test. This is the lowest U_t -value resulting in no erosion at the cross-dike coordinate. It is assumed that the derived threshold flow velocity is representative for each cross-dike coordinate.

The second step in the analysis using the hydrodynamic-erosion model is to calibrate the influence factors to account for increased hydraulic loads and/or decreased grass cover strength at transitions. The threshold flow velocity U_t and/or the inverse strength parameter C_E could be considered as calibration parameters to account for a lower grass cover strength at transitions. The increased hydraulic loads at transitions should be included in the model analysis using the depth-averaged turbulence intensity parameter r_0 as calibration parameter. A range of values for the calibration parameter needs to be determined. Next, the model is used to calculate the erosion depth at the location of the transition for each value of the calibration parameter. The mean erosion depth at the transition is compared with the measured erosion depth near the transition. The value of the calibration parameter that results in the least difference between the modelled and measured mean erosion depth is assumed to be representative for the influence of the transition on grass cover erosion.

This approach for the analysis of influence factors for transitions on grass cover erosion with the hydrodynamic-erosion model requires data from the wave overtopping tests. The input dike profile is defined in terms of the crest width, the length of the slope, the slope steepness and the berm width. The grass cover erosion needs to be expressed in terms of the mean erosion depth and the length of the eroded grass cover, while it is also required to know the cross-dike location at where erosion was observed.

3.2.2. Model 2: Cumulative overload method

The analysis of influence factors for transitions using the cumulative overload method is comparable to the analysis using the hydrodynamic-erosion model: the strength of the grass cover needs to be determined and, next, the influence factor(s) for the transition type are calibrated (Figure 3.4).

The grass cover strength is represented by the critical flow velocity U_c in the cumulative overload method. A range of U_c -values needs to be determined and, subsequently, a cumulative damage number D is calculated for each U_c -value. The modelled cumulative damage numbers for different U_c -values are compared to the damage number that corresponds to the observed damage category. The critical flow velocity that results in the least difference between the modelled damage number and the damage number for the

observed damage category is selected as the representative critical flow velocity. It is again assumed that the derived critical flow velocity is representative for all cross-dike coordinates. The load factor α_M and the strength factor α_s in the cumulative overload method can be considered as calibration parameters for transitions. A range of values for α_M ($\alpha_M \geq 1$) or α_s ($\alpha_s \leq 1$) must be defined to determine the damage number for each value of the influence factors. The modelled damage numbers for each value of the load factor α_M is compared to the damage number that corresponds to the observed damage category (Figure 3.4). The load factor for which the modelled damage number is closest to the damage number for the damage category is selected as the representative load factor for the transition.

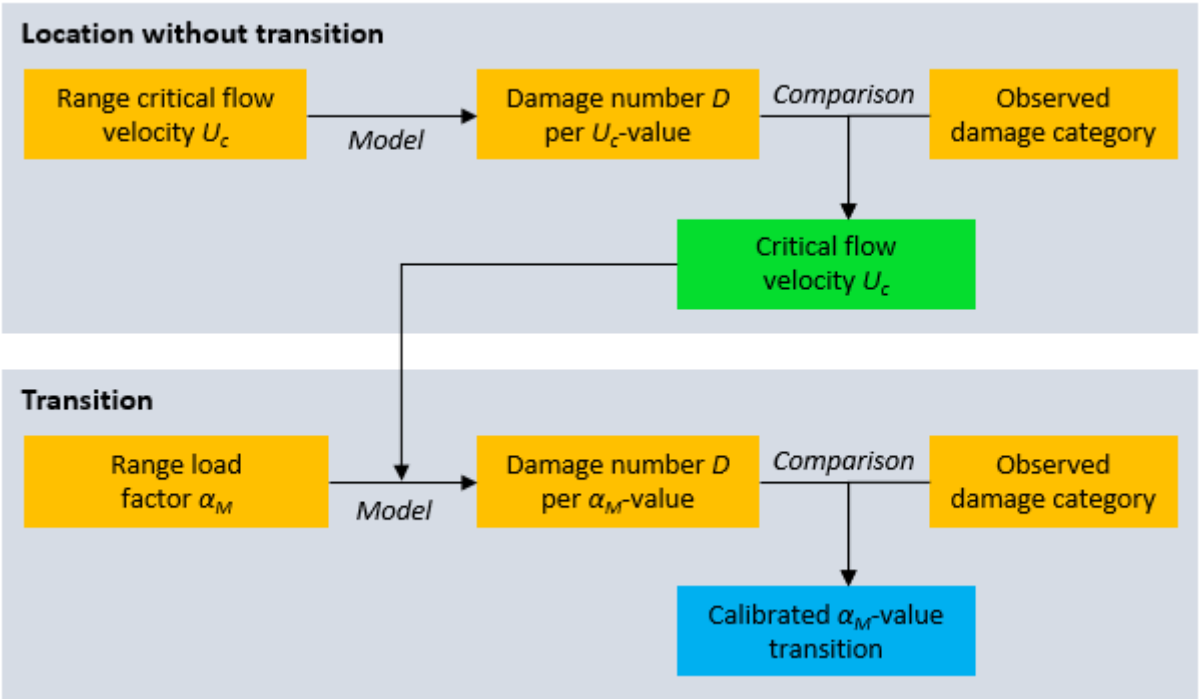


Figure 3.4 Overview of the approach for determining influence factors for a transition on grass cover erosion using the cumulative overload method.

Data required for the analysis using the cumulative overload method consists of dike profile data (landward slope steepness) and erosion data (observed damage numbers and location of damage).

3.3. Application to transition landward toe

Both erosion models are introduced in Section 3.1. and the approach for calibrating the erosional effects of transitions is described in Section 3.2. Next, this model approach is applied to seven tests sections with a geometrical transition at the landward toe (type T6) using the hydrodynamic-erosion model (Subsection 3.3.1.) and the cumulative overload method (Subsection 3.3.2.).

Seven test sections are selected (Section 2.2.) to be considered in the analysis of transition type T6 with both erosion models. Table 3.8 provides the dike profile data for each test section in terms of the crest length L_{crest} , the slope length L_{slope} , the berm length L_{berm} and the slope steepness $\cot(\alpha)$.

Table 3.8 Profile dimensions per test section with the crest length L_{crest} , the slope length L_{slope} , the berm length L_{berm} and the steepness of the landward slope $\cot(\alpha)$. Data for the tests at Boonweg, Kattendijke, Afsluitdijk and Tholen are obtained from Bakker et al. (2008a), Bakker et al. (2008b), Bakker et al. (2009) and Bakker et al. (2011), respectively.

Test section	L_{crest} [m]	L_{slope} [m]	L_{berm} [m]	$\cot(\alpha)$ [-]
Boonweg 1 (Bakker et al., 2008a)	2.5	27.0	5.0	2.9
Boonweg 2 (Bakker et al., 2008a)	2.5	27.0	5.0	2.9
Kattendijke 1 (Bakker et al., 2008b)	2.0	15.0	2.0	3.0
Kattendijke 2 (Bakker et al., 2008b)	2.5	17.5	2.0	3.0
Afsluitdijk 1 (Bakker et al., 2009)	0.5	7.8	6.0	2.3
Afsluitdijk 2 (Bakker et al., 2009)	0.7	7.5	3.2	2.3
Tholen 4 (Bakker et al., 2011)	2.0	14.0	3.0	2.3

3.3.1. Model 1: Hydrodynamic-erosion model

The hydrodynamic-erosion model is applied to seven wave overtopping tests (1) to determine the threshold flow velocity U_t based on the measured erosion depth along the landward slope and (2) to determine the increase of the hydraulic load by calibration of the turbulence intensity parameter r_0 based on the measured erosion depth at the transition.

The friction coefficient was set to $f = 0.01$ for each test section (Van Hoven et al., 2013). The turbulence intensity parameter is assumed to be $r_{0,c} = 0.17$ and $r_{0,s} = 0.10$ at the dike crest and at the landward slope, respectively (Van Hoven et al., 2013). The strength parameter is set to $C_E = 1.0 \cdot 10^{-6} \text{ s/m}$, which is the representative value for a good grass quality (Hoffmans, 2012).

An analysis of the seven test sections with a geometrical transition at the landward toe is provided (Section 2.2). The factual reports of the wave overtopping tests provide pictures and descriptions of grass cover erosion at each test section. These reports were studied to estimate the dimensions of grass cover erosion at the landward slope and the geometrical transition. The dimensions are given in terms of the mean erosion depth and the length of the eroded grass cover after each simulation with a mean overtopping discharge q_m . The width of the eroded grass cover is not considered in the model analysis, because it is not considered in the hydrodynamic-erosion model.

Table 3.9 shows the dimensions of grass cover erosion at the lower part of the landward slope after each simulation per test section. The marked boxes show which simulations with mean overtopping discharge q_m are included in the model analysis to derive the threshold flow velocity U_t per test section.

Table 3.9 Mean erosion depth and length of the eroded grass cover at the slope after each simulation per test section. Erosion values are given as depth [m] x length [m]. Marked boxes show the simulations that are used to derive threshold flow velocities. Test data for Boonweg, Kattendijke, Afsluitdijk and Tholen are obtained from Bakker et al. (2008a), Bakker et al. (2008b), Bakker et al. (2009) and Bakker et al. (2011), respectively.

	Erosion (depth [m] x length [m]) after simulation with mean overtopping discharge q_m [l/s/m]						
	$q_m = 0.1$	$q_m = 1$	$q_m = 5$	$q_m = 10$	$q_m = 30$	$q_m = 50$	$q_m = 75$
Boonweg 1	0 x 0	0 x 0	-	0 x 0	0 x 0	0 x 0	0 x 0
Boonweg 2	0 x 0	0 x 0	-	0 x 0	0 x 0	0 x 0	0 x 0
Kattendijke 1	0 x 0	0 x 0	-	0 x 0	0 x 0	0 x 0	-
Kattendijke 2	-	-	-	-	0 x 0	0 x 0	-
Afsluitdijk 1	-	0 x 0	-	0 x 0	0 x 0	0.10 x 2.50	0.15 x 7.80
Afsluitdijk 2	-	0 x 0	-	0 x 0	-	-	-
Tholen 4	-	0 x 0	0 x 0	0 x 0	0 x 0	-	-

The approach for deriving threshold flow velocities per test section was introduced in Subsection 3.2.1. The threshold flow velocity is determined based on the measured erosion depths at the end of the landward slope for each test section. For each test section, the minimum threshold flow velocity is derived using simulations that did not result in grass cover erosion (Table 3.9).

Erosion dimensions at the transition are also determined in terms of the mean erosion depth and the length of the eroded grass cover (Table 3.10). Grass cover erosion at the transition was observed at each test section. Besides, the erosion dimensions kept increasing during the wave overtopping simulations with higher mean overtopping discharges. The marked boxes show which simulations with mean overtopping discharge q_m are included in the model analysis to calibrate the turbulence intensity parameter r_0 test section.

Table 3.10 Mean erosion depth and length of the eroded grass cover at the transition after each simulation per test section. Erosion values are given as depth [m] x length [m]. Marked boxes show the simulations that are used to calibrate turbulence intensity parameter r_0 . Test data for Boonweg, Kattendijke, Afsluitdijk and Tholen are obtained from Bakker et al. (2008a), Bakker et al. (2008b), Bakker et al. (2009) and Bakker et al. (2011), respectively.

	Erosion (depth [m] x length [m]) after simulation with mean overtopping discharge q_m [l/s/m]						
	$q_m = 0.1$	$q_m = 1$	$q_m = 5$	$q_m = 10$	$q_m = 30$	$q_m = 50$	$q_m = 75$
Boonweg 1	0 x 0	0 x 0	-	0 x 0	0 x 0	0.10 x 1.00	0.30 x 2.00
Boonweg 2	0 x 0	0 x 0	-	0 x 0	0 x 0	0 x 0	0.30 x 2.00
Kattendijke 1	0 x 0	0 x 0	-	0 x 0	0 x 0	0.20 x 2.00	-
Kattendijke 2	-	-	-	-	0 x 0	0.30 x 2.00	-
Afsluitdijk 1	-	0 x 0	-	0.10 x 0.80	0.20 x 2.40	0.25 x 2.40	0.35 x 2.40
Afsluitdijk 2	-	0 x 0	-	0.30 x 2.00	-	-	-
Tholen 4	-	0 x 0	0.20 x 0.50	0.40 x 1.50	-	-	-

To account for increased hydraulic loads at the geometrical transitions, the depth-averaged turbulence intensity parameter r_0 is calibrated using the hydrodynamic-erosion model. The default value for the turbulence intensity along the landward slope is assumed to be $r_0 = 0.10$ (Van Hoven et al., 2013). The calibration values for the turbulence intensity parameter range from $r_0 = 0.10$ (no load increase) to $r_0 = 0.60$ in steps of 0.05. The turbulence intensity parameter is manually calibrated by comparison of the modelled erosion depth per r_0 -value to the measured erosion. The r_0 -value that results in the least difference between modelled and measured mean erosion depths is determined as most representative for the influence of the geometrical transition on grass cover erosion.

An example for deriving U_t and for calibrating r_0 is provided in Table 3.11 for test section Boonweg 1. A threshold flow velocity of $U_t = 22$ m/s is derived by comparison of the modelled erosion depth per U_t -value to a measured erosion depth $d = 0.00$ m (no erosion). Despite the differences in modelled erosion depths are small between different U_t -values, a minimum U_t can be determined for which the hydraulic load does not exceed the grass cover strength. Subsequently, the modelled erosion depth per r_0 -value is compared to the measured erosion depth $d = 0.30$ m. Table 3.11 shows that this results in a calibrated turbulence intensity parameter of $r_0 = 0.25$.

Table 3.11 Modelled erosion depth d_s [m] at the end of the landward slope per threshold flow velocity U_t [m/s] and erosion depth d_t [m] at the transition per turbulence intensity parameter r_0 [-] for Boonweg section 1. A minimum threshold flow velocity $U_t = 22$ m/s (marked) is derived based on no observed erosion at the slope; the calibrated turbulence intensity parameter is $r_0 = 0.25$ (marked) based on a measured erosion depth of 0.30 m at the transition.

Derivation threshold flow velocity U_t											
U_t [m/s]	18	19	20	21	22						
d_s [m]	0.09	0.05	0.03	0.01	0.00						
Calibration turbulence intensity parameter r_0											
r_0 [-]	0.10	0.15	0.20	0.25	0.30	0.35	0.40	0.45	0.50	0.55	0.60
d_t [m]	0.00	0.03	0.12	0.33	0.68	1.19	1.84	2.65	3.60	4.68	5.88

3.3.2. Model 2: Cumulative overload method

The cumulative overload method is also applied to the selected test sections with a geometrical transition at the landward toe. In Subsection 3.2.2. was introduced that the critical flow velocity U_c is derived based on the observed damage category at the end of the landward slope, after which the load factor α_M is calibrated based on the observed damage category at the geometrical transition.

An assessment of the observed damage categories at each test section has been provided by Van der Meer (2014). Those estimated damage categories have been reconsidered by comparing erosional damage between different test sections and by re-assessing the damage according to the four damage categories.

Subsection 3.3.1. has shown which simulations are selected for (1) derivation of the threshold flow velocity U_t and (2) calibration of the turbulence intensity parameter r_0 using the hydrodynamic-erosion model. Those simulations are also selected for the analysis using the cumulative overload method. An overview of the selected simulations for derivation of the critical flow velocity U_c per test section is provided together with the damage numbers per flow acceleration method that correspond to the observed damage category (Table 3.12). The critical flow velocities are determined based on category 'no damage' at each test section.

Table 3.12 Overview of selected simulations of the mean wave overtopping discharge q_m that are considered for derivation of the critical flow velocity U_c per test section. The damage numbers D [m²/s²] for the observed damage category at the end of the landward slope are given per flow acceleration method per test section.

	q_m [l/s/m]	Damage category numbers D per flow acceleration method α_a		
		$\alpha_{a,vdM}$	$\alpha_{a,SO}$	$\alpha_{a,vB}$
Boonweg 1	0.1; 1; 10; 30; 50; 75	0 – 1000	0 – 500	0 – 2500
Boonweg 2	0.1; 1; 10; 30; 50; 75	0 – 1000	0 – 500	0 – 2500
Kattendijke 1	0.1; 1; 10; 30; 50	0 – 1000	0 – 500	0 – 2500
Kattendijke 2	30; 50	0 – 1000	0 – 500	0 – 2500
Afsluitdijk 1	1; 10; 30	0 – 1000	0 – 500	0 – 2500
Afsluitdijk 2	1; 10	0 – 1000	0 – 500	0 – 2500
Tholen 4	1; 5; 10	0 – 1000	0 – 500	0 – 2500

Similarly, the damage numbers for observed damage category at the transition for different flow acceleration methods per test section for calibration of load factor α_M are given in Table 3.13.

Table 3.13 Overview of selected simulations of the mean wave overtopping discharge q_m that are considered for calibration of the load factor α_M per test section. The damage numbers D [m^2/s^2] for the observed damage category at the geometrical transition are given per flow acceleration method per test section.

	q_m [l/s/m]	Damage category numbers D per flow acceleration method α_a		
		$\alpha_{a,vdM}$	$\alpha_{a,SO}$	$\alpha_{a,vB}$
Boonweg 1	0.1; 1; 10; 30; 50; 75	4000	2000	9000
Boonweg 2	0.1; 1; 10; 30; 50; 75	4000	2000	9000
Kattendijke 1	0.1; 1; 10; 30; 50	7000	3500	13000
Kattendijke 2	30; 50	7000	3500	13000
Afsluitdijk 1	1; 10; 30; 50; 75	7000	3500	13000
Afsluitdijk 2	1; 10	4000	2000	9000
Tholen 4	1; 5; 10	7000	3500	13000

Table 3.14 provides an example for deriving U_c and for calibrating α_M for test section Boonweg 1 using the flow acceleration method $\alpha_{a,vdM}$ according to Van der Meer et al. (2015). The modelled damage number D_s per U_c -value is compared to the damage number for the observed damage category at the end of the landward slope. A minimum critical flow velocity $U_c = 10$ m/s is derived based on category ‘no damage’. The calibration parameter, load factor α_M , ranges from $\alpha_M = 1.0$ (no load increase) to the theoretical maximum value $\alpha_M = 2.0$ (Hoffmans et al., 2018) using a step size of 0.1. The load factor α_M is manually calibrated by comparison of the modelled damage number per α_M -value to the damage number for the observed damage category. The α_M -value that results in the least difference between the modelled damage number and the damage category number is determined as most representative for the influence of the geometrical transition on grass cover erosion. This results in a calibrated load factor $\alpha_M = 1.3$ (Table 3.14).

Table 3.14 Modelled damage numbers D_s [m^2/s^2] at the end of the landward slope per critical flow velocity U_c [m/s] and damage numbers D_t [m^2/s^2] at the transition per load factor α_M [-]. A minimum critical flow velocity $U_c = 10$ m/s (marked) is derived based on the observed damage category ‘no damage’; the calibrated load factor is $\alpha_M = 1.3$ (marked) based on the observed damage category ‘various damages’. The flow acceleration method $\alpha_{a,vdM}$ is according to Van der Meer et al. (2015).

Derivation critical flow velocity U_c											
U_c [m/s]	9.0	9.5	10	10.5	11						
D_s [m]	2107	1182	603	272	116						
Calibration load factor α_M											
α_M [-]	1.0	1.1	1.2	1.3	1.4	1.5	1.6	1.7	1.8	1.9	2.0
D_t [m]	603	1245	2187	3513	5193	7311	9904	12968	16532	20520	24984

4. Results

This chapter provides the results of the influence of the geometrical transition at the landward toe (type T6) on grass cover erosion. Two erosion models are used: the hydrodynamic-erosion model (Section 4.1.) and the cumulative overload method (Section 4.2.). The results of both models are compared in Section 4.3.

4.1. Model 1: Hydrodynamic-erosion model

The hydrodynamic-erosion model is used to derive the representative influence factors for the geometrical transition at the landward toe on grass cover erosion. The model approach was introduced in Subsection 3.3.1.

The modelled erosion depth per r_0 -value is compared to the measured erosion depth at the geometrical transition. Examples are provided for the test sections Afsluitdijk 2 and Tholen 4 (Figure 4.1). For both test sections, the calibrated turbulence intensity parameter is $r_0 = 0.45$ based on the least difference between the modelled and measured mean erosion depth at the transition.

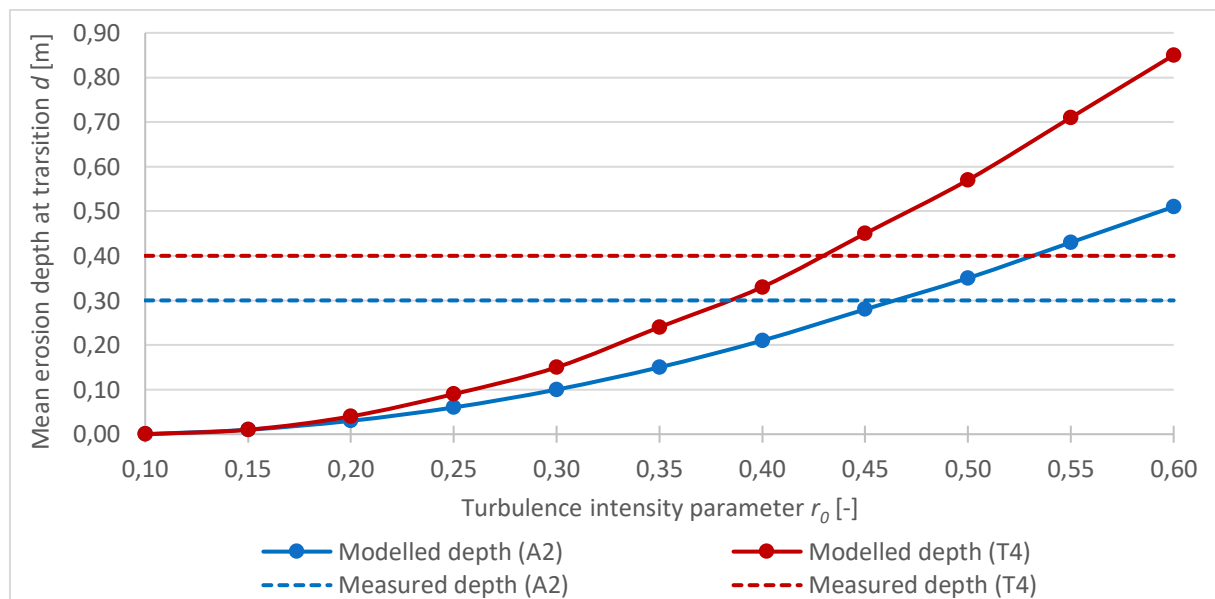


Figure 4.1 Calibration of the turbulence intensity parameter r_0 to quantify the influence of the geometrical transition on grass cover erosion. The modelled erosion depth (dotted line) is compared to the measured mean erosion depth (straight line) at the transition for test sections Afsluitdijk 2 (A2) and Tholen 4 (T4).

The results for all test sections are provided in Table 4.1. Extensive results of the analysis using the hydrodynamic-erosion model are given in Appendix 3.

The strength of the grass cover is expressed in terms of the threshold flow velocity U_t . The grass cover strength varies strongly between the test sections: the derived threshold flow velocities range from $U_t = 14$ m/s to $U_t = 22$ m/s (Table 4.1). The threshold flow velocities are used as input for calibration of the turbulence intensity parameter r_0 . The calibration results show that $r_0 = 0.25$ is derived for both test sections at Boonweg and also at Kattendijke, while $r_0 = 0.20$ is calibrated for Afsluitdijk section 1 (Table 4.1). The calibration results further show that $r_0 = 0.45$ is derived for Afsluitdijk section 2 and Tholen section 4, which is a relatively high value for the turbulence intensity parameter compared to the five other test sections.

Table 4.1 Overview of the derived threshold flow velocity U_t and the calibrated turbulence intensity parameter r_0 for each test section using the hydrodynamic-erosion model. The modelled mean erosion depth d is compared to the observed erosion depth d_o at the geometrical transition at the landward toe. Marked boxes indicate the calibrated values for the turbulence intensity parameter r_0 per test section.

	U_t [m/s]	d_o [-]	Mean erosion depth d [m] per turbulence intensity parameter r_0 [-]										
			0.10	0.15	0.20	0.25	0.30	0.35	0.40	0.45	0.50	0.55	0.60
Boonweg 1	22	0.30	0.00	0.03	0.12	0.33	0.68	1.19	1.84	2.65	3.60	4.68	5.88
Boonweg 2	22	0.30	0.00	0.03	0.12	0.33	0.68	1.19	1.84	2.65	3.60	4.68	5.88
Kattendijke 1	19	0.20	0.00	0.02	0.08	0.20	0.40	0.69	1.06	1.50	2.01	2.58	3.20
Kattendijke 2	19	0.30	0.00	0.02	0.09	0.22	0.42	0.70	1.05	1.46	1.93	2.45	3.02
Afsluitdijk 1	17	0.35	0.03	0.15	0.42	0.86	1.46	2.21	3.07	4.04	5.12	6.28	7.53
Afsluitdijk 2	14	0.30	0.00	0.01	0.03	0.06	0.10	0.15	0.21	0.28	0.35	0.43	0.51
Tholen 4	16	0.40	0.00	0.01	0.04	0.09	0.15	0.24	0.33	0.45	0.57	0.71	0.85

4.2. Model 2: Cumulative overload method

The approach for the analysis of the influence of the geometrical transition at the landward toe on grass cover erosion using the cumulative overload method was introduced in Subsection 3.3.2. Three methods are considered to account for the flow acceleration of overtopping waves along landward slopes: the graphical approach (Van der Meer et al., 2015), the iterative model for acceleration of overtopping waves (Schüttrumpf and Oumeraci, 2005) and the analytical model for acceleration of overtopping waves at dike crests and landward slopes (Van Bergeijk et al., 2019b).

Each flow acceleration method is used to derive the critical flow velocity U_c and to calibrate the load factor α_M for each test section. The extensive results of the model analysis using the cumulative overload method are provided in Appendix 4.

Table 4.2 provides an overview of the derived critical flow velocities per test section for each method for the flow acceleration. The highest critical flow velocities are derived using a constant acceleration factor per test section according to Van der Meer et al. (2015), while the lowest critical flow velocities are obtained using the iterative method for flow acceleration by Schüttrumpf and Oumeraci (2005).

Table 4.2 Derived critical flow velocities U_c per test section using three flow acceleration methods: $\alpha_{a,vdM}$ (Van der Meer et al., 2015), $\alpha_{a,SO}$ (Schüttrumpf and Oumeraci, 2005) and $\alpha_{a,vB}$ (Van Bergeijk et al., 2019b).

	Boonweg	Boonweg	Kattendijke	Kattendijke	Afsluitdijk	Afsluitdijk	Tholen
	1	2	1	2	1	2	4
$U_{c,vdM}$ [m/s]	10.0	10.0	8.5	8.5	7.5	6.0	6.5
$U_{c,SO}$ [m/s]	7.5	7.5	6.5	6.5	6.0	5.0	5.0
$U_{c,vB}$ [m/s]	9.5	9.5	8.0	8.0	7.0	5.5	6.5

Figure 4.2 shows the calibration of load factor α_M for test section Tholen 4. The modelled erosion is expressed in terms of D_{rel} : the relative calculated damage number with respect to the damage number for failure for each flow acceleration method. The least difference between the modelled relative damage number and the failure criterium ($D_{rel} = 1.00$) is used to calibrate the load factor α_M . The calibrated load factor is $\alpha_M = 1.8$ using $\alpha_{a,vdM}$, while $\alpha_M = 1.7$ is calibrated using $\alpha_{a,SO}$ and $\alpha_{a,vB}$. The calibrated load factor α_M is given per test section and per flow acceleration method in Table 4.3. The calibrated values for α_M per test section are quite similar for the different flow acceleration methods.

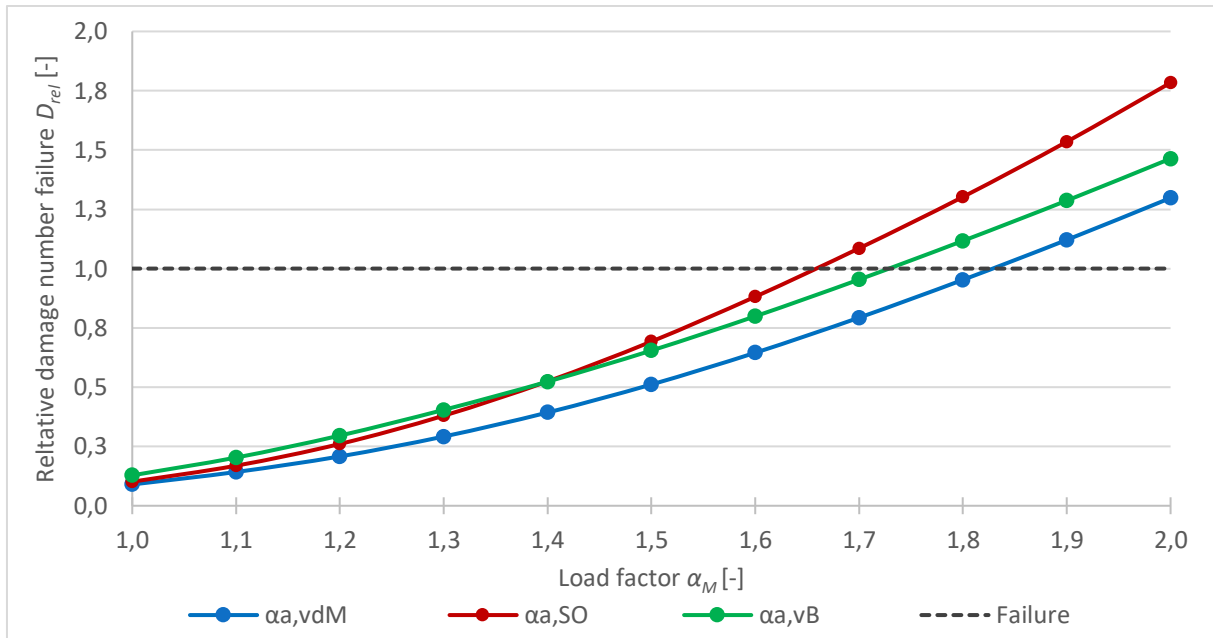


Figure 4.2 Calibration of the load factor α_M to quantify the influence of the geometrical transition on grass cover erosion for test section Tholen 4. The vertical axis shows the relative damage number D_{rel} [-], which is the modelled damage number divided by the damage number for the category failure. The modelled damage number (dotted line) is compared to $D_{rel} = 1.00$ (straight line) for three flow acceleration methods: $\alpha_{a,vdM}$ (Van der Meer et al., 2015), $\alpha_{a,SO}$ (Schüttrumpf and Oumeraci, 2005) and $\alpha_{a,vB}$ (Van Bergeijk et al., 2019b).

Table 4.3 Calibrated load factors α_M per test section using three flow acceleration methods: $\alpha_{a,vdM}$ (Van der Meer et al., 2015), $\alpha_{a,SO}$ (Schüttrumpf and Oumeraci, 2005) and $\alpha_{a,vB}$ (Van Bergeijk et al., 2019b).

	Boonweg 1	Boonweg 2	Kattendijke 1	Kattendijke 2	Afsluitdijk 1	Afsluitdijk 2	Tholen 4
$\alpha_{M,vdM}$ [-]	1.3	1.3	1.6	1.5	1.0	1.6	1.8
$\alpha_{M,SO}$ [-]	1.4	1.4	1.6	1.6	1.0	1.6	1.7
$\alpha_{M,vB}$ [-]	1.3	1.3	1.5	1.4	1.0	1.5	1.7

4.3. Comparison of the model results

Two erosion models, the hydrodynamic-erosion model and the cumulative overload method, are applied for the analysis of influence factors that are representative for the load increase at the geometrical transition at the landward toe for grass cover erosion. Besides, three different flow acceleration methods are used for the cumulative overload method. So, four different models are considered to analyse the influence of the geometrical transition on grass cover erosion. This section compares the derived values for the grass cover strength parameters (Subsection 4.3.1.) and the calibrated influence factors for the geometrical transition at the landward toe (Subsection 4.3.2.).

4.3.1. Grass cover strength parameter

The strength of the grass cover is defined in terms of the threshold flow velocity U_t and the critical flow velocity U_c for the hydrodynamic-erosion model and the cumulative overload method, respectively. The derived threshold flow velocities and the critical flow velocities for different test sections are compared (Figure 4.3).

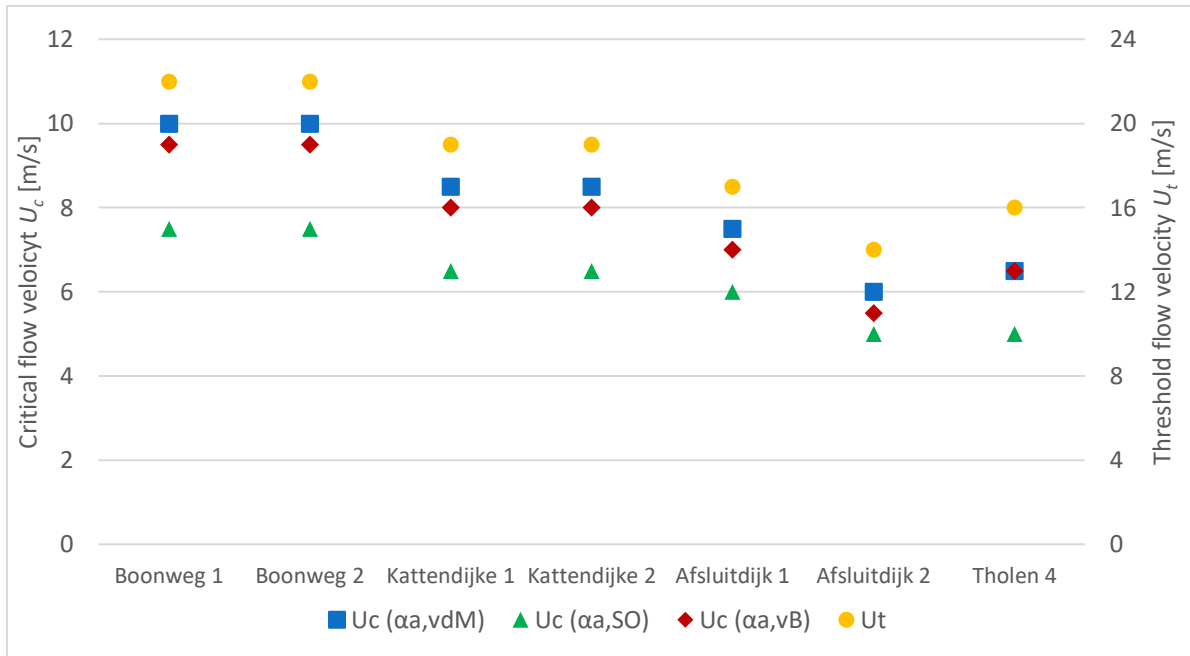


Figure 4.3 Comparison of the derived critical flow velocity U_c (left vertical axis) for three flow acceleration methods to the derived threshold flow velocity U_t (right vertical axis) per test section. Flow acceleration methods are $\alpha_{\alpha, v d M}$ (Van der Meer et al., 2015), $\alpha_{\alpha, S O}$ (Schüttrumpf and Oumeraci, 2005) and $\alpha_{\alpha, v B}$ (Van Bergeijk et al., 2019b).

The iterative method (Schüttrumpf and Oumeraci, 2005) results in the lowest critical flow velocity for each test section. Generally, the derived critical flow velocity is 0.5 m/s higher using a constant flow acceleration factor compared to the critical flow velocity that results from the analytical model. This shows that the flow acceleration methods according to Van der Meer et al. (2015) and Van Bergeijk et al. (2019b) result in comparable U_c -values.

The threshold flow velocity U_t is compared to the critical flow velocity U_c for each flow acceleration method. For a constant flow acceleration factor ($\alpha_{\alpha, v d M}$) yields $U_t \approx 2.3 \cdot U_c$. Using the iterative method ($\alpha_{\alpha, S O}$) gives $U_t \approx 2.9 \cdot U_c$, while $U_t \approx 2.4 \cdot U_c$ results from the analytical model ($\alpha_{\alpha, v B}$). For comparison of the threshold flow velocity U_t to the critical flow velocity U_c , it is most suitable to consider the cumulative overload method using $\alpha_{\alpha, v B}$ according to Van Bergeijk et al. (2019), because this flow acceleration method is also used in the hydrodynamic-erosion model.

The ratio between the threshold flow velocity and the critical flow velocity ($U_t \approx 2.4 \cdot U_c$) can be related to the different criteria of erosion in both models. In the cumulative overload method, the erosion criterium is defined as $\sqrt{\alpha_M} \cdot U > U_c$ (Equation 16) with overtopping velocity U , while the erosion criterium for the hydrodynamic-erosion model includes an extra turbulence parameter (ω): $\omega \cdot U > U_t$ (Equation 13). This parameter is defined as $\omega = 1.5 + 5 \cdot r_0$. To derive the critical flow velocity, the transition is not considered, so $\alpha_M = 1.0$. The assumption $r_0 = 0.10$ along the landward slope results in $\omega = 2.0$. Combination of both equations results in $U_t = 2 \cdot U_c$, which means that the hydraulic load in the hydrodynamic-erosion model is twice as large as the hydraulic load in the cumulative overload method, using the same flow acceleration method.

The remaining difference between U_t and U_c can be related to approach for deriving the parameter values. The threshold flow velocities are derived based on an exact erosion depth ($d = 0.00$ m) at the end of the slope, while the critical flow velocities are determined by selecting the minimum critical flow velocity for which the modelled damage number lies within the range for the erosion category 'no damage' ($0 \leq D \leq 500 \text{ m}^2/\text{s}^2$ for $\alpha_{a,vB}$).

4.3.2. Influence factor geometrical transition

The derived threshold flow velocity U_t is used to calibrate the turbulence intensity parameter r_0 per test section using the hydrodynamic-erosion model. The calibration values for the turbulence intensity parameter range from $r_0 = 0.10$ to $r_0 = 0.60$ in steps of 0.05. Derived critical flow velocities U_t are used as input for calibration of load factor α_M using the cumulative overload method. The load factor values for calibration are $\alpha_M = 1.0$ to $\alpha_M = 2.0$ in steps of 0.1.

In Subsection 4.3.1. is shown that the hydraulic load in the hydrodynamic-erosion model is twice as large as the load in the cumulative overload method, according to the theory. This was determined for the case without an increased hydraulic load at the transition: $r_0 = 0.10$ and $\alpha_M = 1.0$. Equation 17 is derived using the erosion criteria $\sqrt{\alpha_M} \cdot U > U_c$ (cumulative overload method) and $(1.5 + 5 \cdot r_0) \cdot U > U_t$ (hydrodynamic-erosion model) in combination with $U_t = 2.0 \cdot U_c$.

$$r_0 = \frac{2\sqrt{\alpha_M} - 1.5}{5} \quad \text{Equation 17}$$

Equation 17 is used to compare the step size of calibration parameter α_M for the cumulative overload method to the step size of r_0 for the hydrodynamic-erosion model (Table 4.4). The results show that the range of r_0 -values that is used for calibration ($r_0 = 0.10$ to $r_0 = 0.60$) is larger than the range of r_0 -values that agrees to the calibration range for α_M ($r_0 = 0.10$ to $r_0 = 0.27$). The applied step size for r_0 in the calibration is relatively large compared to the step size of load factor α_M .

Table 4.4 Comparison of the step size of the calibration parameter α_M for the cumulative overload method to the range $r_{0,eq}$ (according to Equation 17) and to the calibration range r_0 for the hydrodynamic-erosion model.

α_M [-]	1.0	1.1	1.2	1.3	1.4	1.5	1.6	1.7	1.8	1.9	2.0
$r_{0,eq}$ [-]	0.10	0.12	0.14	0.16	0.17	0.19	0.21	0.22	0.24	0.25	0.27
r_0 [-]	0.10	0.15	0.20	0.25	0.30	0.35	0.40	0.45	0.50	0.55	0.60

According to Hoffmans et al. (2018), the steepness of the landward slope (θ) can be used to describe the load increase at geometrical transitions for the cumulative overload method (Equation 18).

$$\alpha_T = 1 + \sin(0.5 \cdot \theta) \quad \text{Equation 18}$$

Theoretical load factors for the geometrical transition at the landward toe are $\alpha_T = 1.16$ for test sections Boonweg 1 and 2 and Kattendijke 1 and 2 based on $\cot(\alpha) = 2.9$ and $\cot(\alpha) = 3.0$, respectively. The theoretical load factor is $\alpha_T = 1.20$ based on $\cot(\alpha) = 2.3$ for Afsluitdijk 1, Afsluitdijk 2 and Tholen 4. The theoretical load factors for geometrical transitions according to Hoffmans et al. (2018) are compared to the calibrated values for parameters r_0 and α_M per test section (Figure 4.4).

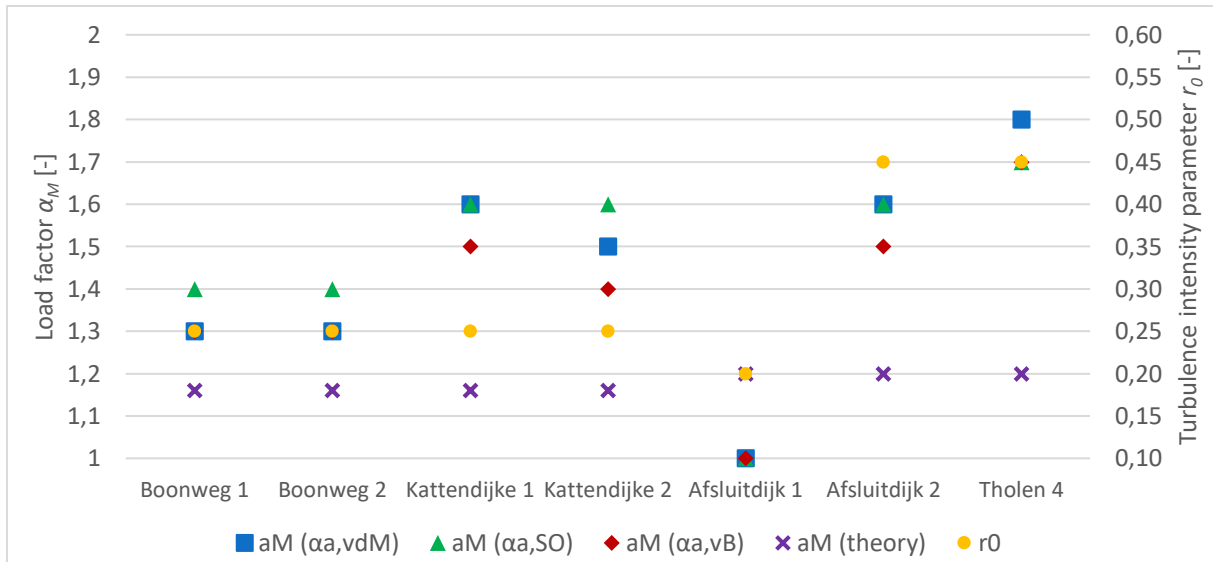


Figure 4.4 Comparison of the calibrated load factor α_M (left vertical axis) for three flow acceleration methods to the calibrated turbulence intensity parameter r_0 (right vertical axis) per test section. Flow acceleration methods are $\alpha_{a,vdM}$ (Van der Meer et al., 2015), $\alpha_{a,SO}$ (Schüttrumpf and Oumeraci, 2005) and $\alpha_{a,vB}$ (Van Bergeijk et al., 2019b). The calibrated load factors are compared to the theoretical load factor based on the steepness of the landward slope $\cot(\alpha)$ (Hoffmans et al., 2018).

Despite different critical flow velocities were derived using three different flow acceleration methods, the calibrated load factors per test section are quite similar between different flow acceleration methods (Figure 4.4). This shows that differences between these three methods are eliminated by first using each flow acceleration method for deriving critical flow velocities and, next, for calibrating the load factors.

Seven cases for the model analysis were described (Section 2.2). It was noticed that bricks were present underneath the grass cover at the geometrical transition at the landward toe at test sections Boonweg 1 and 2. Due to the presence of bricks, the length of the roots in the grass sod is limited. The grass cover strength is likely decreased at the geometrical transition due to these secondary aspects. Therefore, it must be recognized that the calibrated values for r_0 and α_M factors for model cases Boonweg 1 and 2 are not representative for the influence of the geometrical transition on grass cover erosion.

According to the theory, the load factor is high for steep slopes, while a mild slope results in a moderate load factor (Hoffmans et al., 2018). Relatively steep slopes were considered at Afsluitdijk 1 and 2 and Tholen 4 with $\cot(\alpha) = 2.3$, while mild slopes were present at Boonweg 1 and 2 with $\cot(\alpha) = 2.9$ and at Kattendijke 1 and 2 with $\cot(\alpha) = 3.0$. The calibrated values for the turbulence intensity parameter r_0 agree to the theory with $r_0 = 0.25$ for mild slopes (Boonweg 1 & 2 and Kattendijke 1 & 2) and $r_0 = 0.45$ for relatively steep slopes (Afsluitdijk 2 and Tholen 4). Despite the relatively steep slope at test section Afsluitdijk 1, the calibrated turbulence intensity parameter ($r_0 = 0.20$) is quite low compared to the other test sections (Figure 4.4).

Similarly, the calibrated load factor for Afsluitdijk 1 is $\alpha_M = 1.0$ for each flow acceleration method (Figure 4.4). This suggest that the hydraulic load does not increase at the geometrical transition at the landward toe. The highest load factors are calibrated for Tholen section 4 with $\alpha_M = 1.8$ for $\alpha_{a,vdM}$ and $\alpha_M = 1.7$ for $\alpha_{a,SO}$ and $\alpha_{a,vB}$. The calibrated load factors vary from

$\alpha_M = 1.3$ to $\alpha_M = 1.6$ for the test sections with relatively mild slopes at Boonweg and Kattendijke. Because of the variability of the calibrated load factors, it is difficult to select values for the load factor α_M that are representative for the increased hydraulic load at geometrical transitions.

Comparison of the calibration results to the theory by Hoffmans et al. (2018) shows that the calibrated values exceed the theoretical values for each test section except Afsluitdijk 1. Therefore, the theoretical load factors as function of the slope steepness underestimate the influence of the geometrical transition on the hydraulic load on the grass cover, according to the data from the wave overtopping tests. Figure 4.4 further shows that the range of calibrated load factors is broad ($1.0 \geq \alpha_M \geq 1.8$), while the range of theoretical factors is small ($1.16 \geq \alpha_T \geq 1.20$). The step-size in the calibration approach ($\Delta\alpha_M = 0.1$) even exceeds the size of the range of theoretical load factors ($\Delta\alpha_T = 0.04$).

5. Discussion

Before the conclusions are drawn, this chapter provides an analysis of the sensitivity of the model parameters (Section 5.1.) and a reflection to the model approach for analysing the influence of a transition on grass cover erosion by wave overtopping (Section 5.2.).

5.1. Sensitivity analysis

Four aspects are considered in this section. The sensitivity of the calibrated influence factors to the grass cover strength parameters and the erosion rate parameter are discussed in Subsection 5.1.1. and Subsection 5.1.2., respectively. Subsequently, the dependency of the maximum allowed overtopping discharge q_m on the different flow acceleration methods (Subsection 5.1.3.) and the calibrated factors r_0 and α_M is addressed (Subsection 5.1.4.).

5.1.1. Grass cover strength parameter

A major variable that determines the resistance of the grass cover to overtopping waves is the grass cover strength. The grass cover strength depends on the root density in the grass sod. Generally, the root density is highly variable within one test section (Bijlard, 2015) and it is therefore difficult to determine representative parameter values for the grass cover strength at a test section.

The strength of the grass cover is expressed in terms of the threshold flow velocity U_t and the critical flow velocity U_c for the hydrodynamic-erosion model and the cumulative overload method, respectively. For each test section, the value for parameter U_t is determined based on an erosion depth $d = 0.00$ m (no erosion) at the end of the landward slope. Similarly, values for parameter U_c are derived using representative damage numbers for category 'no damage'. This means that minimum values for U_t and U_c are derived based on no observed damage at the landward slope. These derived values represent the minimum strength of the weakest spot in the grass cover along the landward slope.

In the model analysis, it is assumed that the derived values for U_t and U_c per test section are also representative values for the grass cover strength at the geometrical transition at the landward toe. However, the characteristics of the grass cover are highly variable within one test section, which implies that representative values for U_t and U_c are also variable between different locations along the dike profile. If the grass cover strength is higher at the transition compared to the landward slope, the calibrated values for the influence factors (r_0 and α_M) will be higher compared to the case with equal values for the grass cover strength at the transition and the landward slope.

Furthermore, if the actual grass cover strength at a test section exceeds the derived minimum values for U_t and U_c , the actual load increase at the geometrical transition is underestimated when minimum values for U_t and U_c are used for the model calibration. The calibration of the influence factors for Afsluitdijk 1 resulted in $r_0 = 0.20$ and $\alpha_M = 1.0$, which are relatively low values compared to the other test sections (Figure 4.4). These results suggest that the actual grass cover strength at the transition is higher than the derived minimum values for test section Afsluitdijk 1 and that the calibrated values for r_0 and α_M are underestimated.

The modelled mean erosion depth per r_0 -value for different threshold flow velocities U_t is compared to the measured erosion depth at the geometrical transition at Kattendijke 2 to analyse the sensitivity of the calibration parameter r_0 to U_t (Figure 5.1). Similarly, the

sensitivity of the load factor α_M to critical flow velocity U_c is analysed using flow acceleration method $\alpha_{\alpha, vdM}$ (Figure 5.2).

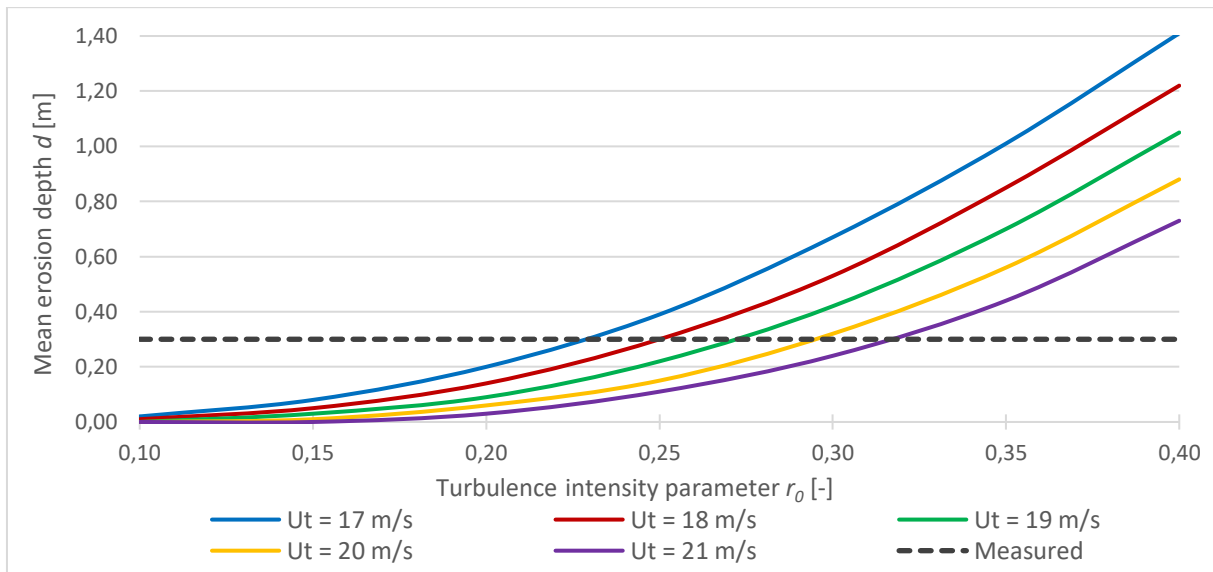


Figure 5.1 Comparison of the modelled mean erosion depth d per turbulence intensity parameter r_0 for different threshold flow velocities U_t to the measured erosion depth ($d = 0.30$ m) at the transition at the landward toe at Kattendijke section 2.

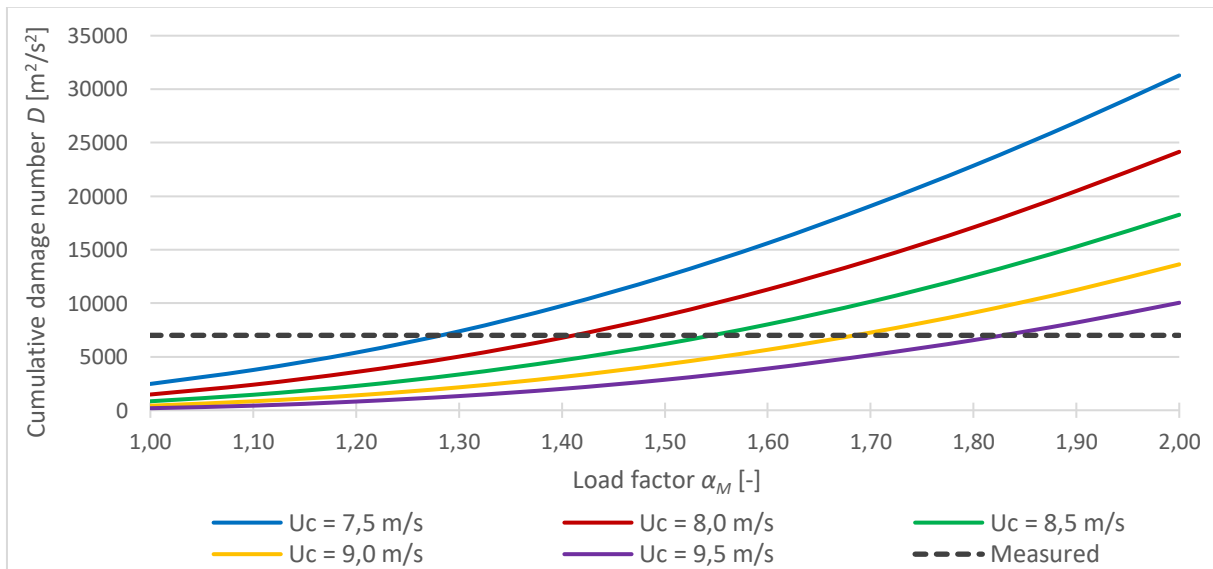


Figure 5.2 Comparison of the modelled damage number D per load factor α_M for different critical flow velocities U_c to the damage number for failure ($D = 7000$ m²/s²) at the transition at the landward toe at Kattendijke section 2. The flow acceleration method according to Van der Meer et al. (2015) is used.

The calibrated r_0 -values vary from $r_0 = 0.22$ for $U_t = 17$ m/s to $r_0 = 0.32$ for $U_t = 21$ m/s. The step size for U_t ($\Delta U_t = 1.0$ m/s) agrees with $\Delta r_0 = 0.02$ for the calibrated turbulence intensity parameter. The calibrated load factor varies from $\alpha_M = 1.28$ for $U_c = 7.5$ m/s to $\alpha_M = 1.82$ for $U_c = 9.5$ m/s. The step size $\Delta U_c = 0.5$ m/s agrees with $\Delta \alpha_M = 0.11$. The step size $\Delta U_t = 1.0$ m/s

for hydrodynamic-erosion model is comparable to the step size $\Delta U_c = 0.5$ m/s for the cumulative overload method (see Subsection 4.3.1.). Equation 17 (Subsection 4.3.2.) shows that $\alpha_M = 1.28$ is comparable to $r_0 = 0.15$ and that $\alpha_M = 1.82$ is comparable to $r_0 = 0.24$. These results show that $\Delta\alpha_M = 0.11$ for steps of $\Delta U_c = 0.5$ m/s in the cumulative overload method is similar to steps of $\Delta r_0 = 0.02$ for $\Delta U_t = 1.0$ m/s using the hydrodynamic-erosion model. So, the sensitivity of the load factor α_M to critical flow velocity U_c is comparable to the sensitivity of the turbulence intensity parameter r_0 to the threshold flow velocity U_t .

5.1.2. Erosion rate parameter

The hydrodynamic-erosion model is used to calibrate the turbulence intensity parameter r_0 for seven test sections. The modelled mean erosion depth for different r_0 -values are compared to the measured erosion depth at the geometrical transition at the landward toe to calibrate r_0 . One major variable for the hydrodynamic-erosion model is the inverse strength parameter C_E . This parameter determines the erosion rate for each wave for which the hydraulic load exceeds the threshold flow velocity. Equation 13 (Subsection 3.1.2.) shows that there is a linear relationship between the parameter C_E and the modelled erosion depth d . Therefore, it is likely that the assumed C_E -value has a significant influence on the calibration results.

For the model analysis, the inverse strength parameter was assumed to be $C_E = 1.0 \cdot 10^{-6}$ s/m, corresponding to a good grass quality (Hoffmans, 2012). To analyse the sensitivity of calibrated r_0 -values to C_E , the values $C_E = 2.0 \cdot 10^{-6}$ s/m (moderate grass quality), $C_E = 3.0 \cdot 10^{-6}$ s/m (poor grass quality) and $C_E = 4.0 \cdot 10^{-6}$ s/m (very poor grass quality) are also considered (Hoffmans, 2012). The sensitivity analysis is applied to test section Afsluitdijk 1 (Figure 5.3). The calibrated turbulence intensity parameter is $r_0 = 0.27$ for a good grass quality and decreases to $r_0 = 0.23$ for a moderate grass quality. The calibrated r_0 -value further decreases to $r_0 = 0.20$ for a poor grass quality and to $r_0 = 0.18$ for a very poor grass quality. Despite the inverse strength parameter C_E for a moderate grass quality is twice as large as the C_E for a good grass quality, the calibrated r_0 -value only decreases from $r_0 = 0.27$ to $r_0 = 0.23$.

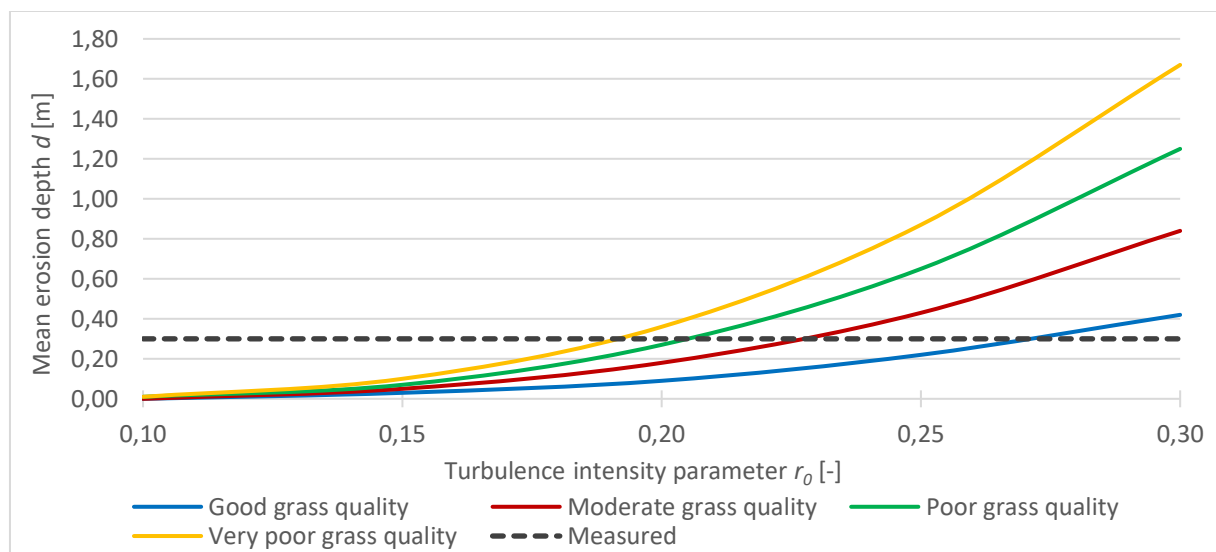


Figure 5.3 Comparison of the modelled mean erosion depth d per turbulence intensity parameter r_0 for different inverse strength parameters C_E to the measured erosion depth ($d = 0.30$ m) at the transition at the landward toe at Afsluitdijk 1.

Figure 5.3 further shows that the modelled mean erosion depth is highly dependent on the inverse strength parameter. The inverse strength parameter for a very poor grass quality is four times as large as the inverse strength parameter for a good grass quality. Because of the linear relationship between the inverse strength parameter and the erosion depth, the modelled erosion depth for a very poor grass quality is also four times as large as the modelled erosion depth for a good grass quality.

The damage at the landward slope and at the geometrical transition after each simulation with a mean overtopping discharge q_m is described in the factual reports. This means that parameters r_0 and α_M can both be calibrated for each simulation using the measured erosion depth and the damage numbers for the observed damage category, respectively. Examples of the calibration of influence factors using several simulations for test section Afsluitdijk 1 are provided for r_0 (Table 5.1) and α_M (Table 5.2).

The results for test section Afsluitdijk 1 show that the calibrated turbulence intensity parameter is $r_0 = 0.35$ after the simulation with $q_m = 10$ l/s/m and decreases to $r_0 = 0.20$ after the simulation with $q_m = 75$ l/s/m (Table 5.1). Similarly, the calibrated load factor is $\alpha_M = 1.5$ after the simulation with $q_m = 10$ l/s/m and decreases to $\alpha_M = 1.0$ after the final simulation with $q_m = 75$ l/s/m (Table 5.2).

Table 5.1 Calibration of the turbulence intensity parameter r_0 by comparison of the modelled mean erosion depth d to the measured erosion depth d_{obs} at the geometrical transition after different simulations with a mean overtopping discharge q_m for test section Afsluitdijk 1. Marked boxes show the calibrated r_0 -values based on the least difference between the modelled and measured erosion depth.

q_m [l/s/m]	U_t [m/s]	d_{obs} [m]	Mean erosion depth d [m] per turbulence intensity parameter r_0 [-]						
			$r_0 = 0.10$	$r_0 = 0.15$	$r_0 = 0.20$	$r_0 = 0.25$	$r_0 = 0.30$	$r_0 = 0.35$	$r_0 = 0.40$
1; 10	17	0.10	0.00	0.00	0.01	0.03	0.06	0.10	0.16
1; 10; 30	17	0.20	0.00	0.01	0.05	0.13	0.25	0.41	0.60
1; 10; 30; 50	17	0.25	0.01	0.05	0.16	0.37	0.66	1.04	1.49
1; 10; 30; 50; 75	17	0.35	0.03	0.15	0.42	0.86	1.46	2.21	3.07

Table 5.2 Calibration of the load factor α_M by comparison of the modelled damage number D to the damage number for the observed damage category D_{obs} at the geometrical transition after different simulations with a mean overtopping discharge q_m for test section Afsluitdijk 1. Flow acceleration according to the method by Van der Meer et al. (2015). Marked boxes show the calibrated α_M -values based on the least difference between the modelled damage number and the damage number for the observed damage category.

q_m [l/s/m]	U_c [m/s]	D_{obs} [m ² /s ²]	Damage number D [m ² /s ²] per load factor α_M [-]						
			$\alpha_M = 1.0$	$\alpha_M = 1.1$	$\alpha_M = 1.2$	$\alpha_M = 1.3$	$\alpha_M = 1.4$	$\alpha_M = 1.5$	$\alpha_M = 1.6$
1; 10	7.5	1000	56	125	232	393	602	868	1154
1; 10; 30	7.5	4000	921	1461	2173	3095	4264	5670	7240
1; 10; 30; 50; 75	7.5	7000	8835	12902	17819	23578	30138	37455	45454

High values for the influence factors r_0 and α_M were calibrated based on the grass cover erosion after simulations with relatively low mean overtopping discharges, $q_m = 10$ l/s/m and $q_m = 30$ l/s/m. Subsequently, the calibrated values of the influence factors decrease for simulations with larger mean overtopping discharges. The results suggest that the erosion rate decreases during the course of the wave overtopping simulator test (Table 5.1 and Table 5.2).

The decrease of the calibrated turbulence intensity parameter r_0 and the load factor α_M suggests that the erosion rate is depth-dependent. In case of test section Afsluitdijk 1, the first damage at the geometrical transition at the landward toe develops relatively fast during the simulation with $q_m = 10$ l/s/m. Once the grass sod is ruptured, the grass sod is washed away by the overtopping wave volumes. This already results in a mean erosion depth of 5 to 10 cm. Subsequently, larger mean overtopping discharges with a maximum of $q_m = 75$ l/s/m are simulated. The clay layer is exposed to the large overtopping wave volumes. However, the mean erosion depth only increases from 0.10 m to 0.35 m during the three simulations with the highest mean overtopping discharges (Table 5.1). The erosion pattern at test section Afsluitdijk 1 suggests that the inverse strength parameter C_E is relatively high for the grass sod and is low for the clay layer underneath.

Three categories for grass cover erosion have been observed at the geometrical transition during the wave overtopping tests at test section Afsluitdijk 1 (Table 5.2). First damage was observed after the simulation with $q_m = 10$ l/s/m. Various damages were observed after the simulation with $q_m = 30$ l/s/m and, finally, the failure criterium was met after the simulation with $q_m = 75$ l/s/m. According to Hoffmans et al. (2018), the cumulative overload method is most reliable for predicting damage category ‘failure’, while ‘first damage’ and ‘various damages are less predictable. This implies that the calibrated load factors are most reliable for test sections at which failure was observed, Kattendijke 1, Kattendijke 2, Afsluitdijk 1 and Tholen 4, while the calibrated load factors for test section Boonweg 1, Boonweg 2 and Afsluitdijk 2 are less reliable.

5.1.3. Flow acceleration method

Three methods to account for the acceleration of overtopping waves along slopes were used in the analysis using the cumulative overload method: a constant flow acceleration $\alpha_{a,vdM}$ (Van der Meer et al., 2015), the iterative method $\alpha_{a,SO}$ (Schüttrumpf and Oumeraci, 2005) and the analytical model $\alpha_{a,vB}$ (Van Bergeijk et al., 2019b). The simulations with the largest mean overtopping discharges, $q_m = 50$ l/s/m and $q_m = 75$ l/s/m, are now considered to compare the acceleration of all overtopping wave volumes between the different flow acceleration methods. Moderate conditions are assumed with a slope length $L_{slope} = 20$ m and a slope angle $\cot(\alpha) = 2.7$. These conditions result in a constant acceleration factor $\alpha_{a,vdM} = 1.47$.

Both the iterative method by Schüttrumpf and Oumeraci (2005) and the analytical model by Van Bergeijk et al. (2019b) are used to calculate the acceleration of overtopping waves along the dike profile as function of the slope length, the slope steepness and the wave overtopping volume. Both models are based on physics. Van Bergeijk et al. (2019b) has shown that the analytical model results in more accurate approximations of the flow acceleration compared to the iterative model by comparison of modelled overtopping flow velocities with flow velocity measurements.

The constant flow acceleration factor $\alpha_{a,vdM}$ (Van der Meer et al., 2015) is a simplification of the analytical method by Schüttrumpf and Oumeraci (2005). The constant flow acceleration factor $\alpha_{a,vdM}$ is determined from a graph as function of the length of the landward slope and the slope steepness $\cot(\alpha)$ (Van der Meer et al., 2015). This graph is derived from the iterative method by considering the largest wave overtopping volumes. Figure 5.4 shows that the flow acceleration factors for the iterative method ($\alpha_{a,SO}$) for the largest wave volumes are relatively low compared to the constant flow acceleration factor $\alpha_{a,vdM} = 1.47$. The difference between the derived flow acceleration factors for the largest wave volumes for both methods is likely

related to the assumptions that were made to derive a graph for constant flow acceleration factors as function of the slope length and slope steepness.

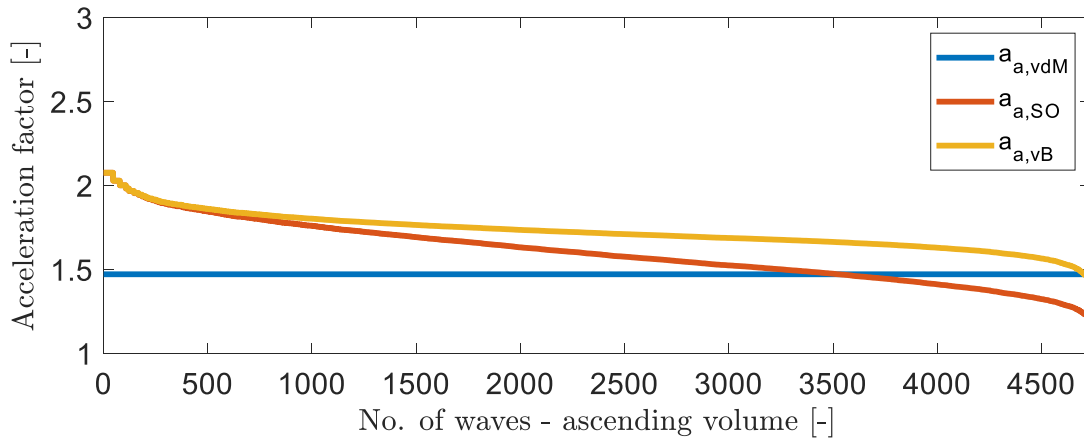


Figure 5.4 Comparison of the acceleration factors of wave overtopping volumes at the end of the slope using the graphical approach (Van der Meer et al., 2015), the iterative method (Schüttrumpf and Oumeraci, 2005) and the analytical approach (Van Bergeijk et al., 2019b) for simulations with the largest mean overtopping discharges ($q_m = 50$ l/s/m & $q_m = 75$ l/s/m). The slope length is $L_{slope} = 20$ m and the slope angle is $\cot(\alpha) = 2.7$.

Figure 5.4 shows that the acceleration factors for the iterative method ($\alpha_{a,SO}$) and the analytical model ($\alpha_{a,vB}$) are quite similar for small wave volumes. However, the difference between the flow acceleration factors for both methods increases for larger wave volumes. The analytical model ($\alpha_{a,vB}$) results in higher acceleration factors compared to the constant flow acceleration $\alpha_{a,vdM} = 1.47$, except for the largest wave volumes.

The damage numbers that were derived for grass cover failure for the cumulative overload method using three flow acceleration methods show the influence of the flow acceleration factors on the cumulative damage number. Based on the tests at the Vechtdijk, the derived damage numbers for failure are $D = 7000$ m²/s², $D = 3500$ m²/s² and $D = 13000$ m²/s² for a constant acceleration factor ($\alpha_{a,vdM}$), the iterative method ($\alpha_{a,SO}$) and the analytical model ($\alpha_{a,vB}$), respectively. The high damage number for $\alpha_{a,vB}$ is related to the relatively high hydraulic loads caused by the high flow acceleration factor for all wave volumes. Similarly, the iterative method $\alpha_{a,SO}$ results in a relatively low damage number for failure, because the flow acceleration factor is relatively low for the major part of the overtopping volumes.

The influence of the flow acceleration method on the maximum allowed mean overtopping discharge q_m is analysed in Figure 5.5. A critical flow velocity $U_c = 7$ m/s is used. For each flow acceleration method, the relative damage number for failure is calculated as function of the mean overtopping discharge q_m . The relative damage number D_{rel} is defined as the modelled damage number divided by the damage for the category 'failure'. Figure 5.5 shows that the maximum allowed overtopping discharge is approximately $q_m = 45$ l/s/m for $\alpha_{a,vdM}$ and $q_m = 48$ l/s/m for $\alpha_{a,vB}$. Table 3.2 is used to translate the maximum allowed overtopping discharge q_m into a minimum required free crest height R_c . Interpolation of R_c as function of q_m gives $R_c = 1.82$ m and $R_c = 1.78$ m for a $\alpha_{a,vdM}$ and $\alpha_{a,vB}$, respectively. Figure 5.5 further shows that $q_m = 75$ l/s/m does not yet result into failure of the grass cover for the iterative method for flow acceleration, which means that the minimum required free crest height is approximately 1.54 m (Table 3.2).

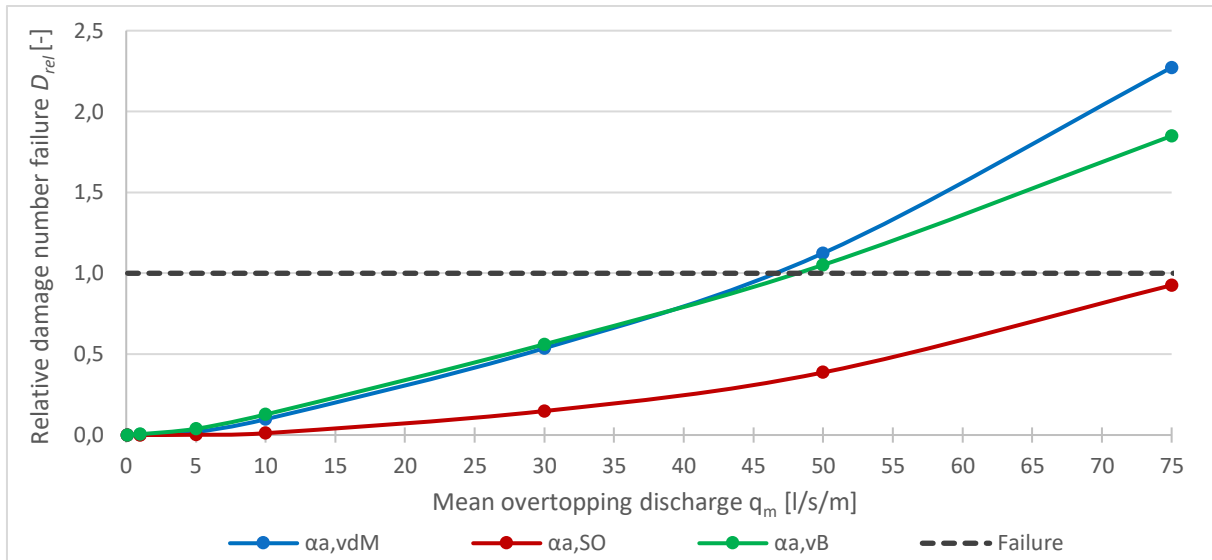


Figure 5.5 Comparison of the modelled relative damage number D_{rel} as function of the mean overtopping discharge q_m to the criterium for failure $D_{rel} = 1.0$ for three flow acceleration methods: $\alpha_{a,vdM}$ (Van der Meer et al., 2015), $\alpha_{a,SO}$ (Schüttrumpf and Oumeraci, 2005) and $\alpha_{a,vB}$ (Van Bergeijk et al., 2019b). The relative damage number is the modelled damage number divided by the damage number for the category ‘failure’. The slope length is $L_{slope} = 20$ m, the slope angle is $\cot(\alpha) = 2.7$ and the critical flow velocity is $U_c = 7$ m/s. Flow acceleration factor is $\alpha_{a,vdM} = 1.47$ according to the method by Van der Meer et al. (2015).

5.1.4. Influence factors

This subsection addresses the sensitivity of the maximum allowed mean overtopping discharge q_m and the minimum required free crest height R_c on the turbulence intensity parameter r_0 and the load factor α_M . Moderate conditions are assumed with a slope length $L_{slope} = 20$ m and a slope angle $\cot(\alpha) = 2.7$. These conditions result in a constant acceleration factor $\alpha_{a,vdM} = 1.47$. The threshold flow velocity is $U_t = 20$ m/s and the critical flow velocity is $U_c = 8$ m/s. Interpolation of the required free crest height R_c per mean overtopping discharge q_m (Table 3.2) is used to determine the minimum R_c for a specific q_m -value.

Figure 5.6 shows the modelled mean erosion depth d as function of the mean overtopping discharge q_m for four r_0 -values. The modelled erosion depth is compared to the failure criterium $d = 0.30$ m. In case of $r_0 = 0.10$ (no increased load at the transition), the modelled erosion depth for $q_m = 75$ l/s/m is much lower than the failure criterium. If $r_0 = 0.25$, the maximum overtopping discharge is $q_m = 60$ l/s/m and the minimum required crest height is $R_c = 1.65$ m. Similarly, $r_0 = 0.45$ results in a maximum overtopping discharge $q_m = 18$ l/s/m and the minimum required crest height $R_c = 2.30$ m. The maximum r_0 -value that was considered for the calibration, $r_0 = 0.60$, results in a maximum $q_m = 10$ l/s/m and a minimum $R_c = 2.61$ m.

The modelled cumulative damage number D as function of q_m is compared to failure criterium $D = 7000$ m²/s² for four α_M -values (Figure 5.7). The failure criterium is not exceeded by $q_m = 75$ l/s/m in case of no increased hydraulic load at the transition ($\alpha_M = 1.0$). The maximum overtopping discharge is $q_m = 60$ l/s/m and the minimum required crest height is $R_c = 1.65$ m for $\alpha_M = 1.3$. If $\alpha_M = 1.6$, the maximum allowed overtopping discharge is $q_m = 40$ l/s/m and the required free crest height is $R_c = 1.90$ m. The maximum allowed overtopping discharge is $q_m = 22$ l/s/m with a minimum free crest height $R_c = 2.20$ m using $\alpha_M = 2.0$.

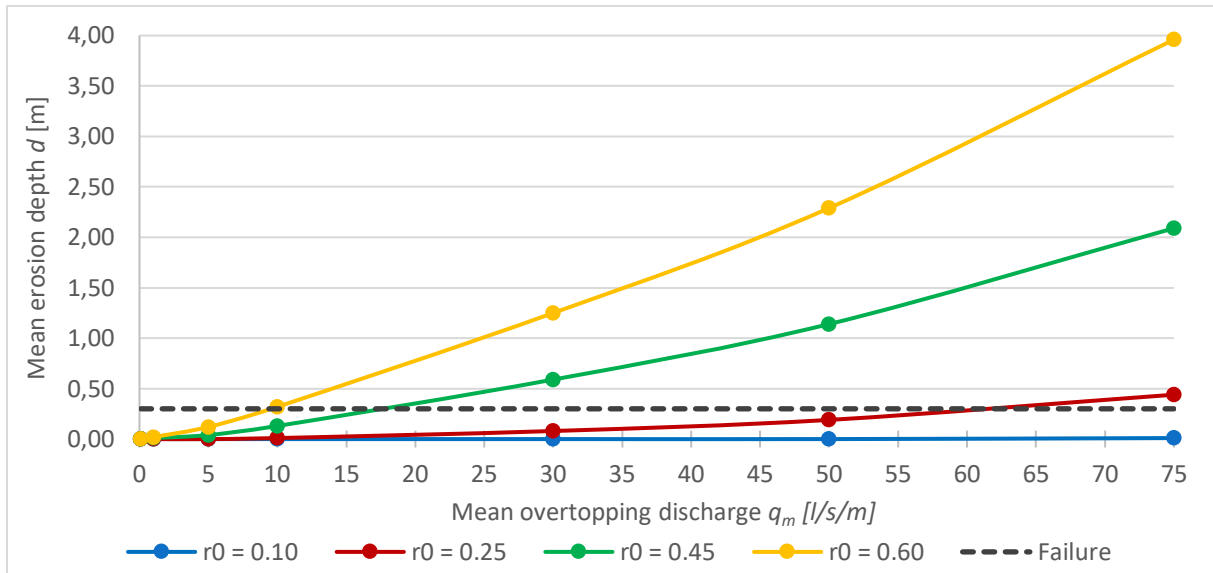


Figure 5.6 Comparison of the modelled mean erosion depth d as function of the mean overtopping discharge q_m for different values for turbulence intensity parameter r_0 to the criterium for failure $d = 0.30$ m. The slope length is $L_{slope} = 20$ m, the slope angle is $\cot(\alpha) = 2.7$ and the threshold flow velocity is $U_t = 20$ m/s.

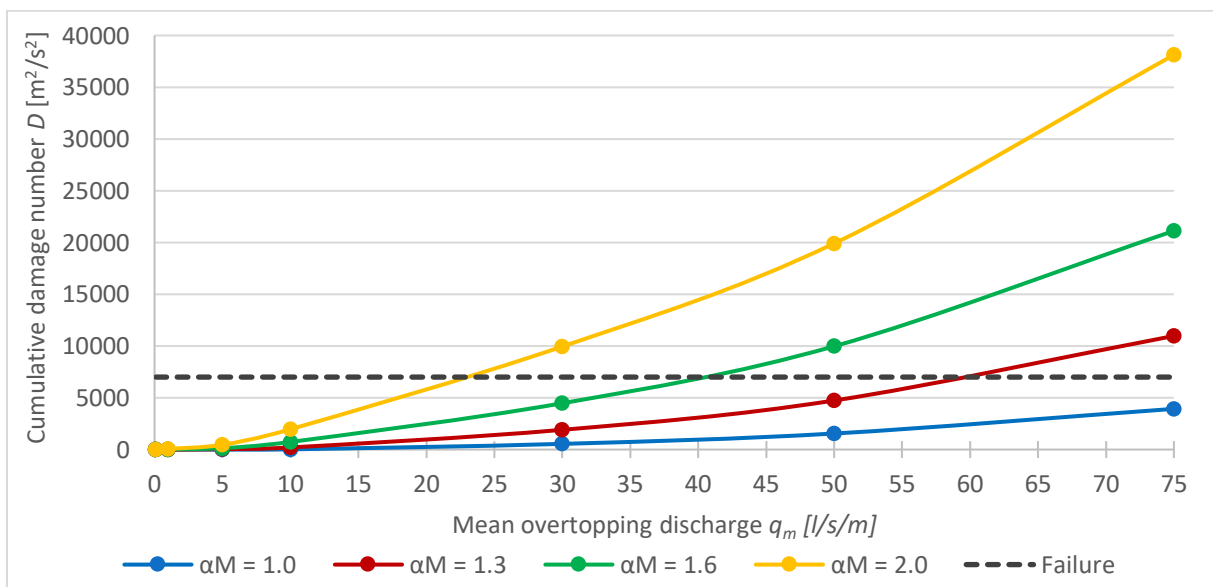


Figure 5.7 Comparison of the modelled cumulative damage number D as function of the mean overtopping discharge q_m for different values for load factor α_m to the criterium for failure $D = 7000$ m²/s². The slope length is $L_{slope} = 20$ m, the slope angle is $\cot(\alpha) = 2.7$ and the critical flow velocity is $U_c = 8$ m/s. Flow acceleration factor is $\alpha_{\alpha, v d M} = 1.47$ according to the method by Van der Meer et al. (2015).

5.2. Model approach

This section provides a reflection on the approach for the model analysis. First, the approach for modelling the influence of transitions on grass cover erosion by wave overtopping is discussed (Subsection 5.2.1.). Subsequently, it is discussed how the model applicability differs between the hydrodynamic-erosion model and the cumulative overload method.

5.2.1. Modelling the influence of transitions on grass cover erosion

This thesis has shown how representative values for the influence of transitions on grass cover erosion can be derived from the results of wave overtopping tests. The approach has been applied using two erosion models: the hydrodynamic-erosion model and the cumulative overload method. Both erosion models are applied to seven test sections with a geometrical transition at the landward toe (type T6).

The approach for modelling the influence of transitions on grass cover erosion can be divided in two steps. First, the grass cover strength parameter (U_t or U_c) is quantified based on the damage along the landward slope. Next, the derived grass cover strength parameter is used as model input for calibrating the influence factor (r_0 or α_M) based on the damage at the transition.

For both erosion models, it appears to be difficult to derive representative values for the grass cover strength parameters at the transition. In this thesis, minimum values of the threshold flow velocity U_t and the critical flow velocity U_c are determined based on no damage at the landward slope at each test section. It is assumed that the values for U_t and U_c are also representative for the grass cover strength at the geometrical transition. However, using a minimum value implies that it is likely that the actual grass cover strength at the transition is underestimated, which will result in relatively low values for the calibrated values for influence factors r_0 and α_M . Furthermore, the assumption that the grass cover strength at the landward slope and at the transition are similar is basically invalid, because measurements have shown that the grass cover strength is highly variable along test sections (Bijlard, 2015). The minimum grass cover strength, however, is expected to be less variable and therefore the minimum threshold and critical flow velocities are assumed to be representative input values for the calibration of the influence factors.

The approach for calibrating influence factors is applied to seven test sections with geometrical transitions. Similarly, the model approach can be applied to other transitions. The major obstacle for the application of the model approach to other transition types is to derive representative values for U_t and U_c . For the geometrical transition at the landward toe, the grass cover strength parameters are determined based on the damage at landward slopes where no other transitions were present. However, if transitions at dike crests are considered, it is less reliable to determine U_t and U_c based on the damage along the landward slope. It is likely that the grass cover erosion at the landward slope is influenced by erosion at the transition at the dike crest.

Basically, the approach for calibrating influence factors is not designed for including secondary aspects in the model approach. However, secondary aspects could be considered in the model analysis by adapting parameter values for the grass cover strength at transitions. For example, lower values for U_t and U_c can be used to account for a locally decreased grass cover strength at damaged spots near transitions in grass covers.

5.2.2. Model applicability

Two erosion models were considered in this thesis: the hydrodynamic-erosion model and the cumulative overload method. Furthermore, three flow acceleration methods for the cumulative overload method were used: a constant flow acceleration factor $\alpha_{\alpha, v d M}$ (Van der Meer et al., 2015), an iterative method $\alpha_{\alpha, S O}$ (Schüttrumpf and Oumeraci, 2005) and an analytical model $\alpha_{\alpha, v B}$ (Van Bergeijk et al., 2019b).

The turbulence intensity parameter r_0 is calibrated using the measured erosion depth at the transition. The load factor α_M is calibrated using the cumulative overload method by comparing the calculated cumulative damage number to the damage number for the observed damage category. Four damage categories are defined: no failure, first damage, various damages and failure. The damage number per category is calculated using the wave overtopping tests at four test sections at the Vechtdijk. At each test section, a grass cover with a moderate quality was present on top of a sand layer (Van der Meer, 2014). In the cumulative overload method, it is assumed that these derived damage numbers per damage category are representative for all test sections. However, the seven test sections that were studied in this thesis were all characterized by a grass cover on top of a clay layer (Van der Meer, 2014). It is likely that these different characteristics have a significant influence on the erosion process. Therefore, the derived damage numbers per damage category in the cumulative overload method are possibly not representative for grass cover erosion at test sections with a grass cover on top of a clay layer.

Using a measured erosion depth is more straightforward than using an observed damage category for calibration of influence factors. Besides, it is doubtful if the derived damage numbers per damage category are representative for test sections with a grass cover on top of a clay layer. Therefore, it is expected to be more reliable to use the hydrodynamic-erosion model, which relies on physics, than using an empirical model like the cumulative overload method.

The required input for the different erosion models is comparable. The hydrodynamic-erosion model requires to specify several parameters: the characteristics of the dike profile (e.g. crest width, slope length and slope steepness), the friction coefficient f for the cover type and the inverse strength parameter C_E . For the cumulative overload method, only the characteristics of the dike profile are required. If a constant flow acceleration is used, the flow acceleration factor $\alpha_{a,vdM}$ is determined based on the slope length and the slope steepness. If the iterative method and the analytical model are used for flow acceleration along the landward slope, it is also required to specify the friction coefficient f for the cover type.

Furthermore, the erosion models require wave characteristics as model input. If a constant flow acceleration method is used, only the initial flow velocity per overtopping wave is required for the cumulative overload method. Using the iterative model for flow acceleration ($\alpha_{a,SO}$), the initial layer thickness per overtopping wave is also required. The hydrodynamic-erosion model and the cumulative overload method using the analytical method for flow acceleration both additionally require the overtopping period and the overtopping discharge per wave.

6. Conclusions and recommendations

This research provides an analysis of the influence of transitions on grass cover erosion by wave overtopping. A model approach is introduced for deriving representative values for load increases and strength decreases by transitions in grass revetments on dikes. This approach describes how influence factors can be derived based on the development of grass cover erosion along the dike profile during wave overtopping tests using the hydrodynamic-erosion model and the cumulative overload method. Three different flow acceleration methods are used for the cumulative overload method.

Four problematic transition types for grass cover erosion are identified based on expert judgment and available data from the wave overtopping tests. Transition type T6, the geometrical transition at the landward toe, is selected for the model analysis. Both erosion models result in influence factors for seven test sections that represent the hydraulic load increase at the geometrical transitions. Finally, the results and the models are compared. This chapter provides the conclusions (Section 6.1.) and recommendations (Section 6.2.).

6.1. Conclusions

In this section, an answer to each research question is provided. Next, it is described how the research objective is met.

1. *Which transition types are most relevant for calibration of load and/or strength parameters using the hydrodynamic-erosion model and the cumulative overload method?*

Transitions types are analysed based on their problematic influence on grass cover erosion (1) according to four experts and (2) based on the availability of data resulting from wave overtopping tests for the transition type. This resulted in four problematic transition types: types T2, T3, T5 and T6. These transition types are determined to be suitable for calibration of parameters that represent the influence of the transition on grass cover erosion.

Horizontal transition types T2 and T3 are identified as vulnerable for grass cover erosion, because the grass cover strength at the transition decreases due to interruption of the grass sod and due to secondary aspects like tire tracks near roads. Besides, surface roughness differences (type T2) are expected to cause turbulence effects that result in hydraulic load increases at the transition.

Geometrical transition types T5 and T6 are also expected to be vulnerable for grass cover erosion. The inclination change results in a load increase at the geometrical transition. Furthermore, the interruption of the grass sod and surface roughness differences (type T5) are expected to increase the influence of the transition on grass cover erosion even more.

2. *What are calibrated values of the turbulence intensity parameter (r_0) to represent the load increase at the geometrical transition at the landward toe using the hydrodynamic-erosion model?*

The hydrodynamic-erosion model is used to determine the grass cover strength per test section in terms of the threshold flow velocity U_t . Minimum values for U_t are determined based on no erosion along the landward slope and resulted in threshold flow velocities that range from $U_t = 14$ m/s to $U_t = 22$ m/s for different test sections. The turbulence intensity parameter r_0 is calibrated based on the mean erosion depth at the transition. The calibrated values range from $r_0 = 0.20$ to $r_0 = 0.45$. Generally, the results show that the calibrated r_0 -

values are higher for relatively steep slopes compared to mild slopes, which agrees to the theory by Hoffmans et al. (2018). The calibration results show that representative values for the load increase at the geometrical transition are $r_0 = 0.25$ for mild slopes with $\cot(\alpha) = 2.9$ and $r_0 = 0.45$ for relatively steep slopes with $\cot(\alpha) = 2.3$.

3. *What are calibrated values of the load factor (α_M) to represent the load increase at the geometrical transition at the landward toe using the cumulative overload method?*

The grass cover strength is derived in terms of the minimum critical flow velocity U_c and is determined based on no damage at the landward slope. Subsequently, the load factor α_M is calibrated based on the damage number for the observed damage category at the transition using the cumulative overload method. Three methods are considered to account for the flow acceleration in the cumulative overload method: a constant acceleration factor $\alpha_{a,vdM}$ (Van der Meer et al., 2015), an iterative method $\alpha_{a,SO}$ (Schüttrumpf and Oumeraci, 2005) and an analytical model $\alpha_{a,vB}$ (Van Bergeijk et al., 2019b). Damage numbers per damage category are derived for the iterative method and the analytical model based on the wave overtopping tests at the Vechtdijk using a similar approach to Van der Meer et al. (2015).

The derived minimum critical flow velocities per test section depend on the flow acceleration method that is applied. The iterative method $\alpha_{a,SO}$ results in relatively low minimum critical flow velocities that range from $U_c = 5.0$ m/s to $U_c = 7.5$ m/s. The analytical model $\alpha_{a,vB}$ gives critical flow velocities between $U_c = 5.5$ m/s and $U_c = 9.5$ m/s. The highest minimum critical flow velocities are derived using a constant flow acceleration factor $\alpha_{a,vdM}$ with values varying from $U_c = 6.0$ m/s to $U_c = 10.0$ m/s. These results for different flow acceleration models show that using a constant flow acceleration factor $\alpha_{a,vdM}$ results in the highest hydraulic loads in the cumulative overload method. This is caused by the relatively high flow acceleration factors for the largest wave overtopping volumes.

Despite the derived critical flow velocities are different between the flow acceleration methods, the calibrated load factors per test section are quite similar for the three flow acceleration methods. The lowest load factor ($\alpha_M = 1.0$) is calibrated for section Afsluitdijk 1 for each flow acceleration method. The highest calibrated load factors are calibrated for test section Tholen 4 with $\alpha_M = 1.8$ for a constant flow acceleration factor $\alpha_{a,vdM}$ and $\alpha_M = 1.7$ for the iterative method $\alpha_{a,SO}$ and the analytical model $\alpha_{a,vB}$. Generally, the theoretical load factors for geometrical transitions as function of the landward slope steepness are exceeded by the calibrated load factors for each flow acceleration method.

Calibrated load factors per flow acceleration vary per test section and, therefore, it is difficult to determine representative values for mild slopes and relatively steep slopes. Upper limits of the calibrated load factor are assumed to be safe values for modelling the influence of geometrical transitions on grass cover erosion. If a constant flow acceleration factor ($\alpha_{a,vdM}$) is used, safe values are $\alpha_M = 1.6$ for mild slopes with $\cot(\alpha) = 2.9$ and $\alpha_M = 1.8$ for relatively steep slopes with $\cot(\alpha) = 2.3$. Using the iterative method ($\alpha_{a,SO}$), safe values are $\alpha_M = 1.6$ for mild slopes and $\alpha_M = 1.7$ for relatively steep slopes. The calibration results further show that $\alpha_M = 1.5$ for mild slopes and $\alpha_M = 1.7$ for relatively steep slopes are safe values using the analytical model ($\alpha_{a,vB}$).

The main objective of this research is introduced as:

To set up a general approach for the model analysis of the effects of transitions on grass cover erosion and to derive representative influence factors for a transition type.

This research has provided a model approach to determine the influence of transition types on grass cover erosion using the results from wave overtopping tests. The approach describes how the influence of a transition can be calibrated in terms of a load and/or strength factor based on the grass cover erosion at the transition. The approach is elaborated for two models for grass cover erosion by wave overtopping: the hydrodynamic-erosion model and the cumulative overload method. The model applied is applied for one transition type: the geometrical transition at the landward toe (type T6). The model analysis results in values for the turbulence intensity parameter r_0 and the load factor α_M for the hydrodynamic-erosion model and the cumulative overload method, respectively.

The derived threshold flow velocity U_t is at least twice as large as the critical flow velocity U_c , which can be related to different criteria for grass cover erosion in the hydrodynamic-erosion model and the cumulative overload method. The calibrated values for turbulence intensity parameter r_0 clearly show that high values ($r_0 = 0.45$) are representative for steep slopes, while low values ($r_0 = 0.25$) are representative for mild slopes. The calibration results using the cumulative overload method are less straightforward and, therefore, it is difficult to specify representative values for the load factor α_M for mild and steep slopes.

6.2. Recommendations

The model approach for deriving representative influence factors for transitions on grass cover erosion by wave overtopping is applied to the geometrical transition at the landward toe (type T6). The approach appears to be a practical way for deriving influence factors. It is recommended to further apply this approach to the other transition types that were identified as problematic: transition types T2 (horizontal transition with roughness difference), T3 (horizontal transition without roughness difference) and T5 (geometrical transition with roughness difference). Besides, it is recommended to apply the model approach to study the influence of secondary aspects, like local strength decreases, on grass cover erosion. This thesis has shown that the hydrodynamic-erosion model is better applicable to determine influence factors for specific dike characteristics, e.g. the landward slope steepness, than the cumulative overload method. Therefore, it is advised to use the hydrodynamic-erosion model for analyses of other transition types and secondary aspects.

The sensitivity of the calibrated turbulence intensity parameter r_0 to the threshold flow velocity U_t is similar to the sensitivity of calibrated load factor α_M to the critical flow velocity U_c . The threshold and critical flow velocity are input parameters for the erosion models and have a direct influence on the calibrated influence factors. It is recommended for future research to improve the method for determining threshold and critical flow velocities. It is of interest to consider the spatial variability of these parameters along dike sections.

The modelled erosion depth in the hydrodynamic-erosion model is linearly dependent on the inverse strength parameter C_E , which means that the calibrated r_0 -values are sensitive to the value of C_E . The model results have shown that the grass cover erodes relatively fast, but the erosion rate decreases during the continuation of the wave overtopping test using higher mean overtopping discharges. Probably, the inverse strength parameter C_E is depth-dependent. It is recommended to analyse the possibilities to distinguish between erosion of the grass sod and erosion of the clay layer to improve the hydrodynamic-erosion model.

Different flow acceleration methods were considered using the cumulative overload method. The method by Van der Meer et al. (2015) uses a constant flow acceleration factor, while it is

known that the flow acceleration depends on the wave overtopping volume. The volume-dependency of the acceleration of overtopping waves along landward slopes is included in the iterative method (Schüttrumpf and Oumeraci, 2005) and the analytical model (Van Bergeijk et al., 2019b). Comparison of modelled overtopping flow velocities to measurements showed that the modelled flow acceleration is more accurate using the analytical model compared to the iterative method (Van Bergeijk et al., 2019b). The iterative method underestimates the flow acceleration along the landward slope. Besides, the cumulative overload method can be easily adapted to include the analytical method for flow acceleration. Therefore, it is recommended to use the analytical method for flow acceleration of overtopping waves for application of the cumulative overload method.

The damage numbers per damage category in the cumulative overload method are calculated using wave overtopping tests at test sections at the Vechtdijk. These test sections were characterized by a grass cover on top of a sandy soil. In this research, the damage numbers per damage category are used for an analysis of transitions on test sections with a grass cover on a clay layer. It is likely that the damage numbers per damage category are not representative for clayey soil types. This possibly explains the large difference between the calibrated load factors and the theoretical load factors for geometrical transitions. Therefore, it is first recommended to derive damage numbers per damage category that are representative for a grass cover on top of a clay layer. Next, the calibration of load factors for the geometrical transition should be repeated using the new derived damage numbers and the calibrated values should again be compared to the theoretical factors. Subsequently, it could be considered to improve the theoretical load factors for geometrical transitions by Hoffmans et al. (2018) if the calibrated load factors are still not comparable to the theoretical values.

7. References

- Aguilar-López, J.P., Warmink, J.J., Bomers, A., Schielen, R.M.J. and Hulscher, S.J.M.H. (2018). *Failure of grass covered flood defences with roads on top due to wave overtopping: a probabilistic assessment method*. Journal of Marine Science and Engineering, 6(3), 74. DOI: 10.3390/jmse6030074.
- Akkerman, G.J., Van Gerven, K.A.J., Schaap, H.A. and Van der Meer, J.W. (2007). *Workpackage 3: development of alternative overtopping-resistant sea defences. Phase 3: wave overtopping erosion tests at Groningen sea dyke*.
- Bakker, J.J., Galema, A.A., Mom, R.J.C., and Steendam, G.J. (2010). *Factual report: Overslagproeven en afschuifproef Afsluitdijk*. Infram, project number 09i068.
- Bakker, J.J., Mom, R.J.C. and Steendam, G.J. (2008a). *Factual report: Golfoverslagproeven Friese Waddenzeedijk*. Infram, project number 07i107B.
- Bakker, J.J., Mom, R.J.C. and Steendam, G.J. (2008b). *Factual report: Golfoverslagproeven Zeeuwse zeedijken*. Infram, project number 08i011.
- Bakker, J.J., Mom, R.J.C. and Steendam, G.J. (2009). *Factual report: Overslagproeven en afschuifproef Afsluitdijk*. Infram, project number 09i002.
- Bakker, J.J., Mom, R.J.C., Steendam, G.J. and Van der Meer, J.W. (2011). *Factual report: Overslagproeven en oploopproof Tholen*. Infram, project number 10i092.
- Bakker, J.J., Melis, R. and Mom, R.J.C. (2013). *Factual report: Overslagproeven Rivierenland*. Infram, project number 12i071.
- Bijlard, R.W. (2015). *Strength of the grass sod on dike during wave overtopping*. Master thesis. Delft University of Technology.
- Bomers, A., Aguilar López, J.P., Warmink, J.J. and Hulscher, S.J.M.H. (2018). *Modelling effects of an asphalt road at a dike crest on dike cover erosion onset during wave overtopping*. Natural Hazards 2018, 1-30. DOI: 10.1007/s11069-018-3287-y.
- Calle, E.O.F. and Van der Meer, M. (2012). *SBW Golfoverslag en Bekledingen deelproject Overgangsconstructies*. Deltares report 1204204-011.
- ComCoast. (2007). *Design, construction, calibration and use of the wave overtopping simulator*.
- 't Hart, R., De Bruijn, H. and De Vries, G. (2016). *Fenomenologische beschrijving*. Deltares report 1220078-000.
- Hughes, S.A., Thornton, C.I., Van der Meer, J.W. and Scholl, B. N. (2012). *Improvements in describing wave overtopping processes*. Coastal Engineering Proceedings, 1(33), 35.
- Hughes, S., Thornton, C., Scholl, B., Youngblood, N., Beasley, J., Tucker, R. and Van der Meer, J.W. (2013). *Wave overtopping resiliency of grass and turf reinforcement mats on sandy soils*. Proceedings ICE, Coasts, Marine Structures and Breakwaters 2013, Edinburgh, UK.

- Hoffmans, G.J.C.M. (2012). *The influence of turbulence on soil erosion*. Eburon Uitgeverij BV.
- Hoffmans, G.J.C.M. (2015). *WTI 2017 Onderzoek en ontwikkeling landelijk toetsinstrumentarium. Product 5.8 Validatie erosiebestendigheid overgangen*. Deltares report 1209437-003-HYE-0001.
- Hoffmans, G., Van Hoven, A., Steendam, G.J., and Van der Meer, J.W. (2018). *Summary of research work about erodibility of grass revetments of dikes*. Proc. Protections 2018, Grange-over-Sands, UK.
- Le, H.T. (2011). *Destructive tests with the wave overtopping simulator. Two years of testing: Hai Phong, Nam Dinh and Thai Binh seadikes*. Communications on Hydraulic and Geotechnical Engineering, 2011-01, Delft University of Technology, Delft, The Netherlands.
- Le, H.T. (2012). *Wave overtopping simulator on a 1/15 slope protected by two local grass species*. Communications on Hydraulic and Geotechnical Engineering, 2012-02, Delft University of Technology, Delft, The Netherlands.
- Le, H.T., Van der Meer, J.W. and Verhagen, H.J. (2012). *Wave overtopping tests on sea dikes in Vietnam*.
- Ministerie van Infrastructuur en Milieu & Ministerie van Economische Zaken. (2017). *Deltaprogramma 2018*. Retrieved June 6th, 2019 from <https://www.deltacommissaris.nl/>
- Ministerie van Verkeer en Waterstaat. (2007). *Voorschrift Toetsen op Veiligheid Primaire Waterkeringen*.
- Peeters, P., De Vos, L., Vandevoorde, B., Taverniers, E. and Mostaert, F. (2012). *Erosiebestendigheid van de grasmat bij golfoverslag. Golfoverslagproeven Tielrodebroek. Version 2_0. WL Rapporten, 713_15b. Waterbouwkundig Laboratorium, INBO en afdeling Geotechniek: Antwerpen, België*.
- Pleijter, G., Van Steeg, P., Ter Horst, W., Van Hoek, M. and Pol, J. (2018). *Data analyse golfoverslag en overloop. Proeven proeflocatie Wijmeers*. HKV Lijn in water & Deltares, project number PR3517.10.
- Schüttrumpf, H. (2001). *Wellenüberlaufströmung bei Seedeichen – Experimentelle und Theoretische Untersuchungen*. PhD-Thesis. (Wave Overtopping Flow at Seadikes – Experimental and Theoretical Investigations). Retrieved June 6th, 2018, from <http://www.biblio.tu-bs.de/ediss/data/20010703a/20010703a.html>.
- Schüttrumpf, H. and Oumeraci, H. (2005). *Layer thicknesses and velocities of wave overtopping flow at seadikes*. Coastal Engineering, 52, p. 473-495.
- Thornton, C., Van der Meer, J.W., Scholl, B., Hughes, S. and Abt, S. (2010). *Testing levee slope resiliency at the new Colorado State University test facility*. Proc. Coastal Structures 2011, World Scientific, Singapore, p. 167-178.

- Thornton, C., Hughes, S., Scholl, B., and Youngblood, N. (2014). *Estimating grass slope resiliency during wave overtopping: results from full-scale overtopping simulator testing*. Proc. Coastal Engineering, 1(34):52.
- Van Bergeijk, V.M., Warmink, J.J., Frankena, M., Hulscher, S.J.M.H. (2019a). *Modelling dike cover erosion by overtopping waves: the effects of transitions*. Coastal Structures.
- Van Bergeijk, V.M., Warmink, J.J., Van Gent, M.R.A. and Hulscher, S.J.M.H. (2019b). *An analytical model for wave overtopping flow velocities on dike crests and landward slopes*. Coastal Engineering, 149, p. 28-38. DOI: 10.1016/j.coastaleng.2019.03.001.
- Van Hoven, A., Verheij, H., Hoffmans, G. and Van der Meer, J.W. (2013). *Evaluation and model development. Grass erosion test at the Rhine dike*. Deltares report 1207811-002-HYE-0007-svb.
- Van der Meer, J.W. (2014). *Samenvatting kengetallen en resultaten golfoverslag- en golfplooppoeven*. Concept edition.
- Van der Meer, J.W., Bernardini, P., Snijders, W. and Regeling, E. (2006). *The wave overtopping simulator*. Retrieved March 18, 2019, from www.vandermeerconsulting.nl/.
- Van der Meer, J.W., Hoffmans, G. and Van Hoven, A. (2015). *WTI Onderzoek en ontwikkeling landelijk toetsinstrumentarium: Product 5.12 Analyses grass erosion in wave run-up and wave overtopping conditions*. Deltares report 1209437-005-HYE-0003.
- Van der Meer, J.W., Hardeman, B., Steendam, G.J., Schüttrumpf, H. and Verheij, H. (2010). *Flow depths and velocities at crest and inner slope of a dike, in theory and with the Wave Overtopping Simulator*. ASCE, Proc. ICCE 2010, Shanghai.
- Van Steeg, P. (2014). *Bureaustudie overgangen met gras in primaire keringen*. Deltares report 1209380-006.
- Van Steeg, P. (2015). *Monitoring en fysieke modelproeven overgangen met grasbekledingen 2016-2020*. Deltares report 1220039-007.
- Van Steeg, P. and Van Hoven, A. (2013a). *Overgangen en overgangsconstructies*. Deltares report 1208394-000.
- Van Steeg, P. and Van Hoven, A. (2013b). *Overgangen bij grasbekledingen in primaire waterkeringen*. Deltares report 1208394-000.
- Young, M.J. (2005). *Wave overtopping and grass cover layer failure on the inner slope of dikes*. MSc-thesis, UNESCO-IHE, Delft.

Appendix 1 Wave overtopping tests in Vietnam and the USA

Similar to the wave overtopping tests in the Netherlands and Belgium, an overview of the tests in Vietnam and the United States is also provided. Similarly, information regarding the Vietnamese wave overtopping tests was found in Le (2011) and Le (2012). Descriptions of tests at the wave overtopping facility in the United States were provided in Thornton et al. (2010) and Thornton et al. (2014).

The Vietnamese wave overtopping simulator was used during tests at four locations from 2009 to 2012. Table A1.1 provides an overview of test conditions of wave overtopping tests in Vietnam. The wave regimes that were applied are constant with $H_s = 1.5$ m and $T_p = 6.0$ s. An increased wave height ($H_s = 2.0$ m) was applied at Yen Binh (section 3 and 4) in 2012. The steepness of the landward slope at Do Son, Thinh Long and Thai Tho is comparable to the test sections in the Netherlands and Belgium. During the tests at Yen Binh, however, a very mild slope (1:15) was tested.

Table A1.1 further shows that Carpet grass, Bermuda grass, Vetiver grass and a mixture of Bermuda grass and Vetiver grass were tested in Vietnam. The root structure and root depth of these grass types differ from the grass types on Dutch and Belgian dikes, which means that the erosion resistance of Vietnamese grass types is not comparable to those of grass types in the Netherlands and Belgium.

The reports of the Vietnamese tests include photographs of erosion along the slopes. Besides, manual measurements of erosion depths were used to compose profiles of erosion along the slope after each wave overtopping simulation. Flow data of the Vietnamese tests consist of measurements of layer thicknesses and overtopping durations. Furthermore, digital camera recordings were used to analyse front velocities of overtopping waves during the Vietnamese tests.

Table A1.1 Overview test conditions of wave overtopping tests in Vietnam including the wave height H_s , the wave period T_p , the steepness of the landward slope $\cot(\alpha)$ and the revetment type.

Location – year (reference)	Section	H_s [m]	T_p [s]	$\cot(\alpha)$ [-]	Revetment type
Do Son – 2009 (Le, 2011)	1	1.5	6.0	2.0	Vetiver grass
Thinh Long – 2010 (Le, 2011)	1	1.5	6.0	3.0	Bermuda grass
	2	1.5	6.0	3.0	Bermuda grass
	3	1.5	6.0	3.0	Bermuda grass
Thai Tho – 2010 (Le, 2011)	1	1.5	6.0	3.0	Bermuda & Vetiver grass
	2	1.5	6.0	3.0	Bermuda & Vetiver grass
	3	1.5	6.0	3.0	Bermuda & Vetiver grass
Yen Binh – 2012 (Le, 2012)	1	1.5	6.0	15.0	Bermuda grass
	2	1.5	6.0	15.0	Bermuda grass
	3	1.5 & 2.0	6.0	15.0	Carpet grass
	4	2.0	6.0	15.0	Carpet grass

The wave overtopping facility at Colorado State University in the United States was used during 22 wave overtopping tests in 2010 and 2012. The tests in 2010 included grass types that were representative for dikes in the New Orleans District and were built on top of a clayey subsoil (Thornton et al., 2014). The tests in 2012 were representative for the Jacksonville District considering a sandy subsoil (Thornton et al., 2014).

Table A1.2 shows the test conditions that were applied during tests with the wave overtopping facility in the United States. Because the simulator is fixed-in-place, the landward slope angle does not differ between the tests.

Table A1.2 Overview test conditions of wave overtopping tests in the United States including the wave height H_s , the wave period T_p , the steepness of the landward slope $\cot(\alpha)$ and the revetment type.

Location – year (reference)	Test no.	H_s [m]	T_p [s]	$\cot(\alpha)$ [-]	Revetment type
Colorado State University – 2010 (Thornton et al., 2010)	1	2.4	9.0	3.0	Bare clay
	2	2.4	9.0	3.0	Bermuda grass
	3	2.4	9.0	3.0	Bahia grass
	4	2.4	9.0	3.0	Bermuda grass (reinforced)
	5	2.4	9.0	3.0	Bermuda grass (reinforced)
	6	2.4	9.0	3.0	Bermuda grass (reinforced)
	7	2.4	9.0	3.0	Lime-stabilized clay
	8	2.4	9.0	3.0	Articulated concrete blocks
	9	2.4	9.0	3.0	Dormant Bermuda grass
	10	2.4	9.0	3.0	Dormant Bermuda grass (reinforced)
	11	2.4	9.0	3.0	Dormant Bermuda grass (reinforced)
Colorado State University – 2012 (Thornton et al., 2014)	1	2.4	7.7	3.0	Bahia grass (50% coverage)
	2	2.4	7.7	3.0	Bahia grass (30% coverage)
	3	1.5	7.7	3.0	Bahia grass (30% coverage)
	4	1.4	3.4	3.0	Bahia grass (50% coverage)
	5	2.0	4.5	3.0	Bahia grass (50% coverage)
	6	2.0	4.5	3.0	Bahia grass (50% coverage, reinforced)
	7	2.0	4.5	3.0	Bahia grass (50% coverage)
	8	2.2	6.0	3.0	Bahia grass (50% coverage)
	9	1.4	3.4	3.0	Bahia grass (50% coverage)
	10	2.0	4.5	3.0	Bahia grass (50% coverage)
	11	2.0	4.5	3.0	Bahia grass (50% coverage, reinforced)

Table A1.2 shows that a constant wave regime ($H_s = 2.4$ m and $T_p = 9.0$ s) was applied during tests in 2010. Those tests focused on the erosion resistance of different revetment types to fixed wave conditions. The results show that three grass types (Bahia grass, Bermuda grass and Dormant Bermuda grass) were tested. Also, five of eleven tests in 2010 included grass mat reinforcement systems. Other revetment types that were tested are bare clay, lime-stabilized clay and articulated concrete blocks.

The tests at the wave overtopping facility in the United States addressed the effect of all kinds of wave regimes to one grass type (Bahia grass) in 2012. Table shows that two tests considered a grass coverage of 30%, while the remaining tests considered 50% grass coverage. Also, two reinforced grass mats were tested. The tests in 2012 showed a wide variety of wave regimes, with wave heights varying from 1.4 to 2.4 m and wave periods between 3.4 and 7.7 s.

The erosion data of the tests at the wave overtopping facility consist of photographs and descriptions of erosion depths and surfaces which were manually measured. The hydraulic data consist of measurements of layer thicknesses and flow velocities.

No transitions were tested at the wave overtopping facility in the United States. Fourteen transitions were tested during the Vietnamese wave overtopping tests (Table A1.3).

Table A1.3 Overview of tested transition types in Vietnam.

Type	Location	Description	Remarks	Case
T3	Thai Tho 1	Concrete beam (horizontal) at slope	-	Yes
T3	Thai Tho 2	Concrete beam (horizontal) at slope	-	Yes
T3	Thai Tho 3	Concrete beam (horizontal) at slope	Erosion related to T9-transition	No
T6	Thinh Long 1	Landward toe	-	Yes
T6	Thinh Long 2	Landward toe	No erosion at transition	No
T6	Thinh Long 3	Landward toe	No erosion at transition	No
T6	Thai Tho 1	Landward toe	No erosion at transition	No
T6	Thai Tho 2	Landward toe	No erosion at transition	No
T6	Thai Tho 3	Landward toe	No erosion at transition	No
T9	Thai Tho 2	Concrete beam (vertical) at slope	Erosion related to T3-transition	No
T9	Thai Tho 3	Concrete beam (vertical) at slope	-	Yes
T13	Thinh Long 2	Trees (\varnothing 0.10 m)	-	Yes
T13	Yen Binh 1	Round concrete obstacle at slope	-	Yes
T13	Yen Binh 4	Square concrete obstacle at slope	-	Yes

Concrete frames, consisting of horizontal and vertical beams, were present in the grass revetment at Thai Tho during the Vietnamese wave overtopping tests (Figure A1.1). Three T3-transitions were tested at Thai Tho. Each transition regards to a horizontal concrete beam at the slope. At section 1 and at section 2, erosion started to develop near the horizontal beam. At the third section, erosion was also observed near the horizontal beam, however, initiation of erosion took place along the vertical concrete beam. At Thai Tho, section 2 and section 3, also vertical beams (type T9) were present in the grass revetment. Erosion at section 3 started near the vertical beam, while erosion started near the horizontal beam at section 2 (Figure A1.1). The landward toe was tested at six Vietnamese sections. However, erosion was only observed at section 1 at Thinh Long. Therefore, only one T6-case is appropriate to consider in the model studies. Furthermore, three objects (type T13) have been considered during the Vietnamese wave overtopping tests. Grass cover erosion was observed at each object, which consisted of trees, a round concrete obstacle and a squared concrete obstacle.



Figure A1.1 Presence of a concrete frame with horizontal and vertical beams in the grass revetment at Thai Tho, Vietnam, before testing (left) and after testing (right). Figure adapted from Le (2011).

Appendix 2 Damage numbers per flow acceleration method

Representative damage numbers were derived for four damage categories from the wave overtopping tests at the Vechtdijk in 2011 using the cumulative overload method and constant flow acceleration factors (Van der Meer et al., 2015). Table A2.1 provides an overview of the wave overtopping simulations that were applied until a damage category was observed. The simulations are expressed in terms of mean overtopping discharges (q_m). Generally, simulations per mean overtopping discharge lasted six hours. Durations of final simulations are indicated and test characteristics are given in terms of the distance between the start of the slope and the eroded spot (L), the landward slope steepness ($\cot(\alpha)$) and the constant acceleration factor ($\alpha_{a,vdM}$) according to Van der Meer et al. (2015) (Table A2.1).

Table A2.1 Overview data wave overtopping tests at the Vechtdijk in 2011. Simulated mean overtopping discharges q_m [l/s/m] until observation of damage category are given together with the duration of the final simulations. Test characteristics are given in terms of the of the distance between the start of the slope and the eroded spot L , the landward slope steepness $\cot(\alpha)$ and the constant acceleration factor $\alpha_{a,vdM}$ according to Van der Meer et al. (2015).

	Simulated mean overtopping discharge q_m [l/s/m] and duration final simulation	L [m]	$\cot(\alpha)$ [-]	$\alpha_{a,vdM}$ [-]
Section 1 (Hs = 1 m)				
First damage	0.1; 1; 10; 30 (1:58 h)	5	4.9	1.14
Various damages	0.1; 1; 10; 30 (6:00 h)	5	4.9	1.14
Failure	0.1; 1; 10; 30; 50 (2:07 h)	5	4.9	1.14
No damage	-	-	-	-
Section 2 (Hs = 2 m)				
First damage	0.1; 1 (6:00 h)	10	3.0	1.36
Various damages	0.1; 1; 5; 10 (3:00 h)	10	3.0	1.36
Failure	-	-	-	-
No damage	0.1; 1; 5; 10; 30; 50 (0:23 h)	12	3.0	1.36
Section 3 (Hs = 2m)				
First damage	0.1; 1; 5; 10 (4:00 h)	14	4.9	1.15
Various damages	0.1; 1; 5; 10; 30 (2:00 h)	14	4.9	1.15
Failure	-	-	-	-
No damage	0.1; 1; 5; 10; 30; 50 (1:01 h)	14	4.9	1.15
Section 4 (Hs = 3 m)				
First damage	0.1; 1; 5 (2:00 h)	3.5	4.9	1.12
Various damages	0.1; 1; 5 (6:00 h)	3.5	4.9	1.12
Failure	0.1; 1; 5; 10; 30 (1:03 h)	16	4.9	1.21
No damage	-	-	-	-

The cumulative overload method is applied to derive representative damage numbers for the flow acceleration method by Van der Meer et al. (2015). From this analysis was concluded that derive damage numbers per damage category were most comparable for a critical flow velocity $U_c = 3.5$ m/s.

The analysis of by Van der Meer et al. (2015) is reproduced (Figure A2.1) and is applied to recalculate representative damage numbers for the volume-dependent flow acceleration methods by Schüttrumpf and Oumeraci (2005) and Van Bergeijk et al. (2019b) (Figure A2.2 and Figure A2.3, respectively).

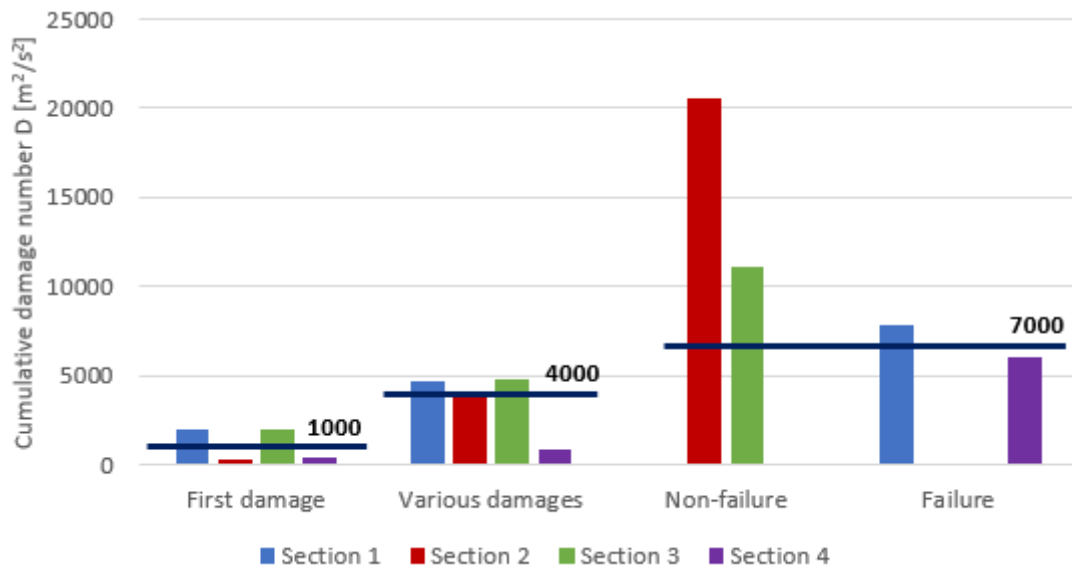


Figure A2.1 Reproduced cumulative damage numbers per damage category per test section together with threshold damage numbers per category using the flow acceleration method by Van der Meer et al. (2015).

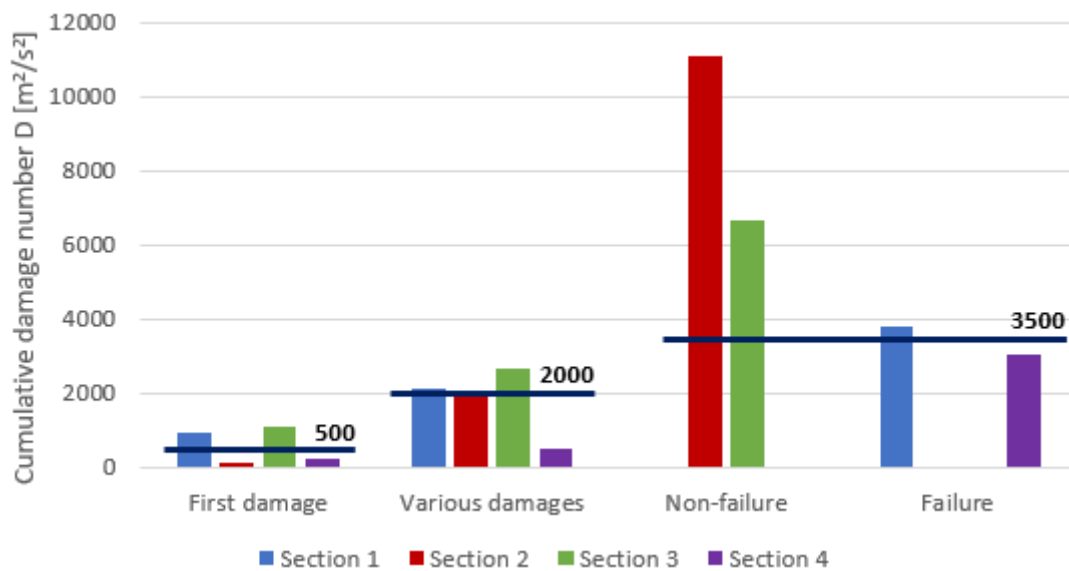


Figure A2.2 Reproduced cumulative damage numbers per damage category per test section together with threshold damage numbers per category using the flow acceleration method by Schüttrumpf and Oumeraci (2005).

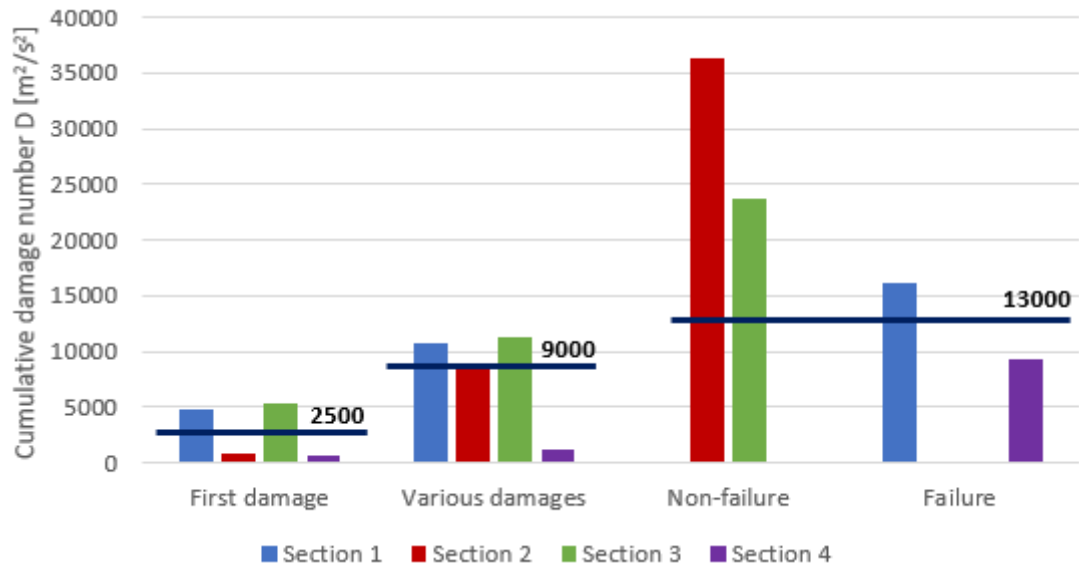


Figure A2.3 Reproduced cumulative damage numbers per damage category per test section together with threshold damage numbers per category using the flow acceleration method by Van Bergeijk et al. (2019b).

Appendix 3 Results hydrodynamic-erosion model

This appendix provides the extensive results of the analysis using the hydrodynamic-erosion model. Minimum values for the threshold flow velocity U_t are derived for each test section based on an observed erosion depth $d = 0.00$ m at the end of the landward slope (Table A3.1).

Table A3.1 Overview of the derivation of the threshold flow velocity U_t [m/s] per test section by comparison of the modelled mean erosion depth d_s [m] to the measured erosion depth d [m] at the end of the slope. Data per test section is provided in terms of the slope length L_{slope} [m], the crest width L_{crest} [m], the steepness of the landward slope $\cot(\alpha)$ [-] and the simulated mean overtopping discharge q_m [l/s/m]. Marked boxes indicate the derived minimum threshold flow velocities.

	L_{slope} [m]	L_{crest} [m]	$\cot(\alpha)$ [-]	q_m [l/s/m]	d [m]	Modelled mean erosion depth d_s [m] at the slope per threshold flow velocity U_t [m]				
						$U_t = 18$ m/s	$U_t = 19$ m/s	$U_t = 20$ m/s	$U_t = 21$ m/s	$U_t = 22$ m/s
Boonweg 1	27.0	2.5	2.9	0.1; 1; 10; 30; 50; 75	0.00	0.09	0.05	0.03	0.01	0.00
Boonweg 2	27.0	2.5	2.9	0.1; 1; 10; 30; 50; 75	0.00	0.09	0.05	0.03	0.01	0.00
Kattendijke 1	15.0	2.0	3.0	0.1; 1; 10; 30; 50	0.00	0.08	0.04	0.02	0.01	0.00
Kattendijke 2	17.0	0.5	3.0	30; 50	0.00	0.09	0.05	0.03	0.01	0.00
Afsluitdijk 1	7.8	0.5	2.3	1; 10; 30	0.00	0.08	0.04	0.02	0.01	0.00
Afsluitdijk 2	7.5	0.7	2.3	1; 10	0.00	0.05	0.03	0.02	0.01	0.00
Tholen 4	14.0	2.0	2.3	1; 5; 10	0.00	0.05	0.03	0.02	0.01	0.00

The turbulence intensity parameter r_0 is calibrated by comparison of the modelled mean erosion depth to the measured mean erosion depth at the geometrical transition at the landward toe (Table A3.2).

Table A3.2 Overview of the calibration of turbulence intensity parameter r_0 [-] per test section by comparison of the modelled mean erosion depth d_t [m] to the measured erosion depth d [m] at the geometrical transition at the landward toe. Data per test section is provided in terms of the slope length L_{slope} [m], the crest width L_{crest} [m], the berm width L_{berm} [m], the steepness of the landward slope $\cot(\alpha)$ [-], the simulated mean overtopping discharge q_m [l/s/m] and the threshold flow velocity U_t [m/s]. Marked boxes indicate the calibrated values for the turbulence intensity parameter r_0 .

	L_{slope} [m]	L_{crest} [m]	L_{berm} [m]	$\cot(\alpha)$ [-]	q_m [l/s/m]	d [m]	U_t [m/s]	Modelled mean erosion depth d_t [m] at the transition per turbulence intensity parameter r_0 [-]										
								0.10	0.15	0.20	0.25	0.30	0.35	0.40	0.45	0.50	0.55	0.60
Boonweg 1	27.0	2.5	1.0	2.9	0.1; 1; 10; 30; 50;	0.10	22	0.00	0.01	0.05	0.14	0.29	0.54	0.88	1.32	1.84	2.43	3.11
Boonweg 1	27.0	2.5	2.0	2.9	0.1; 1; 10; 30; 50; 75	0.30	22	0.00	0.03	0.12	0.33	0.68	1.19	1.84	2.65	3.60	4.68	5.88
Boonweg 2	27.0	2.5	2.0	2.9	0.1; 1; 10; 30; 50; 75	0.30	22	0.00	0.03	0.12	0.33	0.68	1.19	1.84	2.65	3.60	4.68	5.88
Kattendijke 1	15.0	2.0	2.0	3.0	0.1; 1; 10; 30; 50	0.20	19	0.00	0.02	0.08	0.20	0.40	0.69	1.06	1.50	2.01	2.58	3.20
Kattendijke 2	17.5	2.5	2.0	3.0	30; 50	0.30	19	0.00	0.02	0.09	0.22	0.42	0.70	1.05	1.46	1.93	2.45	3.02
Afsluitdijk 1	7.8	0.5	0.8	2.3	1; 10	0.10	17	0.00	0.00	0.01	0.03	0.06	0.10	0.16	0.23	0.30	0.39	0.48
Afsluitdijk 1	7.8	0.5	2.4	2.3	1; 10; 30	0.20	17	0.00	0.01	0.05	0.13	0.25	0.41	0.60	0.82	1.07	1.34	1.64
Afsluitdijk 1	7.8	0.5	2.4	2.3	1; 10; 30; 50	0.25	17	0.01	0.05	0.16	0.37	0.66	1.04	1.49	2.00	2.57	3.19	3.85
Afsluitdijk 1	7.8	0.5	2.4	2.3	1; 10; 30; 50; 75	0.35	17	0.03	0.15	0.42	0.86	1.46	2.21	3.07	4.04	5.12	6.28	7.53
Afsluitdijk 2	7.5	0.7	2.0	2.3	1; 10	0.30	14	0.00	0.01	0.03	0.06	0.10	0.15	0.21	0.28	0.35	0.43	0.51
Tholen 4	14.0	2.0	0.5	2.3	1; 5	0.20	16	0.00	0.00	0.01	0.02	0.04	0.07	0.10	0.14	0.18	0.23	0.28
Tholen 4	14.0	2.0	1.5	2.3	1; 5; 10	0.40	16	0.00	0.01	0.04	0.09	0.15	0.24	0.33	0.45	0.57	0.71	0.85

Appendix 4 Results cumulative overload method

This appendix provides the extensive results of the analysis using the cumulative overload method. Three flow acceleration methods are considered.

1. Derivation critical flow velocity (U_c) per test section:

a. Flow acceleration method according to Van der Meer et al. (2015) - $\alpha_{\alpha,vdM}$:

Table A4.1 Overview of the derivation of the critical flow velocity U_c [m/s] per test section by comparison of the modelled damage number D_s [m^2/s^2] to the damage number D [m^2/s^2] for the observed damage category at the end of the landward slope. Data per test section is provided in terms of the slope length L_{slope} [m], the steepness of the landward slope $\cot(\alpha)$ [-], the flow acceleration factor $\alpha_{\alpha,vdM}$ (Van der Meer et al., 2015) and the simulated mean overtopping discharge q_m [l/s/m]. Marked boxes indicate the derived minimum critical flow velocities.

	L_{slope} [m]	$\cot(\alpha)$ [-]	$\alpha_{\alpha,vdM}$ [-]	q_m [l/s/m]	D [m^2/s^2]	Modelled damage number D_s [m] at the slope per critical flow velocity U_c [m]				
Boonweg 1	27.0	2.9	1.46	0.1; 1; 10; 30; 50; 75	0 - 1000	$U_c = 9.0$ m/s 2107	$U_c = 9.5$ m/s 1182	$U_c = 10.0$ m/s 603	$U_c = 10.5$ m/s 272	$U_c = 11.0$ m/s 116
Boonweg 2	27.0	2.9	1.46	0.1; 1; 10; 30; 50; 75	0 - 1000	$U_c = 9.0$ m/s 2107	$U_c = 9.5$ m/s 1182	$U_c = 10.0$ m/s 603	$U_c = 10.5$ m/s 272	$U_c = 11.0$ m/s 116
Kattendijk 1	15.0	3.0	1.41	0.1; 1; 10; 30; 50	0 - 1000	$U_c = 7.5$ m/s 2333	$U_c = 8.0$ m/s 1372	$U_c = 8.5$ m/s 769	$U_c = 9.0$ m/s 380	$U_c = 9.5$ m/s 166
Kattendijk 2	17.0	3.0	1.42	30; 50	0 - 1000	$U_c = 7.5$ m/s 2460	$U_c = 8.0$ m/s 1473	$U_c = 8.5$ m/s 839	$U_c = 9.0$ m/s 425	$U_c = 9.5$ m/s 190
Afsluitdijk 1	7.8	2.3	1.46	1; 10; 30	0 - 1000	$U_c = 6.5$ m/s 2582	$U_c = 7.0$ m/s 1554	$U_c = 7.5$ m/s 921	$U_c = 8.0$ m/s 528	$U_c = 8.5$ m/s 292
Afsluitdijk 2	7.5	2.3	1.46	1; 10	0 - 1000	$U_c = 5.0$ m/s 1861	$U_c = 5.5$ m/s 1133	$U_c = 6.0$ m/s 667	$U_c = 6.5$ m/s 339	$U_c = 7.0$ m/s 148
Tholen 4	14.0	2.3	1.46	1; 5; 10	0 - 1000	$U_c = 5.0$ m/s 3221	$U_c = 5.5$ m/s 1952	$U_c = 6.0$ m/s 1127	$U_c = 6.5$ m/s 628	$U_c = 7.0$ m/s 306

b. Flow acceleration method according to Schüttrumpf and Oumeraci (2005) - $\alpha_{a,SO}$:

Table A4.2 Overview of the derivation of the critical flow velocity U_c [m/s] per test section by comparison of the modelled damage number D_s [m^2/s^2] to the damage number D [m^2/s^2] for the observed damage category at the end of the landward slope. Data per test section is provided in terms of the slope length L_{slope} [m], the crest width L_{crest} [m], the steepness of the landward slope $\cot(\alpha)$ [-] and the simulated mean overtopping discharge q_m [l/s/m]. Flow acceleration according to Schüttrumpf and Oumeraci (2005). Marked boxes indicate the derived minimum critical flow velocities.

	L_{slope} [m]	L_{crest} [m]	$\cot(\alpha)$ [-]	q_m [l/s/m]	D [m^2/s^2]	Modelled damage number D_s [m] at the slope per critical flow velocity U_c [m]				
Boonweg 1	27.0	2.5	2.9	0.1; 1; 10; 30; 50; 75	0 - 500	$U_c = 6.5$ m/s 1354	$U_c = 7.0$ m/s 560	$U_c = 7.5$ m/s 187	$U_c = 8.0$ m/s 49	$U_c = 8.5$ m/s 6
Boonweg 2	27.0	2.5	2.9	0.1; 1; 10; 30; 50; 75	0 - 500	$U_c = 6.5$ m/s 1354	$U_c = 7.0$ m/s 560	$U_c = 7.5$ m/s 187	$U_c = 8.0$ m/s 49	$U_c = 8.5$ m/s 6
Kattendijk 1	15.0	2.0	3.0	0.1; 1; 10; 30; 50	0 - 500	$U_c = 5.5$ m/s 1387	$U_c = 6.0$ m/s 620	$U_c = 6.5$ m/s 241	$U_c = 7.0$ m/s 69	$U_c = 7.5$ m/s 8
Kattendijk 2	17.0	2.5	3.0	30; 50	0 - 500	$U_c = 5.5$ m/s 1313	$U_c = 6.0$ m/s 592	$U_c = 6.5$ m/s 228	$U_c = 7.0$ m/s 64	$U_c = 7.5$ m/s 7
Afsluitdijk 1	7.8	0.5	2.3	1; 10; 30	0 - 500	$U_c = 5.0$ m/s 1826	$U_c = 5.5$ m/s 800	$U_c = 6.0$ m/s 341	$U_c = 6.5$ m/s 134	$U_c = 7.0$ m/s 45
Afsluitdijk 2	7.5	0.7	2.3	1; 10	0 - 500	$U_c = 4.0$ m/s 1275	$U_c = 4.5$ m/s 595	$U_c = 5.0$ m/s 243	$U_c = 5.5$ m/s 67	$U_c = 6.0$ m/s 13
Tholen 4	14.0	2.0	2.3	1; 5; 10	0 - 500	$U_c = 4.0$ m/s 1811	$U_c = 4.5$ m/s 847	$U_c = 5.0$ m/s 355	$U_c = 5.5$ m/s 110	$U_c = 6.0$ m/s 22

c. Flow acceleration method according to Van Bergeijk et al. (2019b) - $\alpha_{a,vB}$:

Table A4.3 Overview of the derivation of the critical flow velocity U_c [m/s] per test section by comparison of the modelled damage number D_s [m²/s²] to the damage number D [m²/s²] for the observed damage category at the end of the landward slope. Data per test section is provided in terms of the slope length L_{slope} [m], the crest width L_{crest} [m], the steepness of the landward slope $\cot(\alpha)$ [-] and the simulated mean overtopping discharge q_m [l/s/m]. Flow acceleration according to Van Bergeijk et al. (2019b). Marked boxes indicate the derived minimum critical flow velocities.

	L_{slope} [m]	L_{crest} [m]	$\cot(\alpha)$ [-]	q_m [l/s/m]	D [m ² /s ²]	Modelled damage number D_s [m] at the slope per critical flow velocity U_c [m]				
Boonweg 1	27.0	2.5	2.9	0.1; 1; 10; 30; 50; 75	0 - 2500	$U_c = 6.5$ m/s 5276	$U_c = 7.0$ m/s 2928	$U_c = 7.5$ m/s 1488	$U_c = 8.0$ m/s 666	$U_c = 8.5$ m/s 239
Boonweg 2	27.0	2.5	2.9	0.1; 1; 10; 30; 50; 75	0 - 2500	$U_c = 6.5$ m/s 5276	$U_c = 7.0$ m/s 2928	$U_c = 7.5$ m/s 1488	$U_c = 8.0$ m/s 666	$U_c = 8.5$ m/s 239
Kattendijk 1	15.0	2.0	3.0	0.1; 1; 10; 30; 50	0 - 2500	$U_c = 5.5$ m/s 5784	$U_c = 6.0$ m/s 3115	$U_c = 6.5$ m/s 1566	$U_c = 7.0$ m/s 696	$U_c = 7.5$ m/s 252
Kattendijk 2	17.0	2.5	3.0	30; 50	0 - 2500	$U_c = 5.5$ m/s 6157	$U_c = 6.0$ m/s 3492	$U_c = 6.5$ m/s 1857	$U_c = 7.0$ m/s 884	$U_c = 7.5$ m/s 359
Afsluitdijk 1	7.8	0.5	2.3	1; 10; 30	0 - 2500	$U_c = 5.0$ m/s 7328	$U_c = 5.5$ m/s 4098	$U_c = 6.0$ m/s 1977	$U_c = 6.5$ m/s 855	$U_c = 7.0$ m/s 341
Afsluitdijk 2	7.5	0.7	2.3	1; 10	0 - 2500	$U_c = 4.0$ m/s 6033	$U_c = 4.5$ m/s 4054	$U_c = 5.0$ m/s 2488	$U_c = 5.5$ m/s 1358	$U_c = 6.0$ m/s 649
Tholen 4	14.0	2.0	2.3	1; 5; 10	0 - 2500	$U_c = 4.0$ m/s 4832	$U_c = 4.5$ m/s 2989	$U_c = 5.0$ m/s 1668	$U_c = 5.5$ m/s 870	$U_c = 6.0$ m/s 392

2. Calibration load factor (α_M) per test section:

a. Flow acceleration method according to Van der Meer et al. (2015) - $\alpha_{\alpha, v d M}$:

Table A4.4 Overview of the calibration of load factor α_M [-] per test section by comparison of the modelled damage number D_t [m^2/s^2] to the damage number D [m^2/s^2] for the observed damage category at the geometrical transition at the landward toe. Data per test section is provided in terms of the slope length L_{slope} [m], the steepness of the landward slope $\cot(\alpha)$ [-], the flow acceleration factor $\alpha_{\alpha, v d M}$ (Van der Meer et al., 2015), the simulated mean overtopping discharge q_m [l/s/m] and the critical flow velocity U_c [m/s]. Marked boxes indicate the calibrated values for the load factor α_M .

	L_{slope} [m]	$\cot(\alpha)$ [-]	$\alpha_{\alpha, v d M}$ [-]	q_m [l/s/m]	D [m^2/s^2]	U_c [m/s]	Modelled damage number D_t [m] at the transition per load factor α_M [-]										
							1.0	1.1	1.2	1.3	1.4	1.5	1.6	1.7	1.8	1.9	2.0
Boonweg 1	27.0	2.9	1.46	0.1; 1; 10; 30; 50;	1000	10.0	130	323	647	1111	1716	2499	3486	4668	6071	7651	9497
Boonweg 1	27.0	2.9	1.46	0.1; 1; 10; 30; 50; 75	4000	10.0	603	1245	2187	3513	5193	7311	9904	12968	16532	20520	24984
Boonweg 2	27.0	2.9	1.46	0.1; 1; 10; 30; 50; 75	4000	10.0	603	1245	2187	3513	5193	7311	9904	12968	16532	20520	24984
Kattendijk 1	15.0	3.0	1.41	0.1; 1; 10; 30; 50	7000	8.5	769	1344	2135	3173	4465	5991	7823	9974	12451	15254	18348
Kattendijk 2	17.5	3.0	1.42	30; 50	7000	8.5	839	1446	2272	3341	4655	6193	8021	10144	12573	15288	18269
Afsluitdijk 1	7.8	2.3	1.46	1; 10	1000	7.5	56	125	232	393	602	868	1154	1484	1858	2287	2767
Afsluitdijk 1	7.8	2.3	1.46	1; 10; 30	4000	7.5	921	1461	2173	3095	4264	5670	7240	8979	10891	12997	15259
Afsluitdijk 1	7.8	2.3	1.46	1; 10; 30; 50; 75	7000	7.5	8835	12902	17819	23578	30138	37455	45454	54044	63237	73020	83326
Afsluitdijk 2	7.5	2.3	1.46	1; 10	4000	6.0	667	992	1392	1875	2438	3058	3749	4494	5286	6125	7015
Tholen 4	14.0	2.3	1.46	1; 5	1000	6.5	109	186	299	467	680	930	1238	1587	1955	2348	2766
Tholen 4	14.0	2.3	1.46	1; 5; 10	7000	6.5	628	996	1456	2043	2752	3579	4516	5552	6668	7847	9085

b. Flow acceleration method according to Schüttrumpf and Oumeraci (2005) - $\alpha_{a,SO}$:

Table A4.5 Overview of the calibration of load factor α_M [-] per test section by comparison of the modelled damage number D_t [m^2/s^2] to the damage number D [m^2/s^2] for the observed damage category at the geometrical transition at the landward toe. Data per test section is provided in terms of the slope length L_{slope} [m], the crest width L_{crest} [m], the steepness of the landward slope $\cot(\alpha)$ [-], the simulated mean overtopping discharge q_m [l/s/m] and the critical flow velocity U_c [m/s]. Flow acceleration according to Schüttrumpf and Oumeraci (2005). Marked boxes indicate the calibrated values for the load factor α_M .

	L_{slope} [m]	L_{crest} [m]	$\cot(\alpha)$ [-]	q_m [l/s/m]	D [m^2/s^2]	U_c [m/s]	Modelled damage number D_t [m] at the transition per load factor α_M [-]										
							1.0	1.1	1.2	1.3	1.4	1.5	1.6	1.7	1.8	1.9	2.0
Boonweg 1	27.0	2.5	2.9	0.1; 1; 10; 30; 50;	500	7.5	33	111	255	488	803	1233	1795	2487	3314	4291	5435
Boonweg 1	27.0	2.5	2.9	0.1; 1; 10; 30; 50; 75	2000	7.5	187	455	893	1552	2433	3590	5055	6835	8927	11317	14035
Boonweg 2	27.0	2.5	2.9	0.1; 1; 10; 30; 50; 75	2000	7.5	187	455	893	1552	2433	3590	5055	6835	8927	11317	14035
Kattendijke 1	15.0	2.0	3.0	0.1; 1; 10; 30; 50	3500	6.5	241	483	833	1322	1961	2747	3722	4896	6289	7897	9711
Kattendijke 2	17.5	2.5	3.0	30; 50	3500	6.5	236	474	816	1287	1900	2648	3559	4645	5922	7389	9023
Afsluitdijk 1	7.8	0.5	2.3	1; 10	500	6.0	17	45	102	198	336	508	711	955	1251	1598	1989
Afsluitdijk 1	7.8	0.5	2.3	1; 10; 30	2000	6.0	341	608	996	1540	2280	3201	4269	5493	6893	8428	10097
Afsluitdijk 1	7.8	0.5	2.3	1; 10; 30; 50; 75	3500	6.0	3438	5550	8264	11634	15652	20296	25482	31217	37492	44261	51438
Afsluitdijk 2	7.5	0.7	2.3	1; 10	2000	5.0	243	417	642	932	1291	1703	2175	2692	3254	3867	4526
Tholen 4	14.0	2.0	2.3	1; 5	500	5.0	62	116	204	331	486	685	908	1146	1404	1682	1979
Tholen 4	14.0	2.0	2.3	1; 5; 10	3500	5.0	355	591	912	1329	1835	2423	3085	3799	4558	5372	6243

c. Flow acceleration method according to Van Bergeijk et al. (2019b) - $\alpha_{\alpha,VB}$:

Table A4.6 Overview of the calibration of load factor α_M [-] per test section by comparison of the modelled damage number D_t [m^2/s^2] to the damage number D [m^2/s^2] for the observed damage category at the geometrical transition at the landward toe. Data per test section is provided in terms of the slope length L_{slope} [m], the crest width L_{crest} [m], the steepness of the landward slope $\cot(\alpha)$ [-], the simulated mean overtopping discharge q_m [l/s/m] and the critical flow velocity U_c [m/s]. Flow acceleration according to Van Bergeijk et al. (2019b). Marked boxes indicate the calibrated values for the load factor α_M .

	L_{slope} [m]	L_{crest} [m]	$\cot(\alpha)$ [-]	q_m [l/s/m]	D [m^2/s^2]	U_c [m/s]	Modelled damage number D_t [m] at the transition per load factor α_M [-]										
							1.0	1.1	1.2	1.3	1.4	1.5	1.6	1.7	1.8	1.9	2.0
Boonweg 1	27.0	2.5	2.9	0.1; 1; 10; 30; 50;	2500	9.5	449	987	1804	2972	4511	6425	8802	11690	15084	18949	23328
Boonweg 1	27.0	2.5	2.9	0.1; 1; 10; 30; 50; 75	9000	9.5	1488	3000	5205	8235	12128	16829	22412	28878	36200	44341	53276
Boonweg 2	27.0	2.5	2.9	0.1; 1; 10; 30; 50; 75	9000	9.5	1488	3000	5205	8235	12128	16829	22412	28878	36200	44341	53276
Kattendijke 1	15.0	2.0	3.0	0.1; 1; 10; 30; 50	13000	8.0	1566	2905	4797	7374	10644	14604	19166	24325	30063	36290	42968
Kattendijke 2	17.5	2.5	3.0	30; 50	13000	8.0	1935	3404	5417	8051	11286	15157	19550	24468	29853	35638	41785
Afsluitdijk 1	7.8	0.5	2.3	1; 10	2500	7.0	284	589	997	1550	2249	3067	4004	5035	6163	7399	8719
Afsluitdijk 1	7.8	0.5	2.3	1; 10; 30	9000	7.0	1977	3577	5641	8205	11175	14529	18248	22236	26491	30995	35670
Afsluitdijk 1	7.8	0.5	2.3	1; 10; 30; 50; 75	13000	7.0	13810	21764	31401	42659	55295	69023	83753	99222	115391	132161	149387
Afsluitdijk 2	7.5	0.7	2.3	1; 10	9000	5.5	2488	3549	4774	6132	7575	9109	10716	12393	14118	15874	17663
Tholen 4	14.0	2.0	2.3	1; 5	2500	6.5	398	695	1100	1574	2098	2684	3330	4030	4767	5543	6356
Tholen 4	14.0	2.0	2.3	1; 5; 10	13000	6.5	1668	2641	3847	5256	6802	8508	10385	12398	14520	16727	19027